POLITECNICO DI TORINO

Dipartimento di Ingegneria Strutturale, Edile e Geotecnica

Corso di Laurea Magistrale in Ingegneria Civile

TESI DI LAUREA MAGISTRALE

TIME DEPENDENT-BEHAVIOUR OF COMPOSITE STEEL-CONCRETE SLABS

Relatore:

Prof. Ing. Rosario Ceravolo, Politecnico di Torino

Correlatore:

Prof. Ing. Gianluca Ranzi, The University of Sydney

Desideria Cardullo 221755

Anno accademico 2017/2018

Abstract

This thesis focuses on the service behaviour of composite steel-concrete slabs associated to the time-dependent response induced by concrete creep and shrinkage. The main aims of the thesis are: (i) to provide an overview of the available design guidance and research information relevant to the service behaviour of composite slabs, (ii) to compare the serviceability limit state design procedures specified in the European and Australian guidelines and (iii) to perform extensive parametric studies on realistic floor arrangements to evaluate the key parameters controlling the composite slab design for building floors and identify the influence of service considerations of the adopted design solutions. The initial part of the thesis presents an extensive state of the art review that covers work carried out to date and published in the open literature on the time-dependent behaviour of composite members, i.e. composite slabs, beams and columns. This is followed by a brief introduction of creep and shrinkage effects and how these are included in the calculations relevant to the serviceability limit state design. A numerical model capable of describing the time-dependent response and of predicting deflections of composite slabs is then presented. Particular attention is devoted to the development of shrinkage gradients that have been recently observed experimentally to occur in composite steel-concrete floor systems due to the inability of the concrete to dry from its underside because of the presence of the profiled steel sheeting. The serviceability limit state rules specified in the Australian and European codes are described and compared to highlight key differences in their specifications and how these affect the final design. Extensive parametric studies are performed and presented in the final part of the thesis to highlight the key parameters controlling the design.

Sintesi

L'elaborato mira allo studio del comportamento delle solette composte acciaio-calcestruzzo in condizioni di esercizio, attenzionando la risposta tempo-dipendente indotta dagli effetti di creep e ritiro del calcestruzzo. I pricipali scopi della tesi sono: (i) fornire una visione d'insieme delle linee guida di progettazione disponibili attualmente e ricercare rilevanti informazioni sul comportamento in condizioni di esercizio delle solette composte, (ii) paragonare le procedure di progettazione allo stato limite di servizio specificate nelle linee guida Europee ed Australiane ed (iii) eseguire un esteso studio parametrico riguardante realistiche casistiche di pavimentazione così da stimare i parametri chiave che influenzano il risultato in condizioni di esercizio delle diverse soluzioni di progettazione adottate. La prima parte della stesura presenta un'analisi dettagliata dello stato dell'arte sul comportamento tempo-dipendente di membri composti (solette, travi e colonne composte). Lo stato dell'arte comprende ad ampio spettro le ricerche svolte fino ad oggi e disponibili in letteratura. Questa parte è seguita da una breve introduzione degli effetti di creep e ritiro, e su come questi siano inclusi nel calcolo progettuale allo stato limite di servizio. E' stato inoltre presentato un modello numerico capace di descrivere la risposta tempo dipendente e di predire l'inflessione delle solette composte acciaio-calcestruzzo. Particolare attenzione è stata rivolta allo sviluppo del gradiente di ritiro che è stato recentemente osservato nelle solette composte acciaio-calcestruzzo. Questo è dovuto alla presenza della lamiera in acciaio, che impedisce la libera evaporazione dell'acqua, presente nel calcestruzzo, dall'intradosso della soletta. Le norme relative allo stato limite di servizio, specificate nel codice Australiano ed Europeo, sono state descritte e confrontate al fine di

sottolineare le principali differenze e come quest'ultime possano influire sulla progettazione finale. Un dettagliato studio parametrico è stato presentato nella parte finale dell'elaborato, per mettere in evidenza i parametri fondamentali che controllano la progettazione.

Summary

List of figures

List of tables

Introduction

1.1. Introduction

Composite steel-concrete slabs are widely used for building constructions and represent an economical form of construction commonly used in the world. represent an economical form of construction commonly used in the world. Composite slabs are formed by a reinforced concrete slab cast on a profiled steel sheeting as shown in Figure 1.

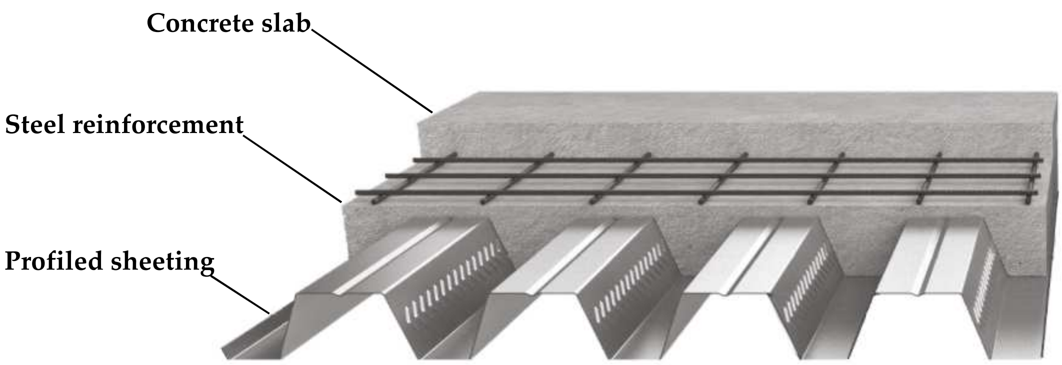

Figure 1: Typical composite steel-concrete slab

A key advantage in using composite slabs relies on that fact that the steel sheeting supports the wet concrete as permanent formwork and, once the concrete has hardened, it acts as external reinforcement by becoming an integral part of the slab. In addition, the simple handling and lightweight of the profiled sheeting can lead to reductions in construction time. Composite steel-concrete building floors are usually governed by the serviceability limit state requirements associated with deflections.

In this context, this thesis focuses on the time-dependent behaviour of composite steel-concrete slabs by placing particular attention to shrinkage effects and how these influence structural deformations and deflections. The presence of steel sheeting prevents free egress of moisture from the underside of slab that leads to the development of a shrinkage gradient through the thickness of the slab. Recent research has shown that the occurrence of the shrinkage gradient can significantly influence and increase deflections. This work highlighted that common industry practice adopted in the past in Australia of specifying a constant shrinkage profile for the composite slab design was non-conservative, because underestimating the time-dependent deflections. For this purpose, a major component of the thesis investigates the design implications of specifying a shrinkage gradient on the calculated deflections and how these results compare to those obtained adopting constant shrinkage profiles or those determined ignoring shrinkage effects, as recommended in some international guidelines. The design model adopted to predict the effects of the shrinkage gradient is the one specified in the Australian composite code published in December 2017 (1). The new Australian service design rules have also been compared against those specified in the European guidelines. An extensive parametric study has been carried out and outlined at the end of the thesis. Its results have highlighted the importance of the serviceability limit state requirements in controlling the final design, such as the slab minimum thickness. The influence of different parameters has also been considered and discussed.

1.2. Layout of the thesis

This thesis is organized in six chapters as detailed below.

The current chapter, i.e. **Chapter 1**, provides a brief introduction to the thesis. **Chapter 2** presents the literature review carried out on the time-dependent behaviour of composite steel-concrete members. For completeness, the review has focused on all composite members, i.e. slabs, columns and beams. **Chapter**

3 describes, after introducing the key concepts related to concrete creep and shrinkage effects, the material properties of concrete and steel that can be used for service calculations. Selected design models for describing the time-dependent behaviour of the concrete are also introduced. In **Chapter 4**, the formulations for the time-dependent analysis of composite slab is derived. The details and use of the cross-sectional analysis are outlined and applied to the prediction of stress and strains variations that take place in the concrete over time. **Chapter 5** shows and discusses the main differences between the service design procedures specified in the Australian (1) and European guidelines (2). **Chapter 6** outlines the results of the extensive parametric studies carried out and aims at identifying the influence of different serviceability models on the design of composite slabs. The results have been obtained by implementing the formulation in a MATLAB program. **Chapter 7** presents the conclusions of this thesis and recommendations for future work.

Literature review

3.1.Introduction

This section presents a review of the literature of composite steel-concrete members. Many researches are mentioned to provide an overall view of the state of the art of time dependent behaviour of composite slabs, columns and beams.

3.2.Composite slabs

Composite slabs are common used in the construction of floors building. Many researches have been dedicated to the ultimate behaviour of composite steel-concrete slabs, while very limited works have been reported on their serviceability condition. Despite this, the serviceability limit state is heavily affected by the time-dependent behaviour of the concrete composite slab and recent work has significantly focused on this aspect. The long-term analysis of the structures in service conditions focus primarily on the time-varying deflection and on creep and shrinkage effects. Notwithstanding the common usage of this kind of construction, structural designers often specify the decking only as loss formwork instead of timber formwork ignoring the composite action and the potential development of shrinkage gradient. They assumed uniform shrinkage distribution through the slab thickness relying on reinforced concrete guidelines. The Australian Standard treats drying shrinkage in a simplified manner, introducing a hypothetical thickness parameter as a term in its equation to calculate drying shrinkage (1). This assumption is suitable for reinforced concrete slabs exposed on both sides (2) (3) .In reality, a shrinkage gradient develops through the slab thickness due to the inability of moisture to egress from the underside of slab, therefore introducing an additional curvature and consequent deflection in composite slabs. For design purposes, the constant shrinkage representation works well for concrete slabs exposed on both faces but, for composite structures with profiled sheeting, it is necessary take into account the non-uniform shrinkage in the calculation of the long-term response.

First analytical models describing the time depended analysis date back to the '90s (4) (5) (6). They assumed uniform shrinkage profile and full shear interaction between the concrete and the profiled sheeting. Other researchers used these theoretical models to predict the long-term response of composite slabs in (7) (8). Later work, based on the same assumptions, presented an analytical procedure using the age-adjusted effective modulus method (9) (10). Subsequent work aimed at demonstrating that the shrinkage distribution is non-uniform through the depth of a composite slabs with steel sheeting. If this is neglected the midspan deflections could be significantly underestimated. This conclusion was valeted by (9) (10). No design guidance was available to engineers to account for the influence of this non-uniform shrinkage. In the last years, further experimental works have shown the importance in considering non-uniform shrinkage in composite slabs (2) (3) (12) and in post-tensioned composite slab (13) (14) when calculating deflection predictions. In these experimental studies, the development of non-uniform shrinkage was monitored on different concrete samples varying the sealing condition, the profile sheeting, the amount of reinforcement, load condition and the concrete thicknesses as showing in the table 1:

Year	Title Article	Specimens
2013	*Long-term behavior of simply-supported post-tensioned composite slabs*	**1 EXP-EXP** **1 EXP-Condeck HP** **1 EXP-PrimeForm**
2013	*An experimental study on the ultimate behavior of simply supported post-tensioned composite slabs*	**2 EXP-EXP** **2 EXP-Condeck HP** **2 EXP-PrimeForm** with different load condition.
2015	*Effects of Non-uniform Shrinkage on the Long-term Behavior of Composite Steel-Concrete Slabs*	**3 EXP-EXP** **3 EXP-PLA** **3 EXP-PrimForm** **3 EXP-Condeck** with different concrete thicknesses
2015	*Non-uniform shrinkage in simply-supported composite steel-concrete slabs*	**2 EXP-Condeck HP** **2 EXP-EXP** with different amount of reinforcement
2012	*Effects of shrinkage on the long-term stresses and deformations of composite concrete slabs*	**1 EXP-KF40** **1 EXP-COATING** **3 EXP-KF70** **3 EXP-COATING** **1 EXP-RF55** **1 EXP-COATING** with different concrete thicknesses

Table 1: Summary of specimens

The experimental data highlighted how the use of the constant profile can underestimate the predictions of the deflections. The latter may be cause of a reduction of the cracking moment such as it was observed in (12). The comparison between experimental and numerical results confirmed that the current use of a constant shrinkage distribution is not-conservative (13) (2). New theoretical models have been developed to incorporate the effect of non-uniform shrinkage in the deflection calculation (3) (12) (15). They extended the approach for the estimation of uniform shrinkage profile that was readily available from design guidelines AS3600-2009. The aim of the tests is to collect experimental data in order to demonstrate the relevance of the assumption of non-uniform shrinkage and to include it in routine design approach. In 2017, G. Ranzi proposed a simplified approach for routine design reformulating the previous long-term formulation. This approach is available on the Australian code (1). Over the last years, finite element analysis have been carried out to investigate the long-term response of composite slabs varying different parameters such as the shape of steel sheeting, thickness and shear span (18).

3.3. Composite columns

The use of composite steel-concrete columns is a good structural solution because it takes advantage of mechanical properties of both materials that together allow to reach better performances than those achieved when the two components are considered in isolation. The first composite columns used in construction were *fully encased* columns, in which the steel profile was totally surrounded by the concrete. The capacity of the concrete provided the protection against corrosion and fire and contributed at limiting the occurrence of local buckling. In this kind of composite columns, the local instabilities are avoided; for this reason, they are widely used for the construction of tall building where the phenomenon of local bucking is common due to the slenderness of elements. Additional typology of composite columns have been introduced over time. Typical and usual classification catalogued the composite columns in four typologies: *fully encased*, *partially encased*, *concrete filled* (CFTs) and *concrete filled double skin member* (CFDST). The second typology is similar to the first one but, in this case, the concrete surround only some part of the steel section. The steel section is partially exposed and so it is not totally protected against the corrosion and fire by the concrete. On the other hand, in the last two typologies the cost of the formwork is eliminated because the concrete is poured into the steel section that acts as permanent formwork. In CFT columns, the central part of concrete can be replaced by another hollow steel tube with much smaller area, which is left unfilled because the concrete is poured within the two steel sections. This structural solution is usually referred to as concrete-filled double-skin tubular columns. The position of the concrete compared to the steel profile changes the performance of the composite system. In CFTs columns the fire and corrosion requirements respectively, are not guaranteed any longer. Despite this, the advantages of the exposed steel tube relies on the confinement and on the protection of the concrete core from the direct exposure to the external environment.

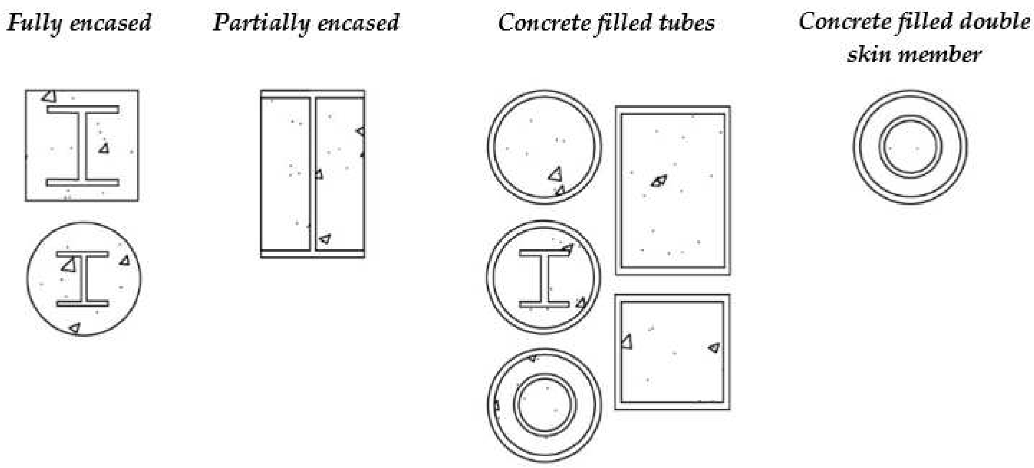

Figure 2: Typical composite column sections

Different studies have been dedicated to both creep and shrinkage effects on composite columns filled. The initial experimental studies date back to 1990, which focussed on the creep response and, reported smaller creep values when compared to conventional reinforced concrete columns due to the inability of moisture to escape from a concrete core within a steel tube (20) (21). The magnitude of this reduction is about 50-60%. Further work validated this range of values (22) (23). The study of moisture diffusion process in concrete is also important to predict the shrinkage effect. The presence of the steel tube influences the long-term deformations. It obstructs the moisture egress and the drying component could be considered null. Several experimental studies, on concrete filled columns, showed the possibility to neglect shrinkage (20) (21) (22) (23). More attention needs to be devoted to understand the time-dependent response of using high-strength concrete in composite columns, because the autogenous shrinkage represents a notable part and it increases with the concretes strength. Despite this, shrinkage strains are smaller for high-strength composite columns than those of lower strength concrete.

Recent work focuses on the long-term shortening of encased columns because very limited research has been conducted over time on this type of composite columns (24). Despite the lack of surrounding steel tube, the moisture diffusion inside the column is however hindered by the inner steel section. For instance, the conventional H steel section where the wide- flange obstructs the moisture dissipation.

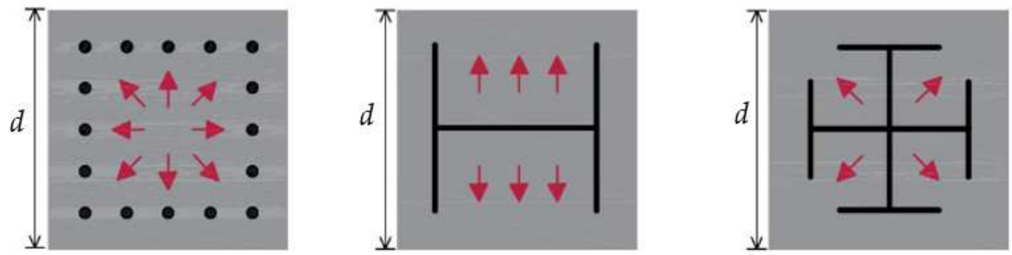

Figure 3: Schematic illustration of moisture diffusion

The study shows that the delayed diffusion of moisture leads to lower long-term deformations of the columns. Therefore, in the prediction of creep and shrinkage strains neglect the influence of steel section means overestimate the long-term deformations. In the calculation of drying creep and shrinkage effects much attention should be given to the type of prolife used and the ratio web length to the size of column. In the case of steel-reinforced concrete columns, a decrease in long-term deformations with an increase of the steel area ratio (the ratio of the cross-sectional area of the encased steel to the total cross-sectional area of the column) was measured (25). Further research highlighted also the dependence of creep and shrinkage strains from of the concrete strengths. The use of high-strength materials has been expanding in the construction of composite columns to improve structural safety and economy and to reduce the columns size and weight. Nevertheless, when high strength steel is used for composite columns, an undesired failure mode may be occurs. It consist on early concrete crushing. If the yield strain of the steel exceeds the crushing strain of concrete, concrete crushing occurs before yielding of the steel. Thus, the yield strength of the steel can not be reached and the use of strength steel is rendered useless. This degrades the capacity of composite columns. Recent work studied different steel sectional shapes and configurations in order to guarantee the use of full yield capacity of steel. It shows that in the case of CFT columns the strength of the confined concrete is significantly increased by lateral confinement due to the presence of steel tube (especially at high levels of concrete stresses when the Poisson's ratio of the concrete is bigger than the one of the steel). Thus, CSE columns could be a good solution to restrain early concrete crushing where high strength steel is used (26). Researches highlighted that confinement depends by the application point of the sustained load (22) (27), in fact at service conditions, confinement effect is not guaranteed if the sustained load is applied to the composite section or only to the steel section, but it develops if applied to concrete component exclusively (19). When confinement effect is not guaranteed, notable results were obtained introducing (at the four corners of the cross section of composite columns) L-shaped steel sections instead of conventional H section. This arrangement maximizes the ultimate moment capacity by increasing the moment arm of the steel. Recent researches had carried to investigate the effect of sustained axial loads on the structural behaviour of high-strength composite columns. (28) Specimens are tested under sustained axial load until crushing failure. From this long-term analysis, the effect of the sustained load on the ultimate behaviour of the columns results negligible. Further work, on the ultimate strengths of SRC columns, confirmed this result (25).

Long-term tests were also performed on recycled aggregate concrete filled steel tubular columns (RACFST) because of the considerable influence of this material on creep and shrinkage effects. The first test reported an increase of 40 % of time-dependent deformations if compared to traditional CFST (29). In order to validate this result, later work provided new experimental data about the influence of concrete strength on time dependent deformation of RACFTS. For different concrete strengths, 30 MPa (C30) and 50 MPa (C50), comparable measured data has been recorded (29). It be observed that the incorporation of recycle aggregates has similar influence on time-dependent behaviour of composite specimens with different concrete strengths (for instance, for C30 specimens is observed an increase of 22,4 % in the $^{\Delta\varepsilon(t)}/_{\varepsilon_0}$ ratio . The latter is only 1,8% different from that registered for C50 specimens) (28).

3.4. Composite beams

Steel-concrete composite beam is another composite element widely used in building and bridge construction. Generally, this solution reaches maximum efficiency in positive moment regions where the bottom area of the slab is subjected to tensile stress. The tensile strength increases due to the presence of steel sheeting. Owing to those advantages, steel-concrete composite beam represents an attractive form of construction. It consists of solid or composite slab and steel beams.

The steel beam and the slab act as a “composite beam” only if connected by mechanical devices otherwise, the composite action is not provided and these two components act independently. Most common connection system consist of shear connectors, welded or bolted to the top flange of the steel.

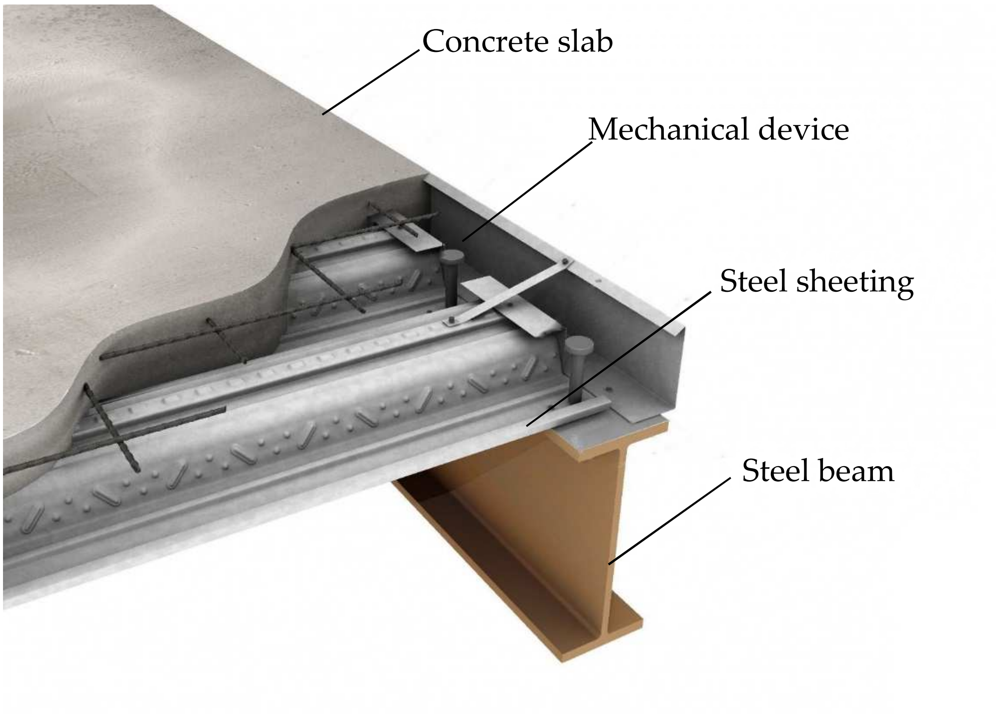

Figure 4: Steel-concrete composite beam

The interaction degree between concrete and steel depends by the deformability of the shear connection. It is possible to provide partial, full or no shear interaction. The latter represent the two limit cases. Full shear interaction implies no relative slip at the interface between the steel and concrete components. Generally, lesser number shear connectors than that required by full shear connection are enough to sustain the applied load in a safety way (30).

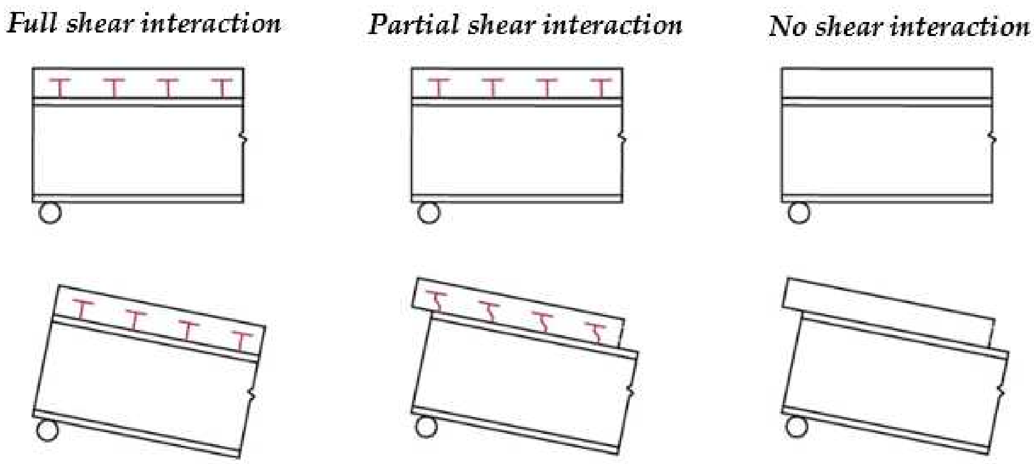

Figure 5: Typical slip displacement before and after loading for a composite beam with full, partial and no shear interaction

The initial model developed about the long-term behaviour of composite beams are only based on full shear interaction theory (4) (5) (31). In the following years it was realized that the interaction degree influence the time dependent composite response of the composite system modifying relevant parameters for serviceability limit state (deflections and stresses). Through extensive experimental and numerical analysis, it has been shown that the degree of shear connection has a direct relationship to deflection of composite beams at service loads. The first works focusing in this area were(32) (33), following by others long-term test concerning the importance to account for partial shear interaction (34) (35) (36). Over time these initial model were improved considering more refined material non-linearity and concrete cracking. These were developed using the finite element method (37) (38) (39) (40) (41) (42) (43) (44) (45) (46), stiffness method (47) (48), and analytical solutions (49). Later works were carried out to date on the long-term behaviour in negative moment regions (50) (51). Recent research focussed on the shrinkage effect on long-term deflection (52). The effect of shrinkage in the concrete slab was found to play a significant role on serviceability behaviour, more so than other parameters including steel-concrete interface slip. The necessity to take into consideration the non-uniform shrinkage profile has showed experimentally. This has already been outlined in previous paragraph on composite slab. Analytical models was suggested in (53) (33) to account the shrinkage gradient through the thickness of concrete. The concrete shrinkage has a significantly influence on the long-term behaviour on the composite system. It has also an effect on the fatigue strength of the connection at the interface at steel and concrete. The fatigue strength can be defined as the bearing capacity of the connection after N load cycles. The results of experimental test (54) showed that generally the shrinkage stresses developed in the steel-concrete interface have an opposite direction compare to the external loads. This opposite effects reduces the stresses and the number of load cycles N leading to fatigue failure are consequently increased. In this way The shrinkage reduces the fatigue hazard. At the other side, the stress developed at the connection due to shrinkage and creep may result in uplift effects. The separation between the beam and the slab can take place, especially in the end region. An analytical model for interfacial stress of composite beams was introduced in (55). It showed that, in order to reproduce uplift effects, the common assumption that the two material have the same curvature must be abandoned. Shrinkage and creep both are the most uncertain phenomenon of concrete structures because they are influenced by the characteristic of the particular concrete mix. The characteristics of material include a widely variability of parameters. In order to involve the uncertainties of creep and shrinkage in the long-term analysis a recent model was introduced. It investigated the stochastic long-term behaviour of steel concrete composite-beams (56). It is clear that there are complex interactions between the beam and composite slab and numerous parameters influence the long-term response. For these reasons, recently, a 3D finite element model was developed (57) as a viable alternative approach to investigate the behaviour of composite beam.

Material properties

4.1.Introduction

This chapter describes the material properties of the constituents of the composite slabs: steel and concrete. The first part of the chapter focuses on the time-dependent effects of concrete (creep and shrinkage) and introduces simple equations to predict typical properties of concrete such as creep coefficient and shrinkage strain. The second part of the chapter deals with the material model to be adopted for the steel at service condition.

4.2.Concrete

The design of concrete structures in-service conditions requires the accurate prediction of time dependent behaviour of a concrete. It is intrinsically linked to two important effects: creep and shrinkage. These time effects may provoke problems with serviceability and durability of the system related with increased deformation and curvature, loss of prestress and cracking (if shrinkage of concrete is restrained). Creep strain develops in concrete over the time due to sustained load contrary to shrinkage that is independent of applied loading. The latter depends on the slab geometry, characteristic of particular concrete mix, drying conditions and relative humidity. When a concrete cross-section is subject to load, it has two components of response. Its initial response, that occurs immediately after the application of the stress, is the instantaneous component. If the cross-section is subject to a sustained load over a prolonged period, a time-dependent or long-term response occurs and it develops as a deformation gradually increasing over time.

The total concrete strain, of an uniaxial-loaded concrete specimen at constant temperature, is commonly calculated as the sum of three components independent from each other: instantaneous strain $\varepsilon_e(t)$, creep strain $\varepsilon_{cr}(t)$ and shrinkage strain $\varepsilon_{sh}(t)$, using the following expression:

$$\varepsilon(t) = \varepsilon_e(t) + \varepsilon_{cr}(t) + \varepsilon_{sh}(t) \tag{3.1}$$

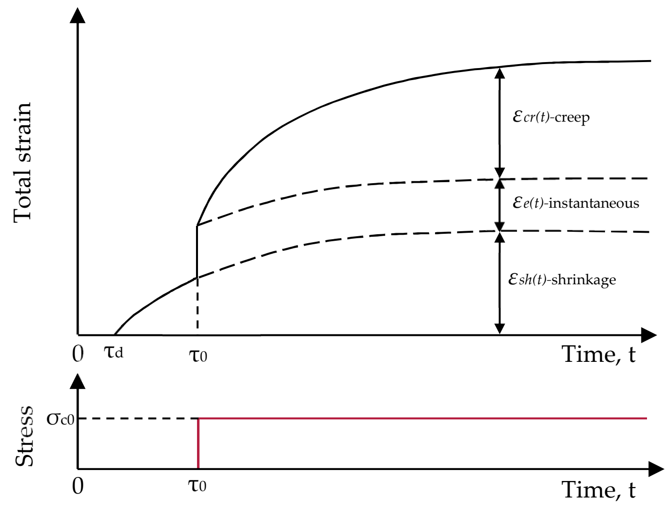

Figure 6: Concrete strain components under sustained load

In this manner, even if not rigorously correct, these three components are treated independently from each other. In reality, creep and shrinkage occur simultaneously. For practical purpose, it can be reasonably assumed that the shrinkage deflection of a slab is independent of the load level and that the creep-induced deflection is roughly proportional to the level of loading. These assumptions justify the calculation of creep and shrinkage-induced deflections separately (Gholamhoseini A, Gilbert RI, Bradford MA and Chang ZT- 2014).

For the prediction of the instantaneous strain, the concrete is assumed to remain in the linear-elastic range. For element in tension, the behaviour can be even considered linearly elastic until concrete reaches its tensile strength. The tensile strength, f_{ct}, is generally define as the maximum stress that the concrete can resist when subjected to direct uniaxial tension. For element in flexure, characteristic flexural tensile strength, $f'_{ct,f}$, is assumed as indirect tensile capacity measured in term of apparent tensile stress at the extreme tensile fibre of the critical cross section .

Linear-elastic uniaxial model is adopted to calculate the instantaneous strain as follow:

$$\varepsilon_e(t) = \frac{\sigma_{c0}}{E_c(t_0)} \tag{3.2}$$

where t_0 is the time of loading, σ_{c0} the stress in concrete at time t_0 and $E_c(t_0)$ is the elastic modulus at time t_0.

For the prediction of creep and shrinkage strain, numerical procedures are presented in the last paragraph 3.2.4 . They are based on Australian standards (1) and other design models for composite structures (e.g. Model Code 90, Model Code 2010, Model GL2000, Model B3, Model B4).

4.2.1. Creep

Creep is a time-dependent effect that develops in concrete due to sustained stress. When concrete is subjected to a sustained stress, it undergoes deformations, which increase with time. Creep strain develops gradually with time at a decreasing rate. In fact, it increases more rapidly at early ages, in the period immediately after first loading, and later the rate of increase slows with time. This phenomenon depends by different complex mechanisms and it may be defined as an increase of deformation with constant stress. The time-dependent deformation is accompanied by no changes in stress.

Creep of concrete evolves in the hardened cement paste composed by many sheets of calcium silicate. The consistence of this paste is gelatinous, in fact the colloidal sheets of calcium are separated by layers of absorbed water; they slide between these spaces causing the well know viscous flow. The viscous flow is one of several different and complex causes of creep, which are not yet totally understood. The creep is ascribed to more than one of the following mechanisms: mechanical deformation theories, plastic theories, viscous and visco-elastic flow theories, delayed elasticity, seepage theory, microcracking. The rate of deformation is a function of the material's properties, environment and loading conditions. Creep decreases with a reduction of water-to-cement ratio (W/C) and with an increase of the aggregate content or maximum aggregate size. The mechanism of creep also depends on temperature and relative humidity. They are inversely proportional: a rise in temperature or relative humidity produces a reduction of creep effects. Creep is also more pronounced in members with large surface-area-to-volume ratios, such as slabs. Finally, creep depends on the loading history, (especially on the magnitude of the applied stress), its duration and the age of the concrete when the stress was first applied. The concrete is a time-dependent material; creep strain value of concrete loaded at an early age $\varepsilon_{cr}(t_1)$ is bigger than the one loaded later $\varepsilon_{cr}(t_2)$. Despite this, in very old concrete, the effect to creep never completely disappears.

$$\varepsilon_{cr}(t_1) > \varepsilon_{cr}(t_2) \qquad t_1 < t_2 \tag{3.3}$$

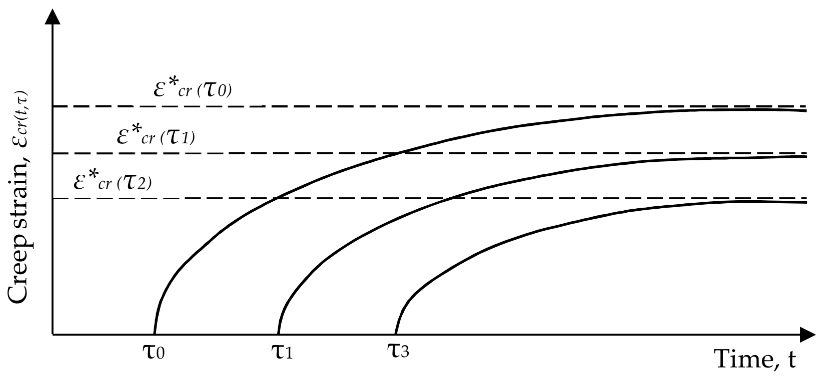

Figure 7: Effect of age at first loading on creep strains

Creep strain can be considered proportional to the stress when the sustained stress is less than about 0.5fc′. Generally, this stress value is not exceeded in concrete structure at service loads and creep is approximately as linear creep. The linear elastic behaviour allows the use of the principle of superposition according the Mc Henry Principle (Mc Henry stated that, whichever is the age at loading and the sign of Δσ, the stress variation Δσ applied at time t_1 has the same effect). Under this simplification, the creep strain can be subdivided into two component: the recoverable and irrecoverable components respectively. When the sustained stress is removed it can be observed a sudden recovery of the elastic deformation and a gradual reduction of creep over time, therefore, not all creep strain is recoverable. The irrecoverable part is known as flow $\varepsilon_{cr.f}$ and represent the majority of creep strain, while the residual recoverable part is often referred to as the delayed elastic strain $\varepsilon_{cr.d}$. The flow component consists of a rapid initial flow strain $\varepsilon_{cr.fi}$ (that occurs in the first day after loading) and a remaining part that it is further subdivided into a basic flow component $\varepsilon_{cr.fb}$ and drying flow component $\varepsilon_{cr.fd}$.

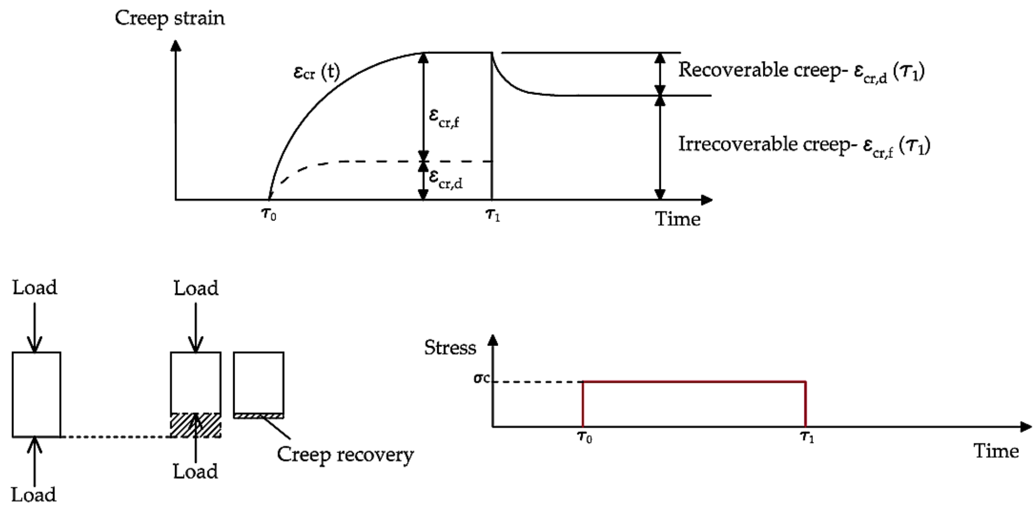

Figure 8: Recoverable and irrecoverable creep components

4.2.1.1. Creep coefficient

The creep coefficient, according the Australian code is defined as the ratio of creep strain at time, t, to the initial elastic strain at time τ. According the Australian Standard (1) (3.1.8.3), the creep coefficient calculated at time t for the stress applied at time τ_0 is determined as:

$$\varphi(t, \tau_0) = k_2 k_3 k_4 k_5 \varphi_{basic} \quad t_1 < t_2 \tag{3.4}$$

where:

k_2 is a factor that depends on the time after loading t, the hypothetical thickness t_h, and the environment, and is given by:

$$k_2 = \frac{\alpha_2 t^{0.8}}{t^{0.8} + 0.15 t_h} \tag{3.5}$$

The coefficient α_2 and the hypothetical thickness t_h are determinated as follows:

$$\alpha_2 = 1.0 + 1.12e^{-0.008t_h} \tag{3.6}$$

$$t_h = \frac{2A}{u_e} \tag{3.7}$$

In which A is the cross-sectional area of the member and u_e is that portion of the section perimeter exposed to the atmosphere plus half the total perimeter of any voids contained within the section.

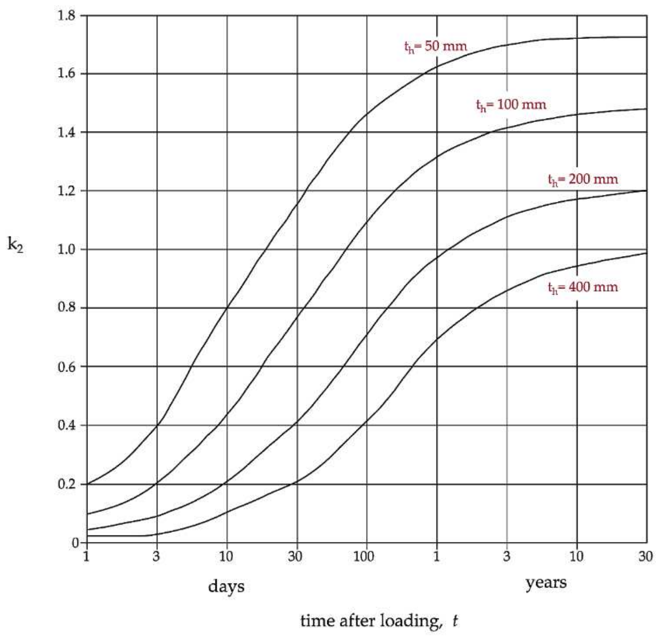

Figure 9: Coefficient k2

The factor k_3 depends on the age at first loading τ_0 (in days) and is given by:

$$k_3 = 2.7/(1 + log(\tau_0)) \qquad \tau_0 \geq 1\ day \tag{3.8}$$

The factor k_4 takes into account the environment and, is shows in the table 2:

0.70	for an arid environment;
0.65	for an interior environment;
0.60	for a temperate environment;
0.50	for tropical/coastal environment

Table 2: Coefficient k_4

The factor k_5 is a modification factor for high strength. It accounts for the reduced influence of the specimen size and the relative humidity on the creep of concrete as the concrete strength increase and, is shall be takes as:

1	for $f'_c \leq 50\ MPa$
$(2.0 - \alpha_3) - 0.02(1.0 - \alpha_3)f'_c$	for $50\ MPa < f'_c \leq 100\ MPa$

Table 3:Coefficient k_5

Where the coefficient α_3 is given by:

$$\alpha_3 = \frac{0.7}{k_4 \alpha_2} \tag{3.9}$$

The basic creep coefficient $\varphi_{basic}$is given in table 4.

$\boldsymbol{f'_c\ (Mpa)}$	20	25	32	40	50	65	80	100
$\boldsymbol{\varphi_{basic}}$	4.5	3.8	3.0	2.4	2.0	1.7	1.5	1.3

Table 4: The basic creep coefficient φ_{basic}

This procedure to calculate the creep coefficient is schematized in the figure 12.

4.2.2. Shrinkage

Shrinkage is a stress-independent effect and, in an unloaded and unrestrained specimen, it causes significant volume changing.

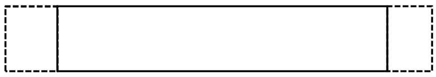

(a) unrestrained specimen

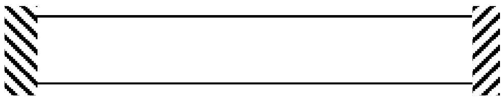

(b) restrained specimen

Figure 10: Restrained and unrestrained conditions

There are different classifications of shrinkage and these can be denoted as *plastic* shrinkage, *chemical* shrinkage, *thermal* shrinkage and *drying* shrinkage.

Plastic shrinkage takes place when the concrete is still wet, whereas chemical, thermal and drying shrinkage occur in the hardened concrete. During the setting process the steel reinforcements are not yet able to control the crack and plastic shrinkage is usually limited or eliminated by adopting specific measures on site, such as applying anti-evaporating membranes or nebulization treatments with water, to avoid the fast evaporation of water and the consequent formation of cracks. At this stage, the exposed zone starts to contract, but this changing of volume is restrained by the inner part that is not free to shorten and it produces tensile stress on the exposed surface of the concrete. If the water evaporation is too fast, the traction exceeds the tensile strength of the concrete and surface cracking occurs (at plastic phase the

modulus of elasticity of concrete is very low). Chemical shrinkage (known as *autogenous shrinkage*) is caused by hydration of the cement paste and by other chemical reactions (e.g. carbonation). This kind of shrinkage occurs quickly in the day after the casting and it is independent of moisture and thermal variations. In this case, the contraction results from transfer of water from big pores to small ones; the bigger tend to contract. Drying shrinkage is the consequence of the evaporation of the water during the drying process. It increases gradually with time at decreasing rate (approaching an asymptotic upper limit). The major loss of water takes place during the first months. Many factors influence the magnitude and rate of development of shrinkage, including the relative humidity, the water to cement ratio, type of aggregate, and the aggregate-to-cement ratio. Drying shrinkage always occurs if the concrete is located in an environment with not saturated humidity (RH>95%), and so all structures made of concrete are potentially affected by drying shrinkage. Drying shrinkage and autogenous shrinkage of concretes with extremely low water-cement ratios are nearly the same. Though the difference between drying shrinkage and autogenous shrinkage increases as the water-cement ratio increases, autogenous shrinkage does not become zero (62) .
The thermal shrinkage is a contraction due to the heat gradually dissipated during the hydration. This effect acts during the first few hours after setting.

4.2.2.1. Design shrinkage strain

The design shrinkage strain of concrete is treated as an imposed deformation and it shall be determined in accordance with the Australian Standard (1) (3.1.7.2). Following this procedure, $\varepsilon_{sh}(t)$, shall be determined as the sum of endogenous shrinkage ε_{she}, (autogenous shrinkage + thermal shrinkage) and drying shrinkage, ε_{shd}.

$$\varepsilon_{sh} = \varepsilon_{she} + \varepsilon_{shd} \tag{3.10}$$

where the endogenous shrinkage strain is given by:

$$\varepsilon_{she} = \varepsilon^{*}_{she}(1.0 - e^{-0.1t}) \tag{3.11}$$

with t being the time in days after casting and ε^{*}_{she} being the final autogenous shrinkage strain defined as:

$$\varepsilon^{*}_{she} = \left(0.06\, f'_{c} - 1.0\right) \times 50 \times 10^{-6} \qquad (f'_{c}\ in\ MPa) \tag{3.12}$$

The basic drying shrinkage $\varepsilon_{shd.b}$ is given by:

$$\varepsilon_{shd.b} = (1.0 - 0.008 f'_{c}) \times\ \varepsilon^{*}_{shd.b} \tag{3.13}$$

where the final drying basic shrinkage strain ,$\varepsilon^{*}_{shd.b}$, depends on the quality of the local aggregates and may be taken as 800×10^{-6} for Sydney and Brisbane, 900×10^{-6} for Melbourne and 1000×10^{-6} elsewhere.

At any time after the commencement of drying $(t - t_d)$, the drying shrinkage may be given by:

$$\varepsilon_{shd} = k_1 k_4 \varepsilon_{shd.b} \tag{3.14}$$

where k_1 depends on the hypothetical thickness, t_h, and is given by:

$$k_1 = \frac{\alpha_1 (t - t_d)^{0.8}}{(t - t_d)^{0.8} + 0.15 t_h} \tag{3.15}$$

and

$$\alpha_1 = 0.8 + 1.2 e^{-0.005 t_h} \tag{3.16}$$

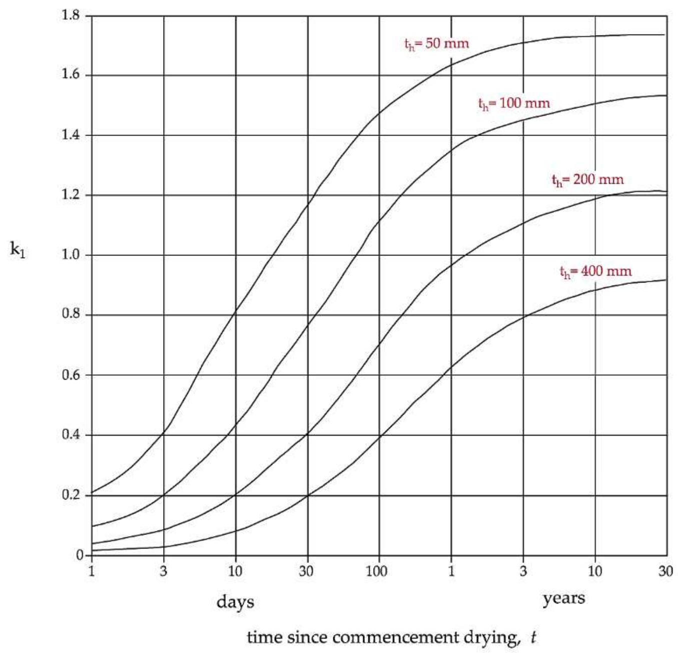

Figure 11: Coefficient k1

This procedure to calculate the design shrinkage strain is schematized in the figure 12.

AS 3600-2009

$$\boldsymbol{\varepsilon(t) = \varepsilon_{ist} + \varepsilon_{sh} + \varepsilon_{cr}}$$

$$\varepsilon_{sh} = \varepsilon_{shd} + \varepsilon_{she}$$

$$\varepsilon_{shd} = \varepsilon_{shd.b} k_1 k_4 \qquad \varepsilon_{she} = \varepsilon^*_{she}(1.0 - e^{-0.1t})$$

$$\varepsilon^*_{she} = \left(0.06\, f'_c - 1.0\right) \times 50 \times 10^{-6}$$

$$\alpha_1 = 0.8 + 1.2 e^{-0.005 t_h}$$

$$k_1 = \frac{\alpha_1 (t - t_d)^{0.8}}{(t - t_d)^{0.8} + 0.15 t_h}$$

$$\varepsilon_{shd.b} = (1.0 - 0.008 f'_c) \times \varepsilon^*_{shd.b}$$

$$\varepsilon^*_{shd.b} = \begin{cases} 800 \cdot 10^{-6} & for\ \text{Sydney and Brisbane} \\ 900 \cdot 10^{-6} & for\ \text{Melbourne} \\ 1000 \cdot 10^{-6} & for\ \text{elsewhere} \end{cases}$$

$$\varepsilon_{cr}(t, t_0) = \frac{\sigma_c(t_0)}{E_c(t_0)} \chi(t, t_0) \varphi(t, t_0)$$

$$E_c = 2400^{0,5} \cdot 0,043 \sqrt{f_{cm}}$$

$$f_{cm} = 0,9 * (f_{ck} + 8)$$

$$\varphi(t, t_0) = k_2 k_3 k_4 k_5 \varphi_{basic}$$

$$\alpha_2 = 1.0 + 1.12 e^{-0.008 t_h}$$

$$k_2 = \frac{\alpha_2 t^{0.8}}{t^{0.8} + 0.15 t_h}$$

$$k_3 = 2.7/(1 + log(\tau_0))$$

$$k_4 = \begin{cases} 0,70 & for\ \text{arid environment} \\ 0,65 & for\ \text{interior environment} \\ 0,60 & for\ \text{temperate enviroment} \\ 0,50 & for\ \text{tropical/coastal environment} \end{cases}$$

$$k_5 = \begin{cases} 1 & for\ f'_c \leq 50\,MPa \\ (2,0 - \alpha_3) - 0,02(1,0 - \alpha_3) f'_c & for\ 50\,MPa < f'_c \leq 100\,MPa \end{cases}$$

$$\alpha_3 = \frac{0.7}{k_4 \alpha_2}$$

Figure 12: Creep strain and shrinkage strain according AS3600-2009.

4.2.3. Other design models for the prediction of material properties

This paragraph presented other design models for the prediction of material properties in the design of concrete structures. They are compared in order to show the influence of using different design model on the calculation of concrete creep and shrinkage strain. In particular, six models are considered: Australian standard 3600-2009, Model Code 90, Model Code 2010, Model GL2000, Model B3, Model B4. Figure 16 summarizes the numerical procedure suggest by Model Code 90. Other similar diagrams are reported in the appendix (Figure A1,A2,A3), aimed at explaining the procedures of the other models. The figure 13 showed the variation with the time of the creep coefficient in the cases of all models. The design shrinkage strains are calculated for two different hypothetical thickness: $t_h = \frac{2 \cdot A_c}{u}$ (figure 14) and $t_h = \frac{A_c}{u}$ (figure 15). These curves (figure 13, 14 and 15) are computed using the inputs showed in table 5 and 6.

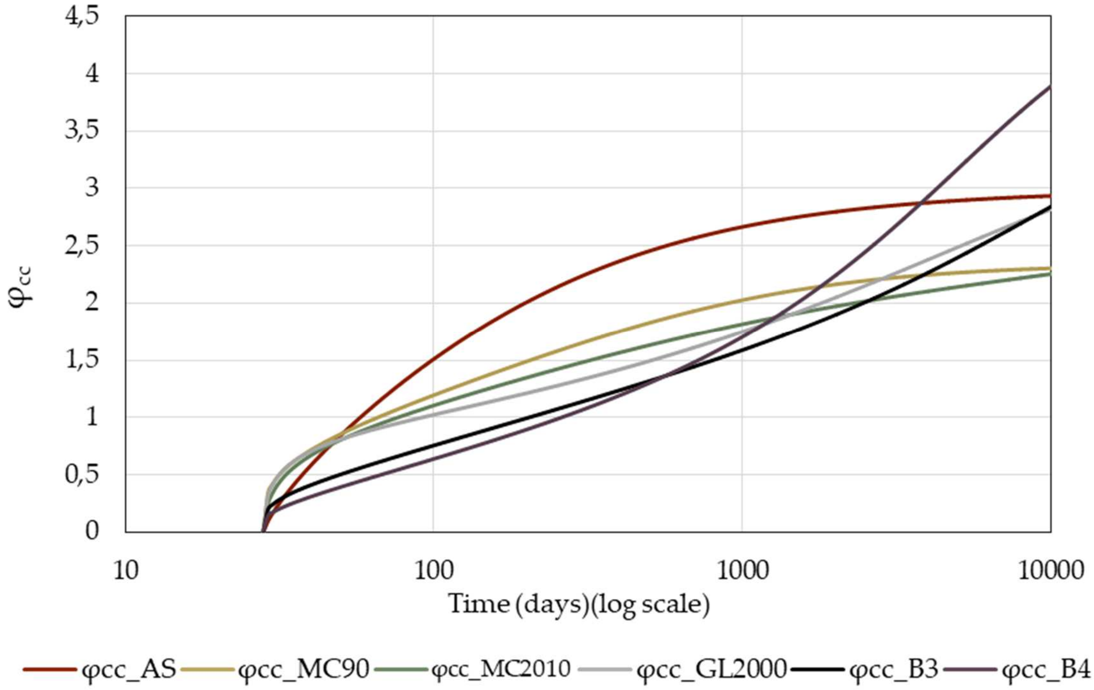

Figure 13: Creep coefficient versus time in the case of different design models.

The figure 13, shows that Model MC 90 and Model MC2010 are far from the results obtained according the Australian code (3), while the results calculated with Model GL2000 and B4 reach and even exc

eed the Australians ones over 30 years. The most relevant difference can be observed for the Model B4; the results obtained with this model are considerably far from the other Models. In the other hand, the model B4 returns the smallest values of design shrinkage strains (figure 14, 15).

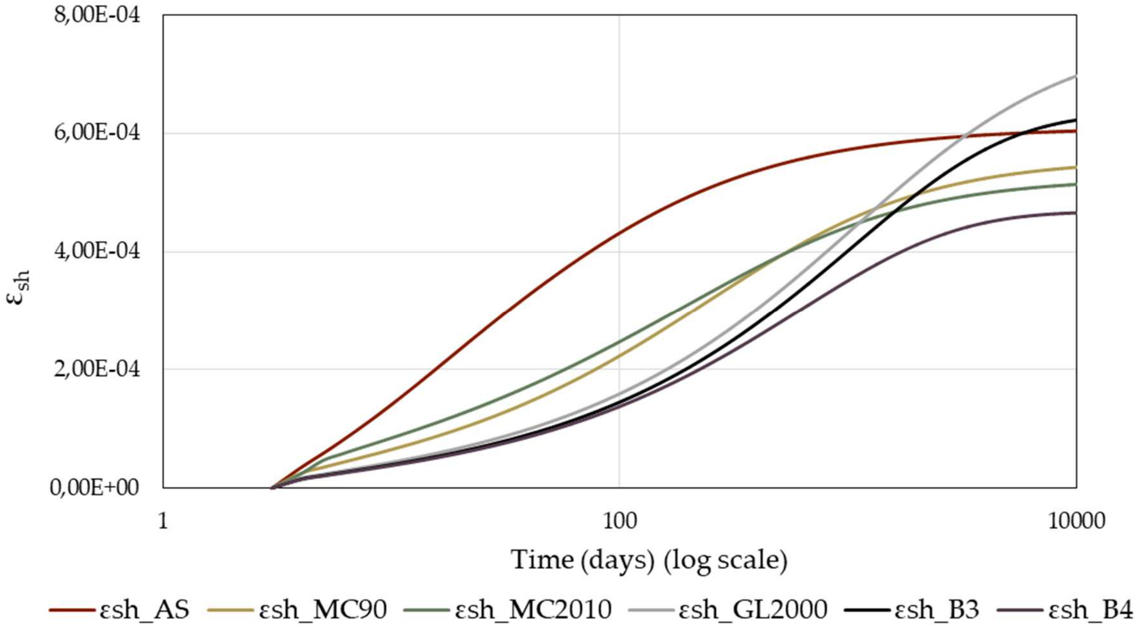

Figure 14: Design shrinkage strain versus time in the case of different design models $\left(t_h = \frac{2 \cdot A_c}{u}\right)$.

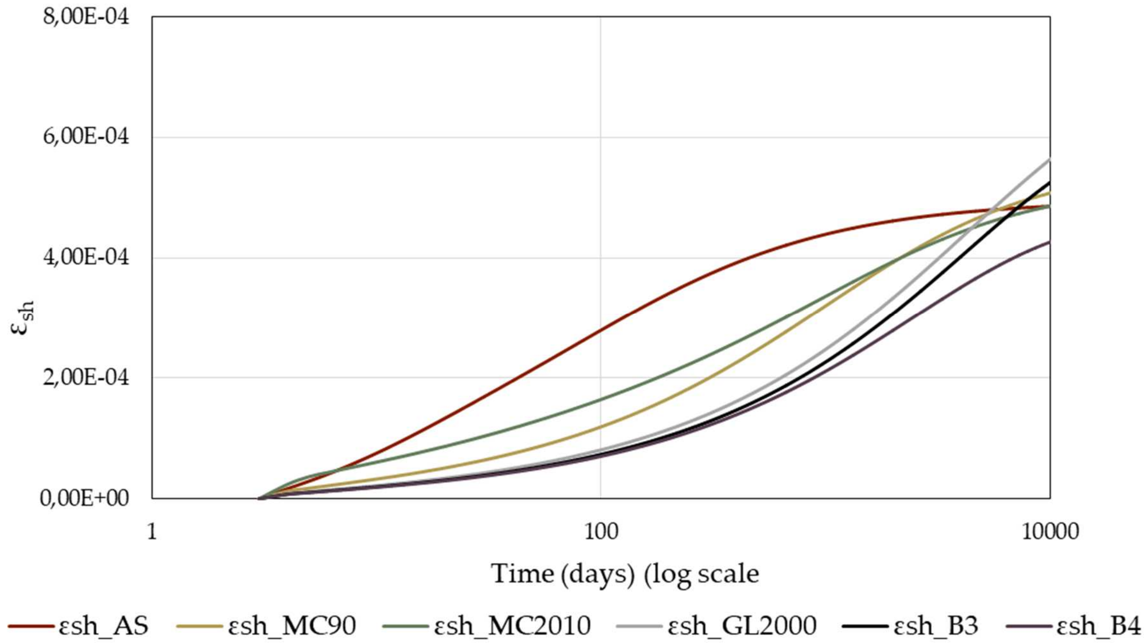

Figure 15: Design shrinkage strain versus time in the case of different design models $\left(t_h = \frac{A_c}{u}\right)$.

Each model has requested different inputs:

Inputs for the prediction of the creep coefficient

AS3600-2009		AS3600-2018		Mcode_90		Mcode_2010		GL2000		B3		B4	
D_c	120	D_c	120	D_c	120	D_c	120	D_c	120	D_c	120	D_c	120
B_c	1000	B_c	1000	B_c	1000	B_c	1000	B_c	1000	B_c	1000	B_c	1000
u	1000	u	1000	u	1000	u	1000	u	1000	u	1000	u	1000
t_0	28	t_0	28	t_0	28	t_0	28	t_0	28	a	1707,8	a	1707,8
t_final	10950	t_final	10950	t_final	10950	t_final	10950	t_final	10950	c	453,0	c	453,0
psi_basic	3,40	psi_basic	3,40	RH_c	50	t_dry	3	t_dry	3	w	172,1	w	172,1
K4	0,65	K4	0,65	fc	32	RH_c	50	RH_c	50	t_0	28	t_0	28
K5	1,00	K5	1,00			fc	32			t_final	10950	t_final	10950
										t_dry	3	t_dry	3
										RH_c	50	RH_c	50
										fc	32	fc	32
												creep parameters	

Table 5: Inputs for the predictions of the creep coefficient in the case of different design models.

Inputs for the prediction of the design shrinkage strain

AS3600-2009		AS3600-2018		Mcode_90		Mcode_2010		GL2000		B3		B4	
D_c	120	D_c	120	D_c	120	D_c	120	D_c	120	D_c	120	D_c	120
B_c	1000	B_c	1000	B_c	1000	B_c	1000	B_c	1000	B_c	1000	B_c	1000
u	1000	u	1000	u	1000	u	1000	u	1000	u	1000	u	1000
t_0	28	t_0	28	t_0	28	t_0	28	t_0	28	t_0	28	t_0	28
t_final	10950	t_final	10950	t_final	10950	t_final	10950	t_final	10950	t_final	10950	t_final	10950
K4	0,65	K4	0,65	RH_c	50	t_dry	3	t_dry	3	t_dry	3	t_dry	3
ε_shd.b*	1E-03	ε_shd.b*	8E-04	fc	32	RH_c	50	RH_c	50	RH_c	50	RH_c	50
				betasc_c	5	fc	32	K_type	1	fc	32	ks	1
						α_bs	800			ks	1,00	k_ta	1
						α_ds1	3					shrinkage parameters	
						α_ds2	0,013						

Table 6: Inputs for the predictions of the design shrinkage strain in the case of different design models.

The creep and shrinkage parameters used for the Model B4 are presented in table 7 and 8, respectively.

Creep parameters-Model B4			
	R	**RS**	**SL**
p1	0,7	0,6	0,8
p2	5,86E-02	1,74E-02	0,0405
p3	3,93E-02	3,93E-02	3,93E-02
p4	3,40E-03	3,40E-03	3,40E-03
p5	7,77E-04	9,46E-05	6,72E-77
p5h	8	1	8
p2w	3	3	3
p3a	-1,1	-1,1	-1,1
p3w	0,4	0,4	0,4
p4a	-0,9	-0,9	-0,9
p4w	2,45	2,45	2,45
p5e	-0,85	-0,85	-0,85
p5a	-1	-1	-1
p5w	0,78	0,78	0,78

Table 7: Creep parameters for Model B4.

Shrinkage Parameters- Model B4			
	R	**RS**	**SL**
τ_cem	0,016	0,08	0,01
p_τ_a	-0,33	-0,33	-0,33
p_τ_w	-0,06	-2,4	3,55
p_τ_c	-0,1	-2,7	3,8
e_cem	3,60E-04	8,60E-04	4,10E-04
p_e_a	-0,8	-0,8	-0,8
p_e_w	1,1	-0,27	1
p_e_c	0,11	0,11	0,11

Table 8: Shrinkage parameters for Model B4

In the chapter 6, the paragraph (6.3.1) presents how the using of different design models on the calculation of concrete creep and shrinkage strain influences the structural behaviour and in particular the structural response in terms of deflection.

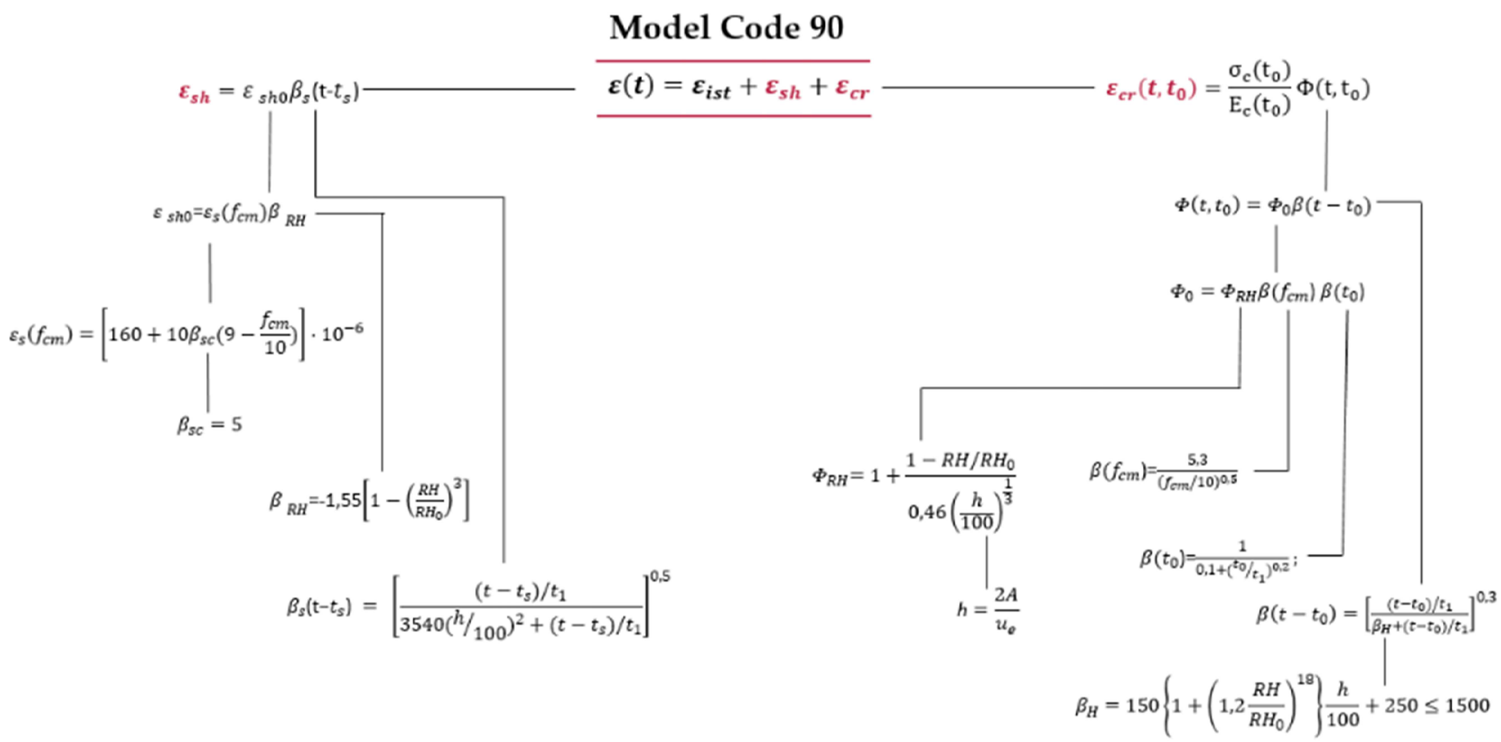

Figure 16: Creep strain and shrinkage strain according Model Code 90

4.2.4. Numerical methods for time-analysis of concrete

4.2.4.1. The effective modulus method (EMM)

Creep effect can be treated as a delayed elastic strain and is can be accounted for by reducing the elastic modulus of concrete with time. The simplest approach aimed at describing this is referred to as Effective Modulus Method and it modifies the concrete modulus by *effective* one,$E_e(t,\tau_0)$, calculated as follows:

$$E_e(t,\tau_0) = \frac{E_c(\tau_0)}{\varphi(t,\tau_0)} \tag{3.17}$$

For concrete subjected to a constant sustained stress, the use of effective modulus allows the rapid determination of creep strain at any time. In fact, the Effective Modulus method not consider stresses variation but assumes a constant sustained stress equal to the final value of the stress history. The total strain at time t can be approximately calculated as:

$$\varepsilon(t) = \frac{1+\varphi(t,\tau_0)}{E_c(\tau_0)}\sigma_c(t) + \varepsilon_{sh}(t) = \frac{\sigma_c(t)}{E_e(t,\tau_0)} + \varepsilon_{sh}(t) \tag{3.18}$$

where $E_e(t,\tau_0)$ is used instead of $E_c(\tau_0)$. The creep strain is independent of the previous stress history but depends only on the current stress in the concrete $\sigma_c(t)$, hence the ageing of the concrete has been ignored. Many times, this simplify assumption is not a limit; in fact this method can give good results for design purpose. Despite it, when the effect of ageing is notable, more sophisticated method is required.

4.2.4.2. The age-adjusted effective modulus method (AEMM)

The age-adjusted effective modulus method developed in 1971 (by Trost), has been recognized during the last few years (by Dilger,Neville and Bazant). It is a practical method to account for creep effects. AEMM can be considered as an improvement of the effective modulus method. The creep strain is now dependent on the stress history exhibited by the concrete. The earlier a concrete specimen is loaded, the grater the final creep strain. This is due to ageing (9). The creep strains can be calculated using an ageing coefficient $\chi(t,\tau_0)$ (<1.0) that reduces the creep coefficient $\varphi(t,\tau_0)$.

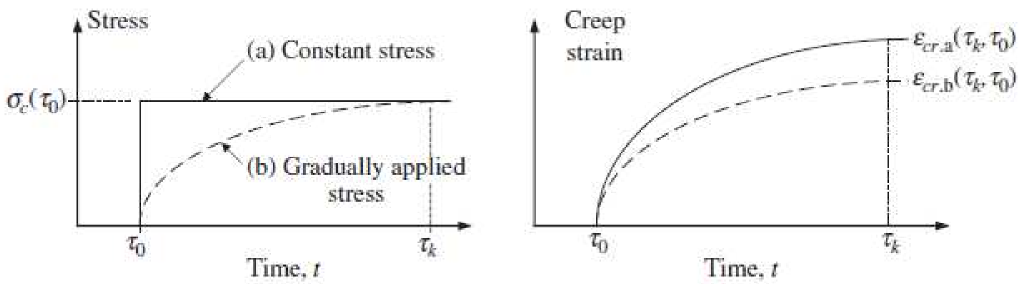

Figure 17: Creep due to constant and variable stress histories (9)

If the stress is gradually applied over the time ($t-\tau_0$) the creep strain at time t may be expressed as:

$$\varepsilon_{cr}(t) = \frac{\sigma_c(t)}{E_c(\tau_0)}\chi(t,\tau_0)\varphi(t,\tau_0) \tag{3.19}$$

where:

$\chi(t,\tau_0) \cong 0.1 \div 0.4$

According AEMM, the overall strain at time t may be expresses as follows:

$$\varepsilon(t) = \frac{\sigma_c(\tau_0)}{E_c(\tau_0)}[1+\varphi(t,\tau_0)] + \frac{\Delta\sigma_c(t)}{E_c(\tau_0)}[1+\chi(t,\tau_0)\varphi(t,\tau_1)] + \varepsilon_{sh}(t)$$

$$= \frac{\sigma_c(\tau_0)}{E_c(t,\tau_0)} + \frac{\sigma_c(t)-\sigma_c(\tau_0)}{\bar{E}_c(t,\tau_0)} + \varepsilon_{sh}(t) \tag{3.20}$$

in which:

$E_c(t,\tau_0)$ is the effective modulus and the age-adjusted effective modulus is determined as:

$$\bar{E}_c(t,\tau_0) = \frac{E_c(\tau_0)}{[1+\chi(t,\tau_0)\varphi(t,\tau_0)]} \tag{3.21}$$

Rearranging the Eq. (3.23), the final stress $\sigma_c(t)$ may be obtained by:

$$\sigma_c(t) = \bar{E}_c(t,\tau_0)[\varepsilon(t) - \varepsilon_{sh}(t)] + \sigma_c(\tau_0)\overline{F_{e,0}} \tag{3.22}$$

where $\overline{F_{e,0}}$ is the age-adjusted creep factor and is given by:

$$\overline{F_{e,0}} = \varphi(t,\tau_0)\frac{[\chi(t,\tau_0)-1]}{[1+\chi(t,\tau_0)\varphi(t,\tau_0)]} \tag{3.23}$$

4.3. Steel

In the service behaviour of composite structures, the steel material properties are assumed to remain linear-elastic. This is acceptable because, at service conditions, the stress in the non –prestressed steel is usually less than the yield stress, f_y, and so the strain-stress curve can be considered linear ignoring plastic and nonlinear effects. In this elastic range the steel stress, σ_s, is proportional to the steel strain ε_s:

$$\sigma_s = E_s \varepsilon_s \tag{3.24}$$

where E_s is the elastic modulus of steel.

The stress-strain curve in compression is also assumed to be linear-elastic similar to that in tension.

At service condition, the non-prestressed steel reinforcement can be useful to reduce both instantaneous and time-dependent deformations and they also provide crack control. The design for serviceability is associated with the determination of suitable types and quantities of reinforcement in order to control cracking or deformation.

Time-dependent analysis of composite slabs

5.1.Introduction

For the time-dependent analysis of the composite slabs, the determination of strains, stresses and deflections is required at different instants in times during the life of the structures. Cross-sectional analysis is used under the assumption of Euler-Bernoulli beam theory (cross-sections initially perpendicular to the neutral axis remain perpendicular before and after deformation), that implies a linear strain profile for each cross-section. Compatibility of strains is also assumed, such that there is no slip between the steel sheeting and the concrete. These assumptions allow to express the linear strain profile in terms of strain value at a reference axis ε_r and curvature κ at each cross-section. Equilibrium and constitutive equations are also utilized in solving for these unknown values, and these are briefly outlined below.

Horizontal equilibrium:

$$N_e = N_i = \int \sigma \, dA \tag{4.1}$$

Rotational equilibrium:

$$M_i = M_e = \int y\sigma \, dA \tag{4.2}$$

where subscripts 'i' and 'e' depict the internal (axial force/moment) and external (axial force/moment) respectively.

Once the unknowns are calculated, it is possible to calculate the strains at any depth y given by:

$$\varepsilon_0 = \varepsilon_{r,0} - y\kappa_0 \tag{4.3}$$

For the instantaneous calculations, the concrete and steel materials can be described by the following constitutive relationships:

$$\sigma_{c,0} = E_{c,0}\varepsilon_0 \tag{4.4}$$

$$\sigma_s = E_s\varepsilon_s \tag{4.5}$$

The cross-sectional analysis is used to calculate the deformations at the cross-section that, if integrated over the member length, can provide information on the member response.

The knowledge of the variation values of strains, stresses, and deflections over time allows an accurate prediction of the structure behaviour during its life.

5.2.Short-term Analysis

This section presents a numerical formulation of cross sectional behavior at the age of first loading, not considering any time-dependent effects. The short-term analysis allows the calculation of the material stresses and member deflections at time τ_0 by considering the linearity hypothesis (concrete and non-prestressed reinforcement work in linear-elastic range). At time τ_0 (instant immediately after the first loading), byapplying axial and rotational equilibrium at the cross-section (Eq. 4.1, 4.2), the unknowns of the problem can be calculated. Once calculated the geometric property of the concrete part of the cross-section A_c, B_c and I_c (area, first moment of area end second moment of area, respectively) and the geometric property of each reinforcing bars $A_{s,i}$ (areas of ith layer of non-prestessed steel) using the equations 4.1, 4.3, 4.4 and 4.5 the internal axial force $N_{i,0}$ is given by:

$$N_{i,0} = \int \sigma_{c,0}\, dA + \sum_{i=1}^{n} \left(A_{s(i)} E_{s(i)}\right) E_{s,0} \varepsilon_0$$

$$= \int E_{c,0}(\varepsilon_{r,0} - y\kappa_0)\, dA + \sum_{i=1}^{n} \left(A_{s(i)} E_{s(i)}\right) \varepsilon_{r,0} - \sum_{i=1}^{n} \left(y_{s(i)} A_{s(i)} E_{s(i)}\right) \kappa_0$$

$$= A_c E_{c,0} \varepsilon_{r,0} - B_c E_{c,0} \kappa_0 + \textstyle\sum_{i=1}^{n} \left(A_{s(i)} E_{s(i)}\right) \varepsilon_{r,0} - \textstyle\sum_{i=1}^{n} \left(y_{s(i)} A_{s(i)} E_{s(i)}\right) \kappa_0$$

$$= \left(A_c E_{c,0} + \sum_{i=1}^{n} \left(A_{s(i)} E_{s(i)}\right)\right) \varepsilon_{r,0} - \left(B_c E_{c,0} + \sum_{i=1}^{n} \left(y_{s(i)} A_{s(i)} E_{s(i)}\right)\right) \kappa_0$$

$$= R_{A,0} \varepsilon_{r,0} - R_{B,0} \kappa_0 \tag{4.6}$$

In the same place, using the equations 4.2 the moment resisted is given by:

$$M_{i,0} = -\left(B_c E_{c,0} + \sum_{i=1}^{n} \left(y_{s(i)} A_{s(i)} E_{s(i)}\right)\right) \varepsilon_{r,0} + \left(I_c E_{c,0} + \sum_{i=1}^{n} \left({y_{s(i)}}^2 A_{s(i)} E_{s(i)}\right)\right) \kappa_0$$

$$= -R_{B,0} \varepsilon_{r,0} + R_{I,0} \kappa_0 \tag{4.7}$$

where $R_{A,0}$, $R_{B,0}$ and $R_{I,0}$ represent the cross-sectional rigidities calculated at time τ_0 using a reference axis (axial rigidity, stiffness related to first moment of area, flexural rigidity).

$$R_{A,0} = A_c E_{c,0} + \textstyle\sum_{i=1}^{n} \left(A_{s(i)} E_{s(i)}\right) \tag{4.8}$$

$$R_{B,0} = B_c E_{c,0} + \textstyle\sum_{i=1}^{n} \left(y_{s(i)} A_{s(i)} E_{s(i)}\right) \tag{4.9}$$

$$R_{I,0} = I_c E_{c,0} + \sum_{i=1}^{n} \left({y_{s(i)}}^2 A_{s(i)} E_{s(i)}\right) \tag{4.10}$$

Rewriting the system equations in compact form, the external axial forces and moments resisted can be calculated using:

$$r_{e,0} = D_0 \varepsilon_0 \tag{4.11}$$

The first term $r_{e,0}$ is a vector holding information regarding the external actions imposed on the system at first loading:

$$r_{e,0} = \begin{bmatrix} N_{i,0} \\ M_{i,0} \end{bmatrix} \tag{4.12}$$

The matrix D_0 contains information regarding the cross section proprieties, for instance axial rigidity, flexural rigidity and stiffness relates to the first moment of area.

$$D_0 = \begin{bmatrix} R_{A,0} & -R_{B,0} \\ -R_{B,0} & R_{I,0} \end{bmatrix} \tag{4.13}$$

The term ε_0 is referred to as the strain vector, containing the unknown variables describing the strain distribution through a cross-section.

$$\varepsilon_0 = \begin{bmatrix} \varepsilon_{r,0} \\ \kappa_0 \end{bmatrix} \tag{4.14}$$

The vector ε_0 contain the unknowns of the problems and it is simply obtained with:

$$\varepsilon_0 = D_0^{-1}(r_{e,0}) = F_0(r_{e,0}) \tag{4.15}$$

Where:

$$F_0 = \frac{1}{R_{A,0}R_{I,0} - R_{B,0}^2}\begin{bmatrix} R_{I,0} & R_{B,0} \\ R_{B,0} & R_{I,0} \end{bmatrix} \tag{4.16}$$

By using the constitutive equations 4.4 and 4.5 the stress distribution is readily obtained as follow:

$$\sigma_{c,0} = E_{c,0}\varepsilon_0 = E_{c,0}[1 \quad -y]\varepsilon_0 \tag{4.17}$$

$$\sigma_{s,0} = E_{s,0}\varepsilon_0 = E_{s,0}[1 \quad -y_{s(i)}]\varepsilon_0 \tag{4.18}$$

5.3. Long-term analysis using the age-adjusted affective modulus method

Cross-sectional analysis using the age-adjusted affective modulus method provides a good prediction of the stress and strains variation over time. It allows analyzing the creep and shrinkage effects, and how these develop in the concrete during the time. It is assumed that the time-dependent behavior of concrete is identical in both compression and tension for stress levels in compression less than about one half of the compressive strength of the concrete, and for tensile stresses less that about one half of tensile strength of the concrete (9). The instantaneous analysis defined the basic for a cross-section analysis by establishing the relevant governing equation and principles of the problem. The matrix manipulation of derived equations that followed produces an explicit solution for the strain and curvature at given cross section. In the same way, equilibrium and constitutive equations are required. The long-term analysis introduce also terms associates with time-dependent effects; namely creep and shrinkage. As before, at time $t = t_k$ (general instant at which stresses and deformations are sought), applying axial and rotational equilibrium (Eq. 4.1, 4.2) at the cross-section the external axial forces and moments resisted by the cross-section can be calculated as follow:

$$N_{i,k} = \int \sigma_{c,0}\, dA + \sum_{i=1}^{n} \left(A_{s(i)} E_{s(i)}\right) \varepsilon_k$$

$$= \int \left[\overline{E_{e,k}} \left(\varepsilon_{r,k} - y\kappa_k \; - \left(\varepsilon_{r,sh} - y\kappa_{sh} \right) \right) + \overline{F_{e,0}} \sigma_{c,0} \right] dA +$$

$$+ \sum_{i=1}^{n} \left(A_{s(i)} E_{s(i)}\right) \varepsilon_{r,k} - \sum_{i=1}^{n} \left(y_{s(i)} A_{s(i)} E_{s(i)}\right) \kappa_k$$

$$= A_c \overline{E_{e,k}} \varepsilon_{r,k} - B_c \overline{E_{e,k}} \kappa_k - A_c \overline{E_{e,k}} \varepsilon_{r,sh} + B_c \overline{E_{e,k}} \kappa_{sh} + \overline{F_{e,0}} N_{c,0} +$$

$$+ \sum_{i=1}^{n} A_{s(i)} E_{s(i)} \varepsilon_{r,k} - \sum_{i=1}^{n} y_{s(i)} A_{s(i)} E_{s(i)} \kappa_k$$

$$= R_{A,0} \varepsilon_{r,k} - R_{B,0} \kappa_k - A_c \overline{E_{e,k}} \varepsilon_{r,sh} + B_c \overline{E_{e,k}} \kappa_{sh} + \overline{F_{e,0}} N_{c,0} \qquad (4.19)$$

and:

$$M_{i,k} = -\left(B_c \overline{E_{e,k}} + \sum_{i=1}^{n} \left(y_{s(i)} A_{s(i)} E_{s(i)} \right) \right) \varepsilon_{r,k} +$$

$$+ \left(I_c \overline{E_{e,k}} + \textstyle\sum_{i=1}^{n} \left({y_{s(i)}}^2 A_{s(i)} E_{s(i)} \right) \right) + B_c \overline{E_{e,k}} \varepsilon_{r,sh} - I_c \overline{E_{e,k}} \kappa_{sh} + \overline{F_{e,0}} M_{c,0} =$$

$$= -R_{B,k} \varepsilon_{r,k} + R_{I,k} \kappa_k + B_c \overline{E_{e,k}} \varepsilon_{r,sh} - I_c \overline{E_{e,k}} \kappa_{sh} + \overline{F_{e,0}} M_{c,0} \qquad (4.20)$$

where:

$R_{A,k}$, $R_{B,k}$ and $R_{I,k}$ represent the cross-sectional rigidities calculated at time t_k using a reference axis.

$$R_{A,k} = A_c \overline{E_{e,k}} + \sum_{i=1}^{n} \left(A_{s(i)} E_{s(i)}\right) \tag{4.21}$$

$$R_{B,k} = B_c \overline{E_{e,k}} + \sum_{i=1}^{n} \left(y_{s(i)} A_{s(i)} E_{s(i)}\right) \tag{4.22}$$

$$R_{I,k} = I_c \overline{E_{e,k}} + \sum_{i=1}^{n} \left({y_{s(i)}}^2 A_{s(i)} E_{s(i)}\right) \tag{4.23}$$

and the constitutive equations are modified as below:

$$\sigma_{c,k} = \overline{E_{e,k}}\left(\varepsilon_k - \varepsilon_{sh,k}\right) + \overline{F_{e,0}} \sigma_{c,0} \tag{4.24}$$

$$\sigma_{s,k} = E_{s,k} \varepsilon_k \tag{4.25}$$

with:

$$\varepsilon_k = \varepsilon_{r,k} - y\kappa_k \tag{4.26}$$

$$\varepsilon_{sh,k} = \varepsilon_{r,sh} - y\kappa_{sh} \tag{4.27}$$

The subscrip "r" depict the reference axis and so $\varepsilon_{r,k}$ and $\varepsilon_{r,sh}$ represent the long-term strain and the shrinkage strain at the level of the arbitrary reference axis, respectively.

Rewriting the system equations in compact form the external axial forces and moments resisted can be calculated using:

$$r_{e,k} = D_k \varepsilon_k + f_{cr,k} - f_{sh,k} \tag{4.28}$$

The following revised formulation includes the extra terms accounting for time-dependent concrete response.

The first term $f_{cr,k}$ describes the creep effect produced by a sustained stress $\sigma_{c,0}$. The terms $N_{c,0}$ and $M_{c,0}$ represent the axial force resisted by the concrete at time τ_0 and the flexural moment resisted by the concrete at time τ_0, respectively.

$$f_{cr,k} = \overline{F_{e,0}} \begin{bmatrix} N_{c,0} \\ M_{c,0} \end{bmatrix} = \overline{F_{e,0}} E_{c.0} \begin{bmatrix} A_c \varepsilon_{r,0} - B_c \kappa_0 \\ -B_c \varepsilon_{r,0} + I_c \kappa_0 \end{bmatrix} N_{c,0} \tag{4.29}$$

The vector $f_{sh,k}$ describes the shrinkage effect due the shrinkage strain that acts in the concrete over time.

$$f_{sh,k} = \overline{E_{e,k}} \begin{bmatrix} A_c & -B_c \\ -B_c & +I_c \end{bmatrix} \begin{bmatrix} \varepsilon_{r,sh} \\ \kappa_{sh} \end{bmatrix} \tag{4.30}$$

This vector allows including the shrinkage gradient in the calculation of shrinkage strain.

The vector ε_k contain the unknowns of the problems and it is simply obtained with:

$$\varepsilon_k = D_0^{-1}(r_{e,0} - f_{cr,k} + f_{sh,k}) = F_0(r_{e,0} - f_{cr,k} + f_{sh,k}) \tag{4.31}$$

where:

$$F_k = \frac{1}{R_{A,k} R_{I,k} - R_{B,k}^2} \begin{bmatrix} R_{I,k} & R_{B,k} \\ R_{B,k} & R_{I,k} \end{bmatrix} \tag{4.32}$$

At the end using the constitutive equations 4.24 and 4.25 the stress distribution is readily obtained as follow:

$$\sigma_{c,k} = \overline{E_{e,k}}(\varepsilon_k - \varepsilon_{sh,k}) + \overline{F_{e,0}}\sigma_{c,0} = \overline{E_{e,k}}\{[1 \quad -y]\varepsilon_k - \varepsilon_{sh,k}\} + \overline{F_{e,0}}\sigma_{c,0} \tag{4.33}$$

$$\sigma_{s,k} = E_{s,k}\varepsilon_k = E_{s,k}[1 \quad -y_{s(i)}]\,\varepsilon_k \tag{4.34}$$

It is noteworthy that some forces arise inside the concrete due to creep and shrinkage during the time. In general, creep and shrinkage cause a contraction of the concrete and so there is an increase in the compressive stress in the reinforcements. To maintain the equilibrium the steel reinforcements react with an equal and opposite actions generating tensile stress in the concrete.

5.4.Member Deflections

If the axial strain and curvature are known at regular intervals along a member, it is possible to determine the deformation of that member. According to the Euler-Bernoulli beam theory, the member deflection at any point z along the span may be calculated by double integration of the curvature.

$$v = \iint k(z)dz \tag{4.35}$$

where z is the axis along the member length.

By considering the member subjected to the axial and transverse loads shown in Fig. 14, the deflection at mid-span v_C may be calculated as follow:

$$v_c = \frac{l^2}{96}\,(\kappa_A + 10\kappa_C + \kappa_B) \tag{4.36}$$

where κ_A , κ_C and κ_B are the values of curvature at the supports A and B and at point C (i.e. at the mid-span).

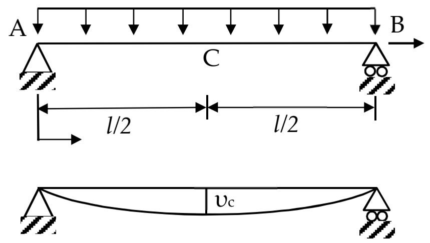

Figure 18: Mid- span deflection of a single span

Serviceability limit state design

6.1.Introduction

This chapter describes the service design procedure recommended for composite steel-concrete slabs by two different international guidelines, i.e. Australian (1) and European (2) code. The first part of the chapter focuses on the deflection calculation at serviceability limit state and it presents both Australian and European procedures. At the end, the results obtained with the two codes are compered and discussed.

6.2.Australian Standard 2327-2017

Australian Standard 2327-2017 suggests refine and simplified calculation to determinate the deflection of composite slab at serviceability limit state conditions.

6.2.1. Slab deflection by refined calculation

The calculation of the deflection by refined calculation (in accordance with the Clause 2.8.2) shall take into account of the following:

- Cracking and tension-stiffening of the concrete.
- Shrinkage and creep properties of the concrete accounting for the presence of the steel sheeting.
- Expected construction procedure.
- Deflection of formwork or settlement of props during construction (particulary when the slab formwork is supported on suspended floors or beams below).
- Relaxation of prestressing strands in post-tensioning composite slabs.

- For slabwith steel sheeting profiles that exhibit slip at service conditions, account shall be taken for the partial interaction behaviour between the steel and the concrete slab in the refined calculation.

6.2.2. Slab deflection by simplified calculation

The calculation of the deflection by simplified calculation shall be applied when the effects of end slip are deemed to insignificant.

This simplified approach consists in a new design model for deflection calculation of composite slabs. It allows deflection predictions by considering a non-uniform shrinkage gradient. The latter is due to the presence of the steel sheeting that prevents moisture egress to occur from the underside of the slab.

According the assumption that the phenomena of creep and shrinkage can be treated independently from each other (as already introduced in the chapter 3); the approach calculates the total deflection of composite slab δ as the sum of three components: the instantaneous deflection δ_0 and the deflection components produced by creep δ_{cc} and shrinkage effects δ_{cs} as follows:

$$\delta = \delta_0 + \delta_{cc} + \delta_{cs} \tag{5.1}$$

6.2.2.1. Instantaneous deflection

The instantaneous deflection δ_0 occurs immediately after the application of the stress. It can be determined under the assumptions of Euler- Bernoulli beam theory. According the kinematic assumption of this theory (the cross-section is infinitely rigid in its own plane, the cross-section of a beam remains plane before and after deformation and the cross section remains normal to the deformed axis of the beam) the relationship of the elastic line is applicable:

$$\frac{\partial^4 w}{\partial x^4} = -\frac{q}{EI} \tag{5.2}$$

In which the differential equation of the fourth order can be easily integrated. Considering a simply-supported slab of length L subjected to a uniformly distributed load q_0, by integration, the mid span instantaneous deflection δ_0 can be calculate thought the well-kwon expression:

$$\delta_0 = \frac{5}{384}\frac{q_0 L^4}{E_C I_{ef}} \tag{5.3}$$

where the instantaneous flexural rigidity $E_c I_{ef}$ is calculated using the mean value of the elastic modulus of concrete at time of first loading and the effective second moment of area of the span. I_{ef}. It involves an empirical adjustment of second moment of area of the cross section to account for tension stiffening. Tension stiffening is a measure of the concrete, which is active in resisting tensile forces generated structural member due to the presence of the steel reinforcement and it is present in regions between primary cracks. It contributes considerably to the member's stiffness after cracking and hence it influences the deflection of the member. For a simply-supported slab, the value I_{ef} is calculated at mid-span adopting the formula:

$$I_{ef} = I_{cr} + (I_{uncr} - I_{cr})({}^{M_{cr}}/_{M_s})^3 \tag{5.4}$$

In which M_s is the maximum bending moment at section; M_{cr} is the cracking moment; I_{uncr} and I_{cr} are the second moment of area of uncracked and cracked sections respectively. I_{ef} is referred to the centroid of the section.

The uncracked and cracked second moment of area can be obtained (respect to its centroid axis) from their cross-sectional rigidities (with respect to an arbitrary reference axis) as follows:

$$I_{uncr} = \frac{R_I R_A - R_B^2}{R_A E_C} \tag{5.5}$$

$$I_{cr} = \frac{R_{I,cr} R_{A,cr} - R_{B,cr}^2}{R_{A,cr} E_C} \tag{5.6}$$

where $R_{A,}$ R_B and R_I are the uncracked cross-sectional rigidities:

Axial rigidity:

$$R_A = A_C E_C + A_{ss} E_{ss} + \sum A_s E_s \tag{5.7}$$

Stiffness related to the first moment of area:

$$R_B = B_C E_C + B_{ss} E_{ss} + \sum y_s A_s E_s \tag{5.8}$$

Flexural rigidity:

$$R_I = I_C E_C + I_{ss} E_{ss} + \sum y_s^2 A_s E_s \tag{5.9}$$

A, B and I are obtained respect to an arbitrary reference axis and represent the geometric area, first moment of the area (B) and second moment of the area, respectively. These geometric properties are calculated for the concrete component "c", the steel sheeting "ss" and steel reinforcement "s". In the same way it is possible obtain the cracked cross-sectional rigidities $R_{Acr,}$ $R_{B,cr}$ and

$R_{I.cr}$ ignoring the contribution of the concrete in tension. In this case, the calculation of the geometric properties of the concrete part of the cross section is carried out by determining the position of the neutral axis on the cracked cross-section $y_{n,0}$. The location of the neutral axis $y_{n,0}$ (for a reinforced concrete rectangular section loaded in pure bending) can be evaluated not consider tension resistance for concrete and equalling to zero the axial forces.

$$N_{e,0} = N_{i,0} = 0 \tag{5.10}$$

$$N_{i,0} = \int_{A_c} E_{c,0}(\varepsilon_{r,0} + y\kappa_{r,0})dA + R_{A,s}\varepsilon_{r,0} + R_{B,s}\kappa_0 = 0 \tag{5.11}$$

Dividing each terms by $\kappa_{r,0}$ and recognizing that $y_{r,0} = {}^{-\varepsilon_{r,0}}/_{\kappa_0}$, Equation (5.11) becomes a quadratic equation, which can be solved to calculate the location of the neutral axis.

In this procedure, the use of an arbitrary reference system allows to calculate the geometric properties only once. These values for the evaluation of the cross-sectional rigidities can be used in the instantaneous, creep and shrinkage deflection predictions, respectively.

The cracking moment is bending moment when cracking occurs. It is possible calculate M_{cr} as the moment at which the tensile stress in the bottom fiber of the concrete equals the stress level required for the concrete to crack.

$$M_{\mathrm{cr}} = \frac{1}{E_c\left[\frac{R_B}{R_0} - y\left(\frac{R_B}{R_0}\right)\right]}\left[f'_{ct,f} - \sigma_{cs}\right] \tag{5.12}$$

where the term $[f'_{ct,f} - \sigma_{cs}]$ represents the stress level to the extreme fibre at which cracking happens.

$f'_{ct,f}$ is the characteristic flexural tensile strength of concrete (modulus of rupture) and it represents the maximum stress that the concrete can withstand.

$$f'_{ct,f} = 0.6\sqrt{f'_c} \tag{5.13}$$

and:

f'_c is the characteristic strength of concrete in compression.

In order to take into consideration the shrinkage gradient caused by the presence of the steel sheeting, the modulus of rupture is reduced by the quantity σ_{cs} (maximum shrinkage-induced tensile stress on the uncracked section at the extreme fibre at which cracking occurs). This term is introduced into the cracking moment equation to allow for the reduction of cracking moment produced by shrinkage effects. Shrinkage reduces member stiffness and it gradually reduces the beneficial effects of tension stiffening. The value of σ_{cs} can be obtained from sectional analysing (respect to arbitrary reference axis on the cross-section) as follows:

$$\sigma_{cs} = \frac{E_{ef,cs}}{R_{I,cs}R_{A,cs} - R_{B,cs}^2}\left[\left(R_{I,cs} - yR_{B,cs}\right)f_{cs1} + +\left(R_{B,cs} - yR_{A,cs}\right)f_{cs2}\right] -$$

$$+E_{ef,cs}(\varepsilon_{r,cs} - y\kappa_{cs}) \tag{5.14}$$

where:

$\boldsymbol{E_{ef,cs}} = \frac{E_c}{1+0.5\varphi_{cc}}$ is the effective concrete elastic modulus.

$\boldsymbol{\varphi_{cc}}$= creep coefficient for concrete calculate at time *t* for a load applied at time t_0 determined in accordance with the paragraph 3.2.1.1.

$\boldsymbol{R_{A,cs}}$, $\boldsymbol{R_{B,cs}}$ and $\boldsymbol{R_{I,cs}}$ = the cross-sectional rigidities computed with $E_{ef,cs}$ as elastic modulus.

$\boldsymbol{\varepsilon_{r,cs}}$ and $\boldsymbol{\kappa_{cs}}$ = the shrinkage strain at the level of the arbitrary reference axis and the shrinkage curvature, respectively.

These terms represent the introduction of the shrinkage gradient in the design model. They are calculated as function of the reference shrinkage strain ε_{cs} (in accordance with the paragraph 3.2.2.1) by assuming both side of the slab to be exposed (uniform shrinkage distribution) and by considering an hypothetical thickness equal to the thickness of the composite slab. Experimental data (e.g. Al-Deen and Ranzi 2015; Al-Deen et al. 2011) has indicated that the shrinkage gradient could vary from a value of 0.2 ε_{cs} at the base of the slab to 1.2 ε_{cs} at the top surface of the slab; assuming valid this simplification by proportion in triangles, shrinkage strain at the level of the arbitrary reference axis can be calculated.

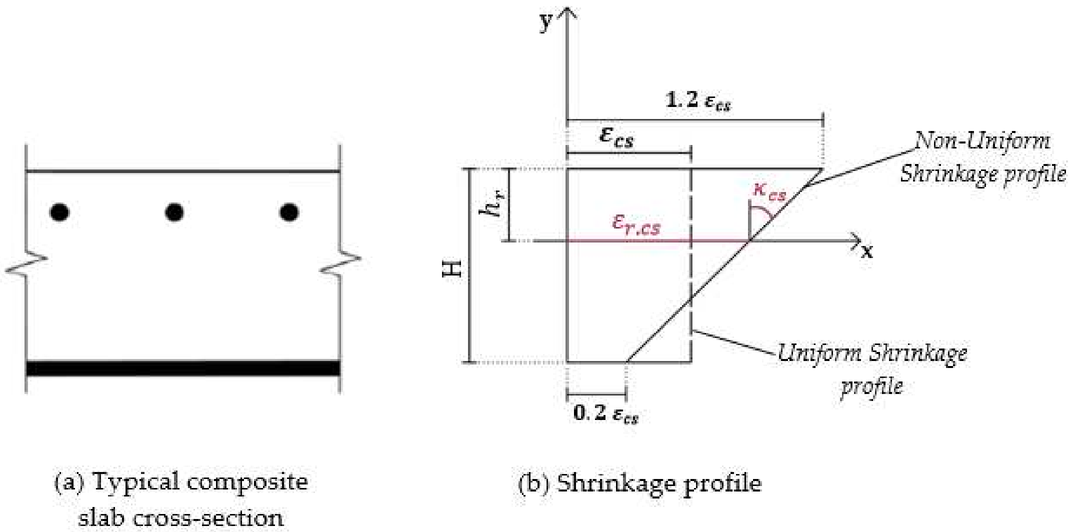

Figure 19: Strain variables describing non-uniform free shrinkage on composite slab

The terms f_{cs1} f_{cs2} are the equivalent loads for shrinkage and are computed as follows:

$$\begin{bmatrix} f_{cs1} \\ f_{cs2} \end{bmatrix} = E_{ef,cs} \begin{bmatrix} A_c \boldsymbol{\varepsilon_{r,cs}} - B_c \kappa_{cs} \\ -B_c \boldsymbol{\varepsilon_{r,cs}} + I_c \kappa_{cs} \end{bmatrix} \tag{5.15}$$

6.2.2.2. Creep deflection

The deflection component produced by creep, δ_{cc} , is evaluated using the creep multiplier α_{cc} according the age-adjusted effective modulus Method (AEMM).

$$\alpha_{cc} = \frac{E_c I_{ef}}{E_{ef,cc} I_{ef,cc}} - 1 \tag{5.16}$$

In order to obtain the deflection component produced by creep, the sustained part of the instantaneous deflection is multiplied by the creep multiplier as follows:

$$\delta_{cc} = \delta_{0,sus}\alpha_{cc} = (\frac{q_{0,sus}}{q_0}\delta_0)\alpha_{cc} \tag{5.17}$$

where:

$E_{ef,cc} = E_c/(1+\varphi_{cc})$ is the effective modulus of the concrete.

and:

$I_{ef,cc}$ is the second moment of area calculated with the concrete effective modulus $E_{ef,cc}$.

6.2.2.3. Shrinkage deflection

The shrinkage deflection δ_{cs} can be evaluated applying on the composite slab an induced curvature κ_{cs} . In the case of a simply-supported member, the deflection is calculated as follows:

$$\delta_{cs} = \frac{\kappa_{cs} L^2}{8} \tag{5.18}$$

$$\kappa_{cs} = (1-\gamma_{cs})\kappa_{cs,cr} + \gamma_{cs}\kappa_{cs,uncr} \tag{5.19}$$

where $\kappa_{cs,uncr}$ and $\kappa_{cs,cr}$ represent the curvatures caused by shrinkage over the uncracked and craked section of the composite slab. Under the simplifying hypothesis of a linear shrinkage profile and recognizing that $\varepsilon_{r,cs}$ and κ_{cs} are the shrinkage strain and the shrinkage curvature at the level of the arbitrary reference axis, respectively. The shrinkage curvatures can be determined with the following expressions:

$$\kappa_{cs,uncr} = \begin{bmatrix} \frac{R_{B,cs,uncr}}{R_{0,cs,uncr}} & \frac{R_{A,cs,uncr}}{R_{0,cs,uncr}} \end{bmatrix} E_{ef,cs} \begin{bmatrix} A_{c,uncr}\varepsilon_{r,cs} - B_{c,uncr}\kappa_{cs} \\ -B_{c,uncr}\varepsilon_{cs} + I_{c,uncr}\kappa_{cs} \end{bmatrix} \tag{5.20}$$

$$\kappa_{cs,cr} = \begin{bmatrix} \frac{R_{B,cs,cr}}{R_{0,cs,cr}} & \frac{R_{A,cs,cr}}{R_{0,cs,cr}} \end{bmatrix} E_{ef,cs} \begin{bmatrix} A_{c,cr}\varepsilon_{r,cs} - B_{c,cr}\kappa_{cs} \\ -B_{c,cr}\varepsilon_{cs} + I_{c,cr}\kappa_{cs} \end{bmatrix} \tag{5.21}$$

6.3.Eurocode 1994

Eurocode 4 suggests that the deflections of composite members at service conditions should be calculated using an elastic analysis (in accordance with the clause 5.4.3 (2)) and neglecting the effects of shrinkage. Moreover, it permits many other simplifications under particular conditions listed below.

- The calculation of deflection may be omitted if following conditions are satisfied:

1. The span/depth ratio of the slab should not exceed the limits give in EN 1992-1-1 (7.4):

$$\frac{l}{d} = K\left[11 + 1{,}5\sqrt{f_{ck}}\frac{\rho_0}{\rho} + 3{,}2\sqrt{f_{ck}}\left(\frac{\rho_0}{\rho} - 1\right)^{\frac{3}{2}}\right] \qquad se\ \rho \leq \rho_0 \qquad (5.22)$$

$$\frac{l}{d} = K\left[11 + 1{,}5\sqrt{f_{ck}}\frac{\rho_0}{\rho - \rho'} + \frac{1}{12}\sqrt{f_{ck}}\sqrt{\frac{\rho'}{\rho_0}}\right] \qquad se\ \rho > \rho_0 \qquad (5.23)$$

2. For external spans, no account need be taken of end slip if the initial slip load in tests (defined as the load causing an end slip of 0,5 mm) exceeds 1,2 times the design service load.

- For an internal span of a continuous slab the deflection may be determined using the following approximations:

1. The second moment of area may be taken as the average of the values for the cracked and un-cracked section;

$$I_{ef} = mean\ (I_{cr}; I_{uncr}) \tag{5.24}$$

2. For concrete, an average value of the modular ratio for both long- and short-term effects may be used.

6.4.Comparison between Australian Standards 2327-2017 and Eurocode 4.

This section shows a comparison of serviceability limit state requirements provided by the two international guidelines above introduced. It may be divided into the following categories: detailing provisions (slab thickness and reinforcement), actions, control of cracking of concrete and calculation of deflections. After that, numerical comparison about long-term deflection calculation of composite slabs are presented.

6.4.1. Detailing provisions

Both Australian and European code contain a section where the details about slab thickness and reinforcement are provided. Minimum values of depth of composite slab, distance between the bars and amount of reinforcement are recommended. The tables 8 and 9 summarize the most relevant points of these sections and show that the text of the two codes is comparable. The detailing provisions specified by both guidelines are not identical but the differences are very small.

Slab thickness

AS 2327-2017 _SECTION 2 (2.2)	UNI EN 1994-1-1_ SECTION 9 (9.2)
The overall depth of the composite slab h shall be not less than **90 mm.**	The overall depth of the composite slab h shall be not less than **80 mm**.
The thickness of the concrete hc above the main flat surface of the top of the ribs of the sheeting shall be not less than **40 mm**.	The thickness of the concrete hc above the main flat surface of the top of the ribs of the sheeting shall be not less than **40 mm**.
If the slab is acting compositely with the beam or is used as a diaphragm, the overall depth h shall not be less than **100 mm** and hc shall not be less than **50 mm.**	If the slab is acting compositely with the beam or is used as a diaphragm, the overall depth h shall not be less than **90 mm** and hc shall not be less than **50 mm.**

Table 8: Slab Thickness requirements

Reinforcement

AS 2327-2017 _SECTION 2 (2.2)	UNI EN 1994-1-1_ SECTION 9 (9.2)
The amount of top reinforcement in the primary span direction shall not be less than the top reinforcement area determined in the transverse direction.	The amount of top reinforcement in both directions shall not be less than 80 mm^2/m
The spacing of the reinforcement bars shall not exceed 2h and **300 mm**, whichever is the lesser.	The spacing of the reinforcement bars shall not exceed 2h and **350 mm**, whichever is the lesser.

Slab depth, h (mm)	**Depth of concrete over profile rib, h_c (mm)**	**Reinforcement area, D500 grade (mm²/m)**
≤ 125	$h_c \geq 40$	135
$125 < h \leq 150$	$h_c \geq 40$	175
$150 < h \leq 175$	$h_c \geq 40$	225
$175 < h \leq 225$	$h_c \geq 45$	290
$225 < h \leq 300$	$h_c \geq 55$	350

Table 9: Reinforcement requirements

6.4.2. Actions

Design for serviceability limit states includes control of simultaneous influence of different actions. Both codes provides appropriate combinations to check that limiting design values are not exceeded. Each combination of actions, provides by AS/NZS 1170 (Section 4) and EN 1990 (Section 6), use ψ factors. These factors allow to take into consideration various design situations. Recommended values of ψ factors are given by Table 4.1 (AS/NZS 1170) and table A1.1 (EN – 1990-1-1). The Australian guideline, compared to Eurocode, allows diversifying the short-term effects from long-term effects using short-term and long-term ψ factors respectively.

6.4.3. Control of cracking of concrete

The table 10 presents the requirements for control cracking of concrete suggest by both codes. According the two guidelines cracking in the concrete components shall be controlled verifying different parameters. Eurocode provides limiting values of crack width given by EN 1992-1-1 (7.3) and recommends not to exceed them, while the Australian code suggests to satisfy some detailing provisions about reinforcement and strength limits. In both cases, the control is provided to ensure durability and structural performance in order to not compromise the structure.

Control of cracking of concrete- SERVICEABILITY LIMIT STATES	
AS 2327-2017 _SECTION 6 (6.3) - AS 3600- SECTION 9 (9.4)	**UNI EN 1994-1-1_SECTION 9 (9.8.1)**
Cracking in the concrete components shall be controlled in terms of : ***Minimum area of reinforcement.*** ***Disposition of bars*** ***Maximum tensile steel stress are satisfied.***	Cracking in the concrete components shall be controlled in terms of : ***Crack width*** It should be estimated according to 7.3 EN 1992-1-1 (7.3).
Where continuous slabs are designed as simply-supported in accordance with Clause 2.4.2, the cross-sectional area of the anti-crack reinforcement above the ribs shall be not less than **0.2%** of the cross-sectional area of the concrete above the ribs for un-propped construction and **0.4%** of this cross-sectional area for propped construction.	Where continuous slabs are designed as simply-supported in accordance with 9.4.2(5), the cross-sectional area of the anti-crack reinforcement above the ribs shall be not less than **0.2%** of the cross-sectional area of the concrete above the ribs for un-propped construction and **0.4%** of this cross-sectional area for propped construction.

Table 10: Control cracking of concrete requirements

6.4.4. Calculation of deflection

In the section regarding the calculation of deflection lies the most significant difference between the two codes. It consists in the approach to take into account the shrinkage effects on the deflection (Table 11). At the serviceability limit state, the Eurocode allows to neglect the shrinkage effects in the calculation of deflections of a composite slabs, while the Australian code not only takes into account the evaluation of the shrinkage deflections but also it redefines the common assumption of constant shrinkage profile considering the use of a shrinkage gradient.

Slab deflection- SERVICEABILITY LIMIT STATES	
AS 2327-2017 _SECTION 2 (2.8)	**UNI EN 1994-1-1_SECTION 9 (9.8.2)**
Shrinkage and creep effects shall be take into consideration. The shrinkage profile to be used in the calculation of the shrinkage deflection and of the cracking moment shall be based on a linearly varying shrinkage distribution.	**Shrinkage effects are not take into consideration.**
Calculation of the deflection of the composite slab could not be omitted.	Calculation of the deflection of the composite slab can be omitted if some conditions are satisfied (Clause 7.4)

Table 11: Control slab deflection requirements

6.5. Numerical comparison

The aim of this chapter is to demonstrate numerically how the choice of the approach to take into account the shrinkage effects influences the long-term deflection. Two worked examples are presented in order to show that the approaches suggested by the European and Australian code lead very different results of total deflection. Two different length spans are analyzed with the aim to show both uncracked and cracked condition. The three component of deflection (instantaneous, creep and shrinkage deflection) are calculated according with AS 2327-2017 and EN 1994-1-1 and the results are compared.

6.5.1. Example 1: Deflection calculation of a composite slab with a span of 2,5 m.

Uncracked section

L	2500 mm
B	1000 mm
g_{sw}	3,13 N/mm^2
g	1.2 N/mm^2
q	3 N/mm^2
t_0	28 days
t_{unpr}	3 days
t_{dry}	14 days
t_f	30 years

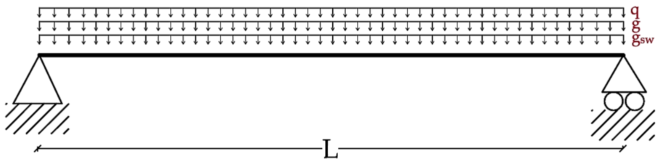

Figure 20: simply-supported composite slab L= 2500 mm

Figure 21: Time analysis

The slab is assumed to be simply-supported. Both propped and unpropped conditions of slab during construction phases are considered. The short-term deflection (instantaneous deflection) and the time-dependent deflections (creep and shrinkage deflection) are calculated according to the procedures suggested by the guidelines: AS 2327-2017-Section 2 and EN1994-1-1-Section 9, respectively.The figure 22 shows that the shrinkage component is the biggest one and so neglecting this component leads considerable smaller values of total deflection than the case in which all components of deflection are considered.

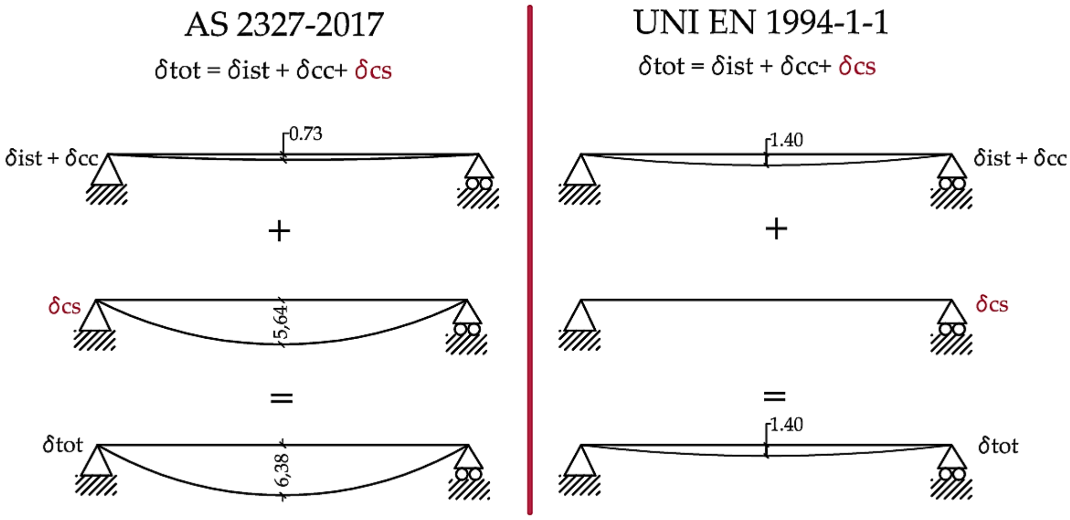

(a) Unpropped

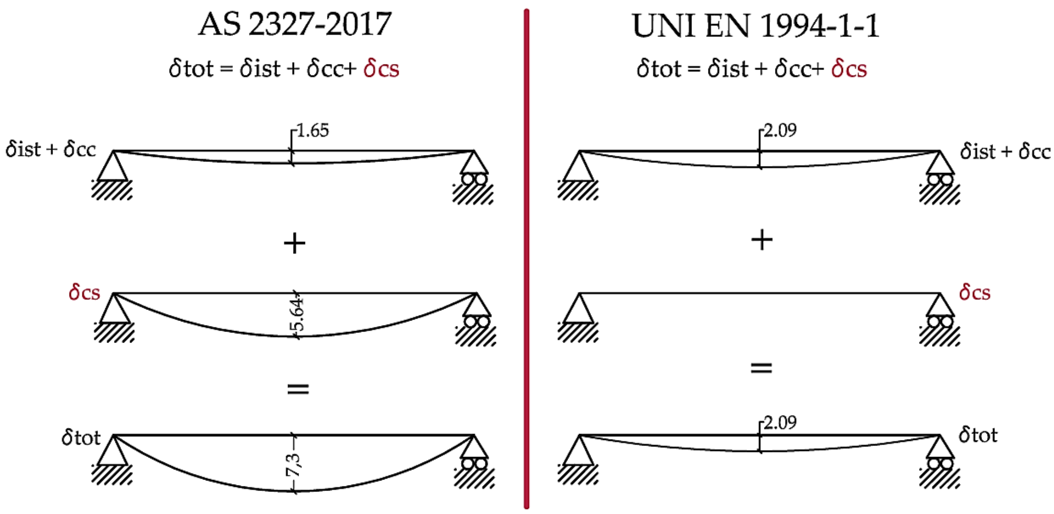

(b) Propped

Figure 22: Instantaneous, creep and shrinkage deflection in the case of an unpropped (a) and propped (b) slab (L=2500 mm)

It is noteworthy that, at serviceability limit state, neglect the shrinkage effect leads to underestimates of the long-term deflections.

6.5.2. Worked example 2: Deflection calculation of a composite slab with a span of 3,5 m.

Uncracked section

L	3500 mm
B	1000 mm
g_{sw}	3,13 $N/_{mm^2}$
g	1.2 $N/_{mm^2}$
q	3 $N/_{mm^2}$
t_0	28 days
t_{unpr}	3 days
t_{dry}	14 days
t_f	30 years

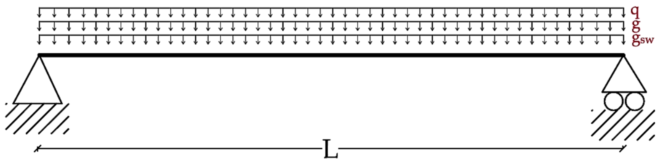

Figure 23:Figure 20: simply-supported composite slab L= 3500 mm

Analogous consideration can be reported about this second worked example.

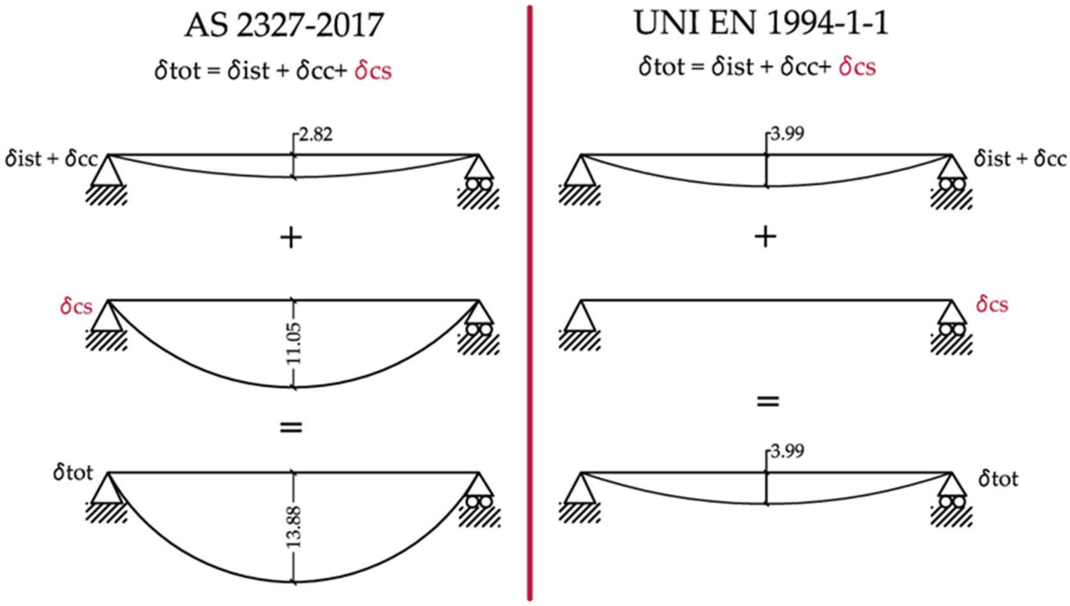

(a) Unpropped

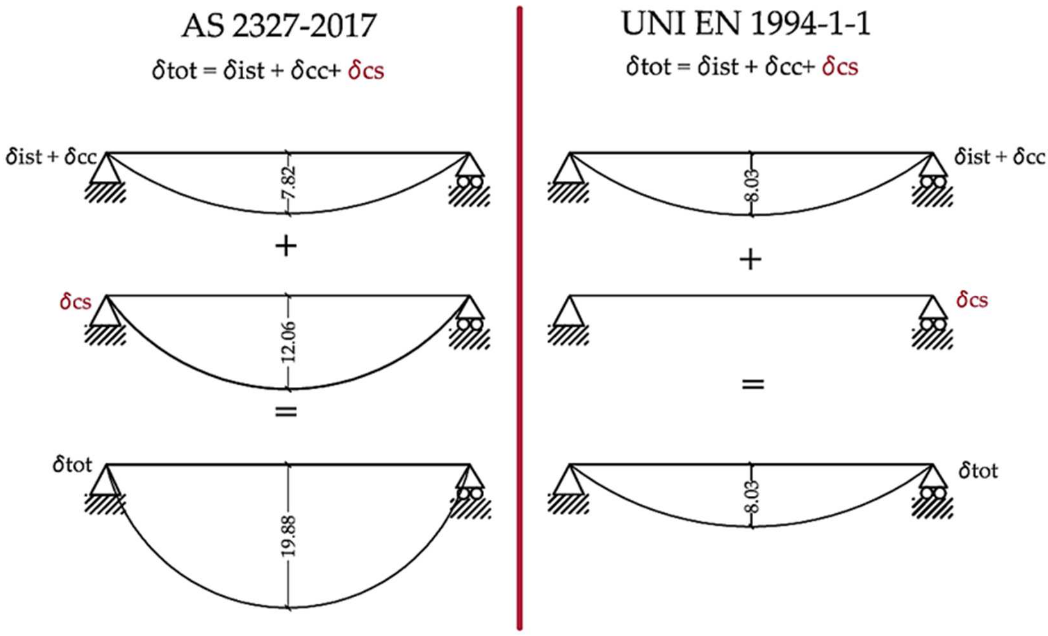

(b) Propped

Figure 24: Instantaneous, creep and shrinkage deflection in the case of an unpropped (a) and propped (b) slab (L=3500 mm)

Parametric study

7.1.Introduction

This chapter introduces the results of a parametric study focussed at identifying the key variables and design criteria controlling the design of composite slabs. For this purpose, four service design models have been considered to see their possible influence of the design solution. For ease of reference, these models have been denoted as Model I, II, III and IV in the following. The difference between these models lies in the approach used to take into account shrinkage effects as follows: (Model I) linear shrinkage gradient specified in accordance to the Australian composite code AS/NZS 2327-2017 (1); (Model II) uniform shrinkage profile based on the shrinkage properties specified in the Australian concrete code AS3600-2009 (3)(Model III), no shrinkage effects while following the other service checked required by the Australian composite code 2327-2017 with opportune variations; (Model IV) no shrinkage effects as suggested in the Eurocode 1994-1-1 (2) (table 12).

Model I	linear shrinkage profile - AS 2327-2017
Model II	uniform shrinkage profile – AS 3600-2009
Model III	no shrinkage effects
Model IV	no shrinkage effects- EN 1994-1-1

Table 12: Models for the prediction of shrinkage effects.

In the parametric study, two profiled steel-sheeting have been used (referred-to as profile 1 and 2). These have a thickness of 1 mm and consist of: (1) Lysaght Bondeck HP and (2) Stramit Condeck. They are widely used in Australia and their geometries (60) (61) are reported in figure 25. In the parametric study, span lengths varied between 2 m and 8 m with length increments of 0.2 m. The strength of the concrete used is 32 and the time-dependent response is evaluated at 30 years from casting.

The variable load and superimposed permanent loads are 3 kPa and 1 kPa, respectively.

Both propped and unpropped construction have been considered in this study.

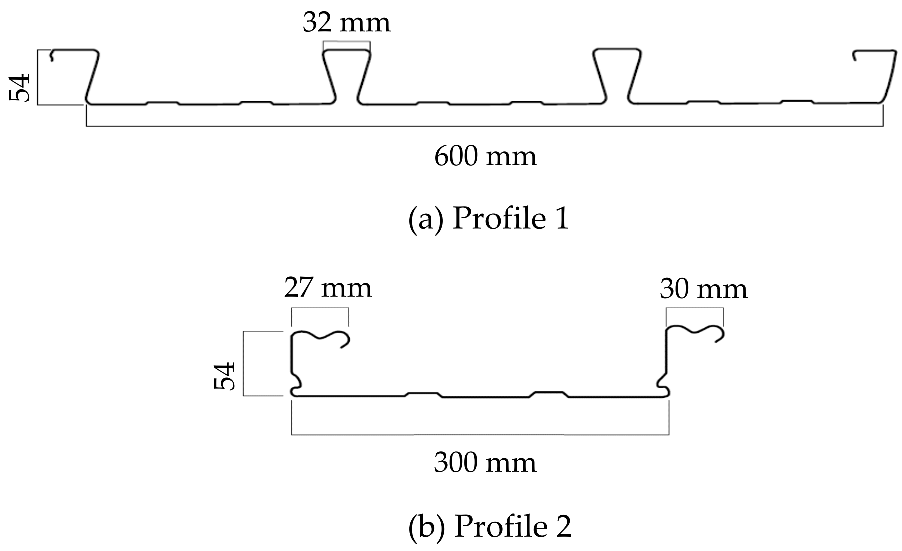

Figure 25: Geometry of the profiled steel sheeting

7.2.The governing limit state for the design of composite slabs

7.2.1. The limit states verification of composite slabs

The ultimate and the serviceability limit states considered in the parametric study are expressed in terms of design ratios.

For SLS, the design ratio is the ratio between the actual deflection of the slab and the value of the limit deflection. The latter is equal to $\frac{\delta_t}{L} = \frac{1}{250}$ for incremental deflection limits and $\frac{\delta_t}{L} = \frac{1}{500}$ for total deflection limits (where L is the span length between supports and δ_t the limit value of mid-span deflection). In the analysis, the age of the concrete at the beginning of the evaluation of the incremental deflection is equal to 28 days.

For ULS, the design ratios are defined as the ratio of the design value of the internal resultants (flexural moment and vertical shear) to the corresponding design resistance.

Design ratio			
SLS		USL	
Total deflection	$\frac{\delta_t}{\delta_{t,lim}} = \frac{\delta_t}{L/250}$	Flexural	$\frac{M_{ed}}{M_{rd}}$
Incremental deflection	$\frac{\delta_{incr}}{\delta_{incr,lim}} = \frac{\delta_t}{L/500}$	Vertical shear	$\frac{V_{ed}}{V_{rd}}$

Table 13: Design ratios

For each lengths span (varied between 2 m and 8 m), the limit states verification has been checked. For both ultimate and service condition, this is satisfied if the design ratios is less or at least equal to one.

7.2.2. The design of the slab thickness

In order to evaluate the key parameters controlling the design of slab thickness, the design ratios (table 13) are compared to each other. The highest design ratio (closer to one) governs the design.

In the parametric study, the use of four different service design model leads to identify the relevant influence of serviceability limit state in the design solutions.

Figure 26 shows the comparison between the results of Models I and II, and their influence on the design of the slab thickness. This figure shows the design ratios and thickness depths for propped slabs constructed with profile 1 in the case of Models I and II.

The figure 26, allows to compare Models I and II and their influence on the design of the slab thickness. This first figure shows the design ratios and thickness depths for propped slab with profile 1 in the case of Models I and II.

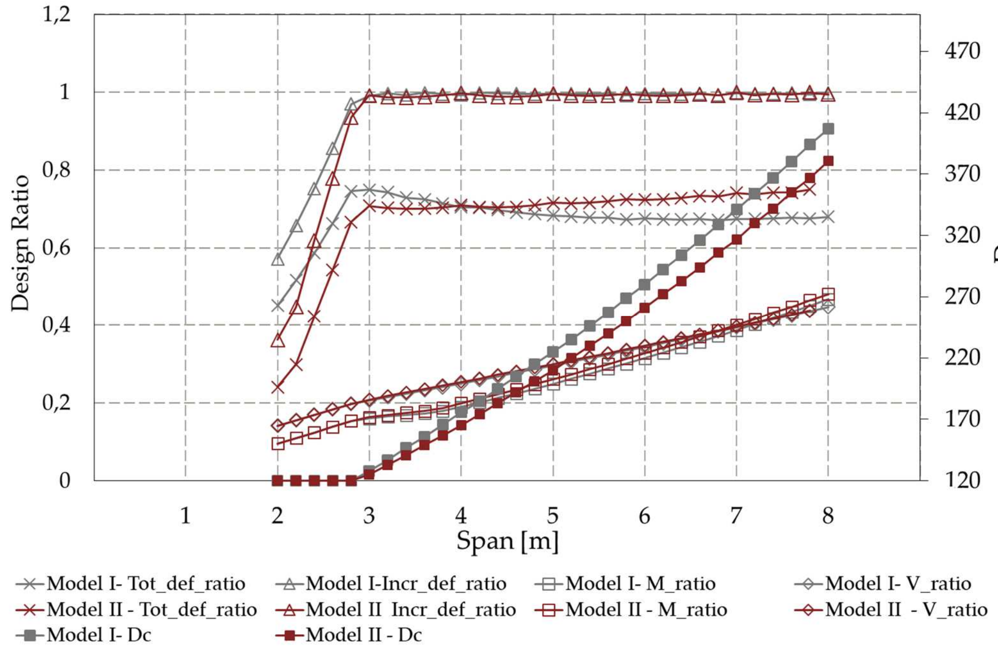

Figure 26: Thickness depth slab and design ratios for a propped slab with profile 1 in the case of Model I and Model II.

The figure 26 leads to stand out important considerations:

- Observing the design ratio-span curves, it is possible understands that the service limit state ratios are always larger than the ultimate ones, in particular, the incremental deflection. This implies that under the assumptions specified for the parametric study, serviceability limit state requirements control the design span depth.

- For span lengths shorter than 2.8 m, the slab thickness is equal to 120 mm. The latter represents the minimum value used in the design (typical value used in the Australian industry practice).
- The results of two models are almost close, and the inclusion of linear shrinkage profile doesn't seem to lead relevant differences. The figure 26 shows that the difference between the Models I and II is negligible for short span and increase relatively for larger ones. This trend is a result of the combined action of cracking and shrinkage c (in particular for the small spans). The model with uniform shrinkage (II) results more cracks in the slab than the Model I. In fact the Model II returns smaller value of M_{cr} (equation 5.12) and in the slab the crack occurs before than the Model I. The smaller value of the cracking moment is due to higher value of the maximum shrinkage-induced tensile stress σ_{cs} (equation 5.14). Therefore, at the same time, a composite slab could be cracked according the Model II and un-cracked according the Model I. Because of the cracking it is necessary a higher values of the thickness for the Model II to satisfy the limit state requirements.

  The shrinkage effects depend on the size of the (uncracked) concrete part of the section (this can be considered recalling the equations 5.20 and 5.21). Therefore the Model I results more affected by the shrinkage effect than the Model II because of its major quantities of the uncracked geometric area. As consequences, the slabs computed with the Model I are less cracked but, in the other hand, the shrinkage effects are large. Therefore, cracking and shrinkage provoke a combined effect on the composite slab. The table 14 shows a numerical example of cracking and shrinkage effect in order to clarify because the different between the depth obtained with Models I and II increase relatively for the larger spans. It is considered a propped slab with thickness equal to 200 mm and two different lengths span (L=4000 mm and L=200 mm). For a span with L=4000 mm M_{cr} results equal to 1,437 E+07 Nmm according with the Model II and 2,092 E+07 Nmm with the Model I. The first value is smaller than the second one due to the high value of σ_{cs} (1,549 MPa> 0,708 MPa). The slab computed with uniform shrinkage results cracked because the cracking moment is lesser than the flexural moment M_s (1,65E+07 Nmm), while in the case of linear shrinkage results $M_{cr} > M_s$ and the section is uncracked. Therefore the cracked condition results different for the Models I and II and this increases the different between the values of design depth.

For smaller span (e.g. L=2000 mm), the slab is uncracked for both Model due to the smaller value of M_s than the M_{cr}. and the design depth optioned with Model I and Model II are very close (Table 15).

	Uniform Shrinkage Model II		**Linear Shrinkage** Model I
L [mm]	4000	=	4000
$\boldsymbol{M_s}$ [Nmm]	**1,65E+07**	=	**1,65E+07**
$\boldsymbol{\sigma_{cs}}$ [MPa]	1,5492	>	0,7084
$\boldsymbol{M_{cr}}$ [Nmm]	**1,4371E+07**	<	**2,0920E+07**
	Cracked section		Uncracked section

Table 14: Numerical comparison between Model I and Model II for a propped slab with L=4000 mm.

	Uniform Shrinkage Model II		Linear Shrinkage Model I
L [mm]	2000	=	2000
$\boldsymbol{M_s}$ [Nmm]	**4,12E+06**	=	**4,12E+06**
$\boldsymbol{\sigma_{cs}}$ [MPa]	1,5492	>	0,7084
$\boldsymbol{M_{cr}}$ [Nmm]	**1,4371E+07**	<	**2,0920E+07**
	Uncracked section		Uncracked section

Table 15: Numerical comparison between Model I and Model II for a propped slab with L=2000 mm.

In order to observe the real difference between the two models, it was necessary avoid different condition of cracking for the two models. The same curves of the figure 26 are been computed blocking the cracking (figure 27). In this way it was possible calculated the design depth with the same quantities of the uncracked geometric area.

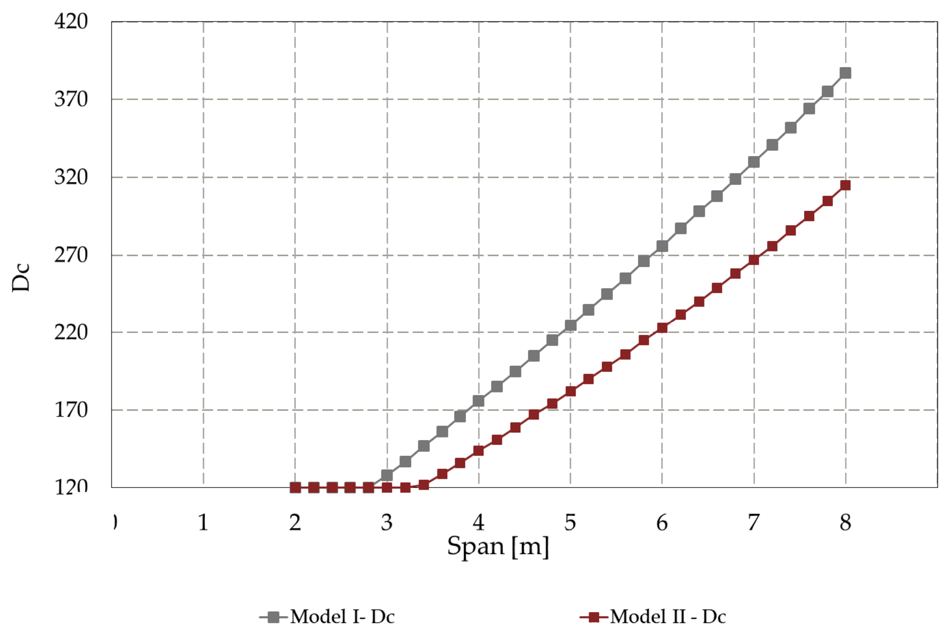

Figure 27: Thickness depth slab for a propped slab with profile 1 in the case of Model I and Model II- without cracking.

The results calculated with Model III, which not considers the effects of shrinkage, are presented in figure 28. With this method, the design solution requires smaller design depths with respect to the previous cases. For small spans (up to 3,8), the minimum thickness of 120 mm is adopted and, for larger spans, the governing limit state is still the incremental deflection (serviceability limit state).

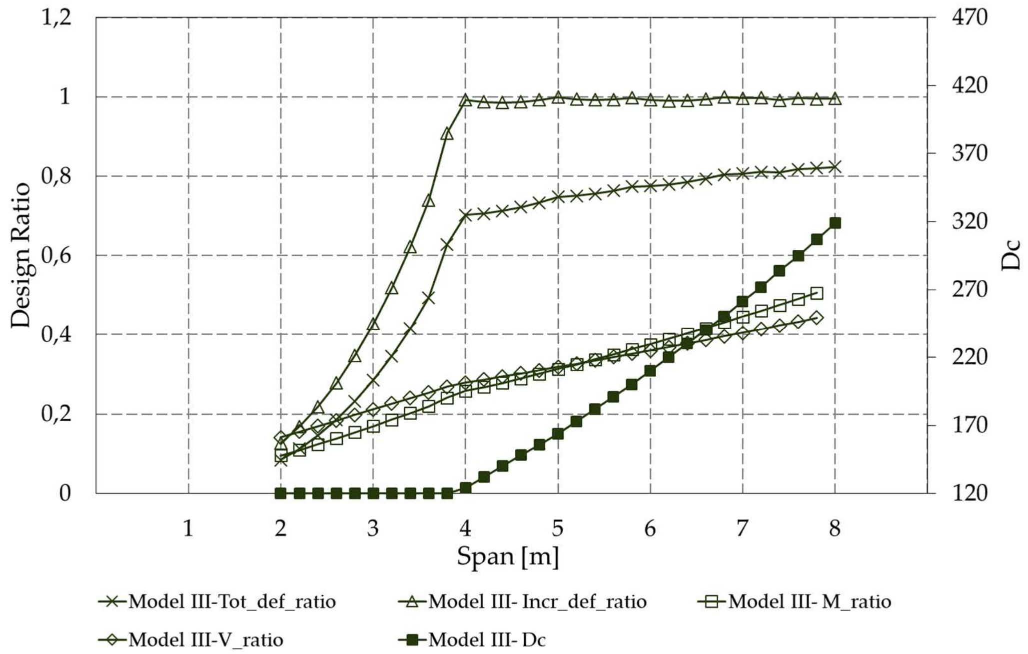

Figure 28: Thickness depth slab and design ratios for a propped slab with profile 1 in the case of Model III.

The depths obtained with the Model IV are even smaller than those calculated with the Model III (Figure 30). For example, the depth of a 8 m span is equal to 249 mm for Model IV and 320 mm for Model III. This is due the fact that, despite both Models not considered the shrinkage effect on the deflection calculation, they use different approach to calculate the other two terms of the total deflection: instantaneous and creep deflection (Model III according AS3600-2009 (3) and Model VI according the EN-1994 (2)). The main difference between the approaches suggest by the codes relies in the term of

I_{ef}. This can be considered recalling the equations 5.4 and 5.24. The European code allows an approximation of the second moment of area calculating as the average of the values for the cracked and un-cracked section (formula 5.24). If the section is cracked I_{ef} calculated with the formula 5.24 results always smaller than with the equation 5.4. A smaller I_{ef} leads a smaller value of deflection and so it is necessary a lesser value of the thickness for satisfying the verifications. These difference between the Model III and Model IV is showed in the Figure 30 through the dimensionless of the results from model Model III against the values obtained with the Model IV. For length span of 8 m (where minimum thickness is not more adopted) the ratio reaches value of 1,3. In terms of design thickness, it means that for high values of length the result obtained with the Model III are far from those of the Model IV.

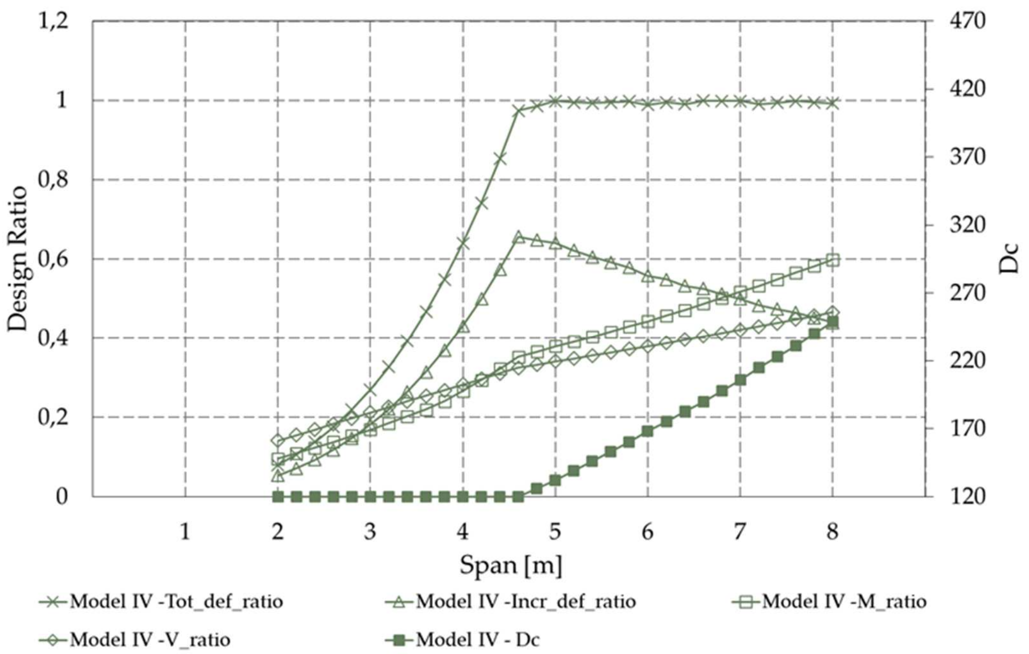

Figure 29: Thickness depth slab and design ratios for a propped slab with profile 1 in the case of Model IV

In addition, the figure 29 shows that for span length greater 4,6 m the design is again governed by the serviceability behaviour of the slab.

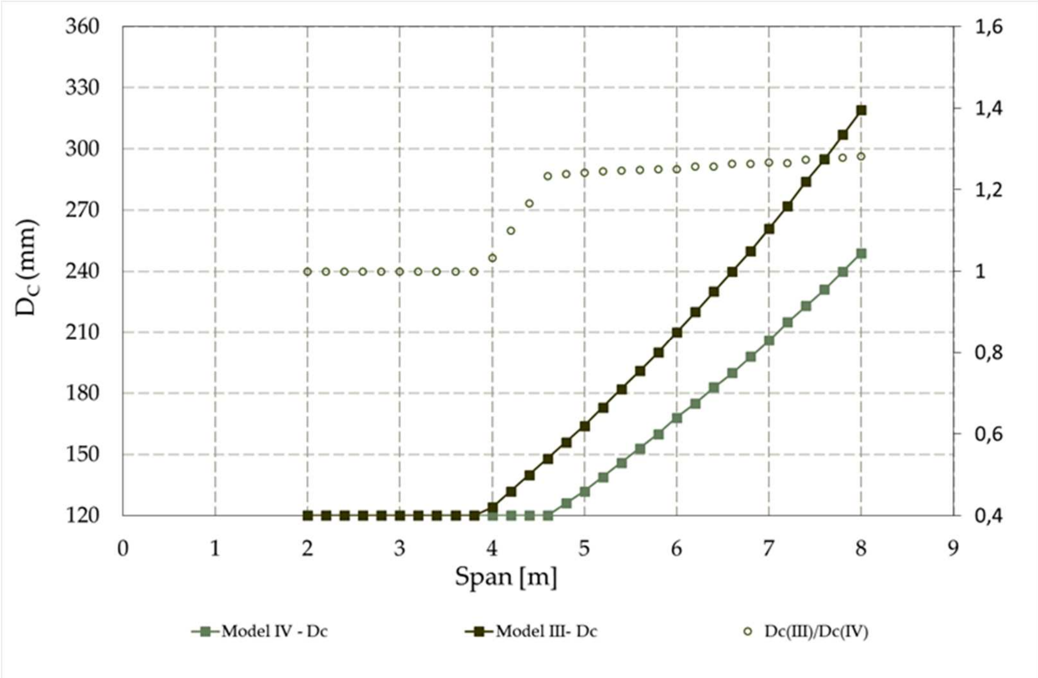

Figure 30: Comparison among design depth computed using model Model III and Model IV for propped slab with profile 1.

Analogous considerations can be reported for unpropped slabs (figures 31-34). If the same slab is not propped during the construction phase the contribution of the dead load to the deflection is neglected and the design depths result smaller than those calculated for propped slab.

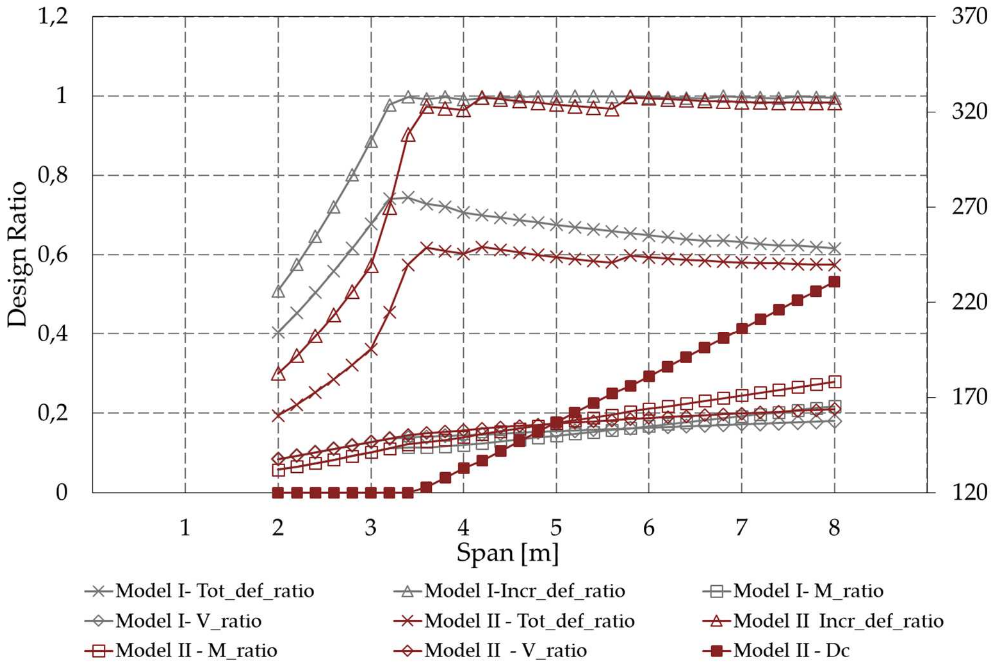

Figure 31: Thickness depth slab and design ratios for an unpropped slab with profile 1 in the case of Model I and Model II.

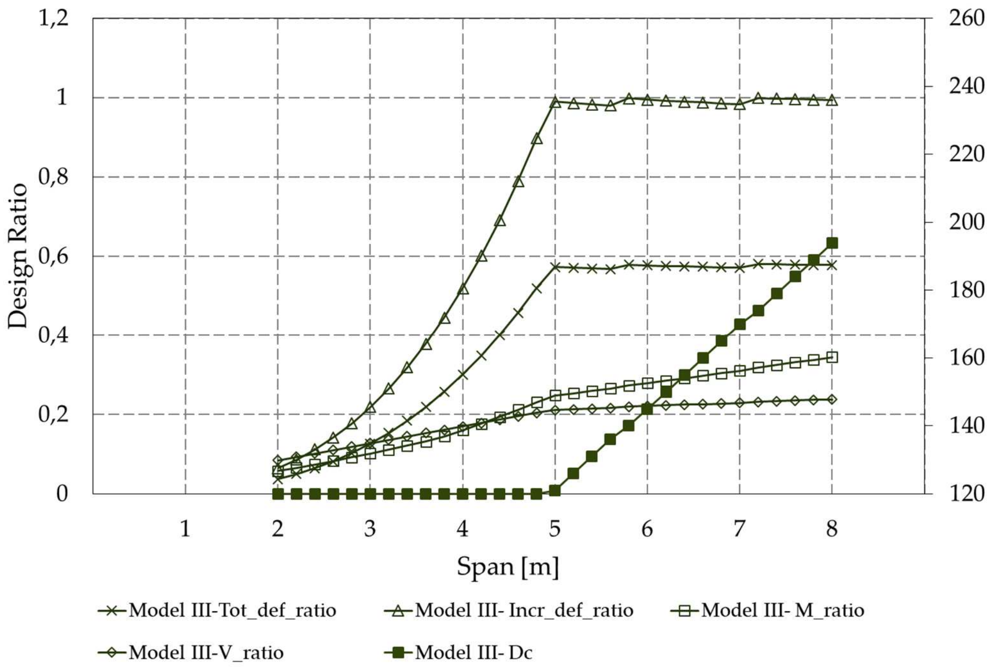

Figure 32:Thickness depth slab and design ratios for an unpropped slab with profile 1 in the case of Model III.

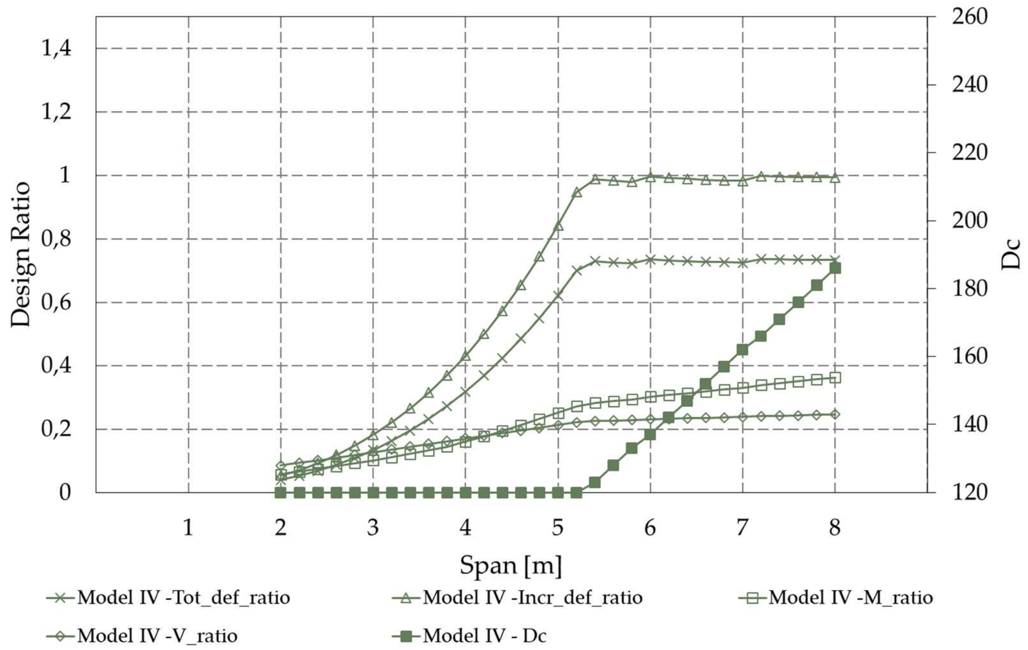

Figure 33: Thickness depth slab and design ratios for an unpropped slab with profile 1 in the case of Model IV

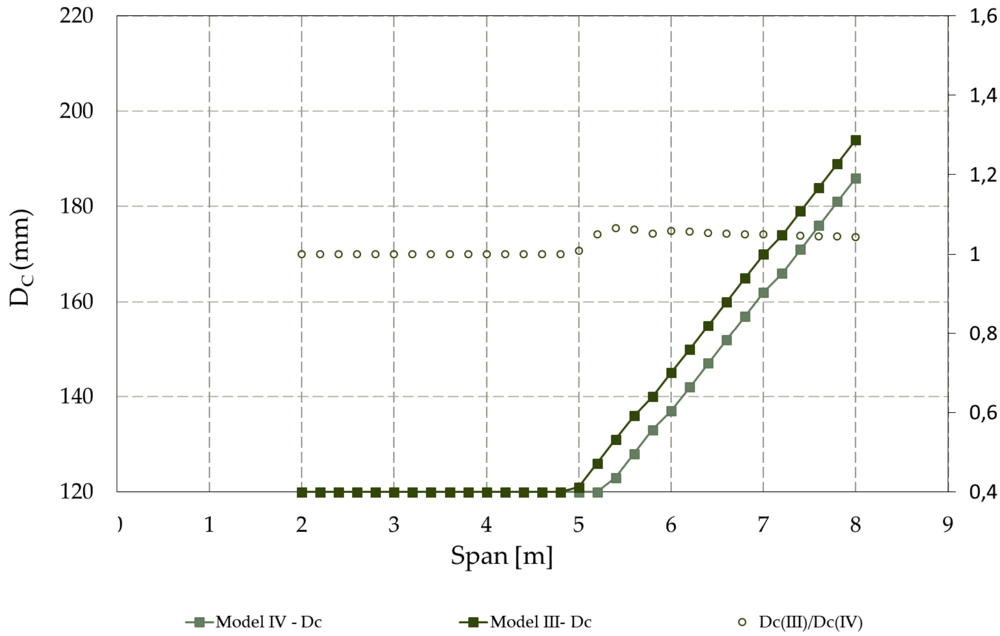

Figure 34: Comparison among design depth computed using model Model III and Model IV for unpropped slab with profile 1.

The same parametric study it was computed using the profile 2. The results for the steel sheeting 2 are similar to the first one and they are showed in the figures 35-42.

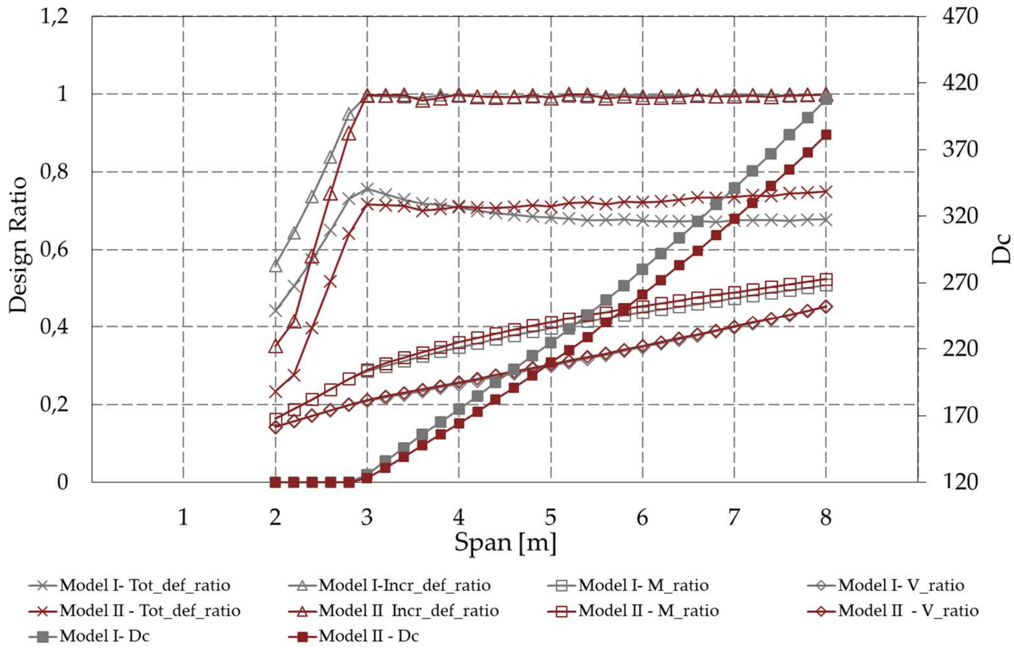

Figure 35: Thickness depth slab and design ratios for a propped slab with profile 2 in the case of Model I and Model II.

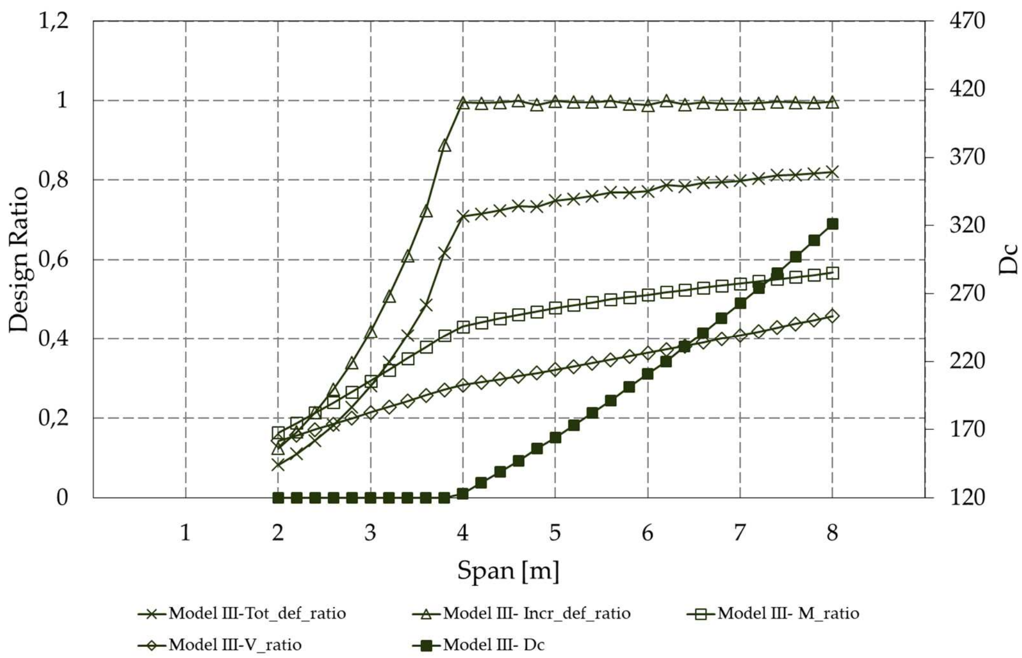

Figure 36: Thickness depth slab and design ratios for a propped slab with profile 2 in the case of Model III

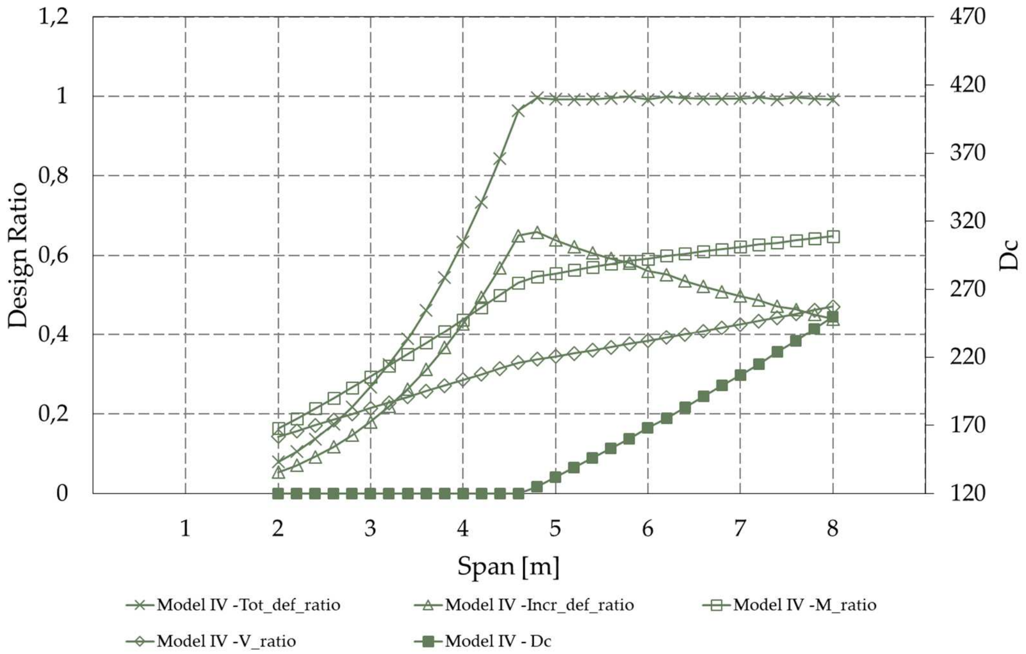

Figure 37: Thickness depth slab and design ratios for a propped slab with profile 2 in the case of Model IV

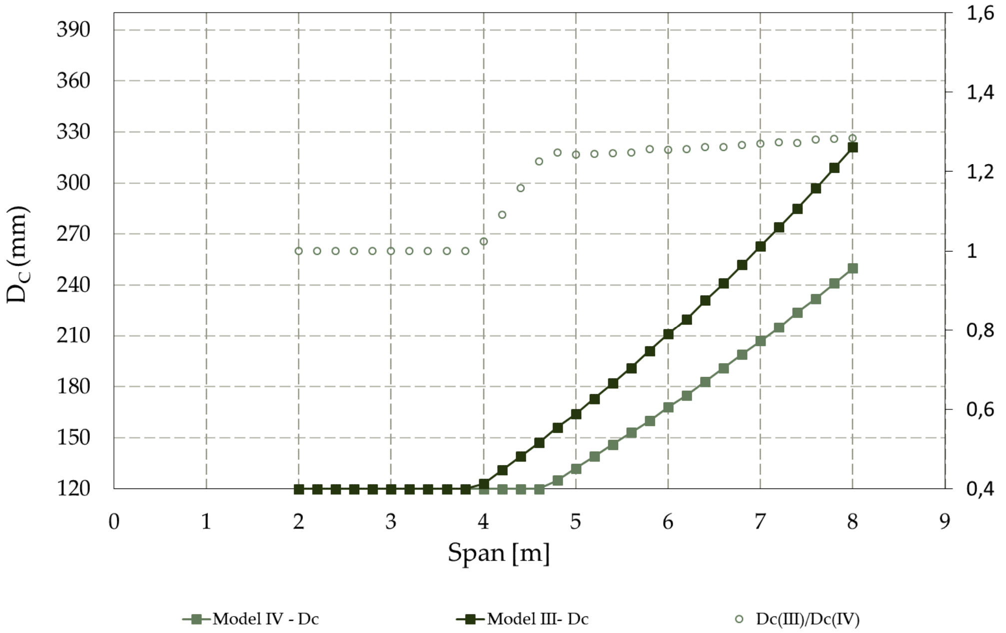

Figure 38: Thickness depth slab and design ratios for a propped slab with profile 2 in the case of Model IV.

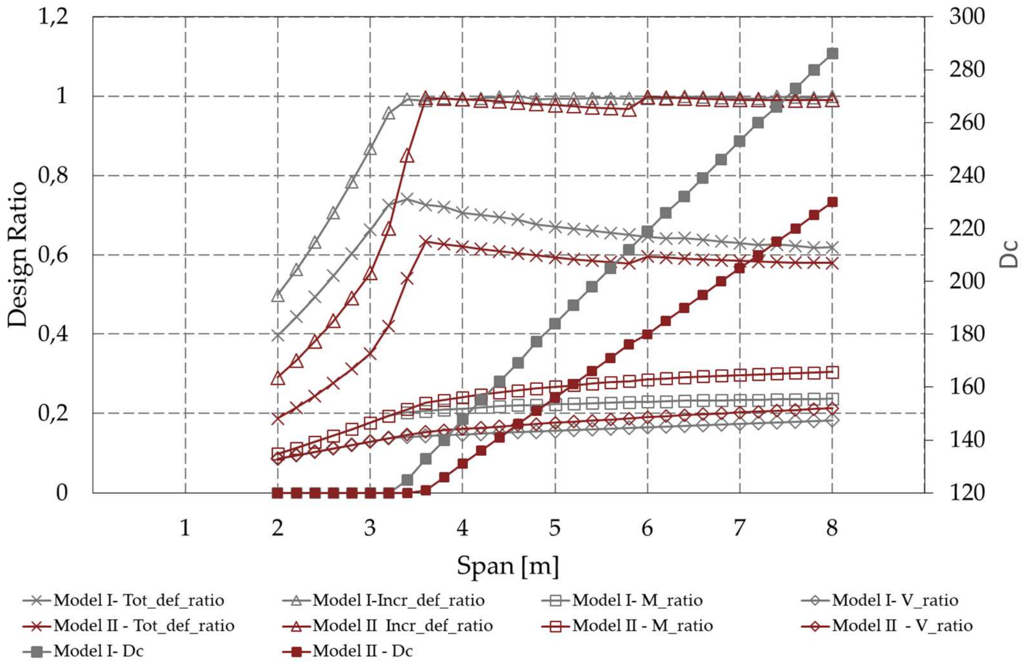

Figure 39: Thickness depth slab and design ratios for an unpropped slab with profile 2 in the case of Model I and Model II.

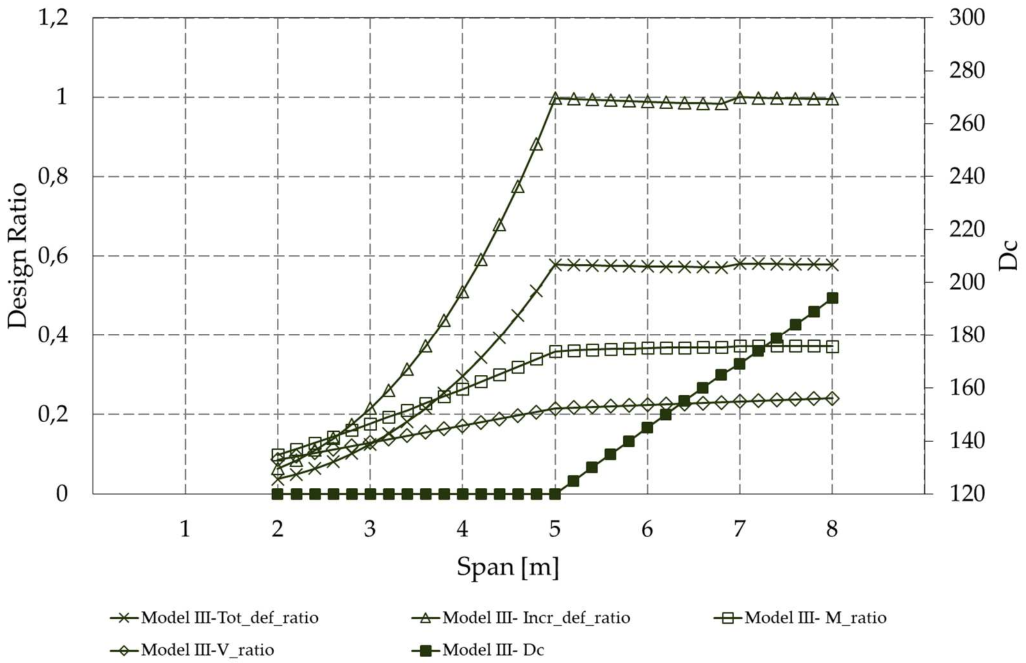

Figure 40: Thickness depth slab and design ratios for an unpropped slab with profile 2 in the case of Model III

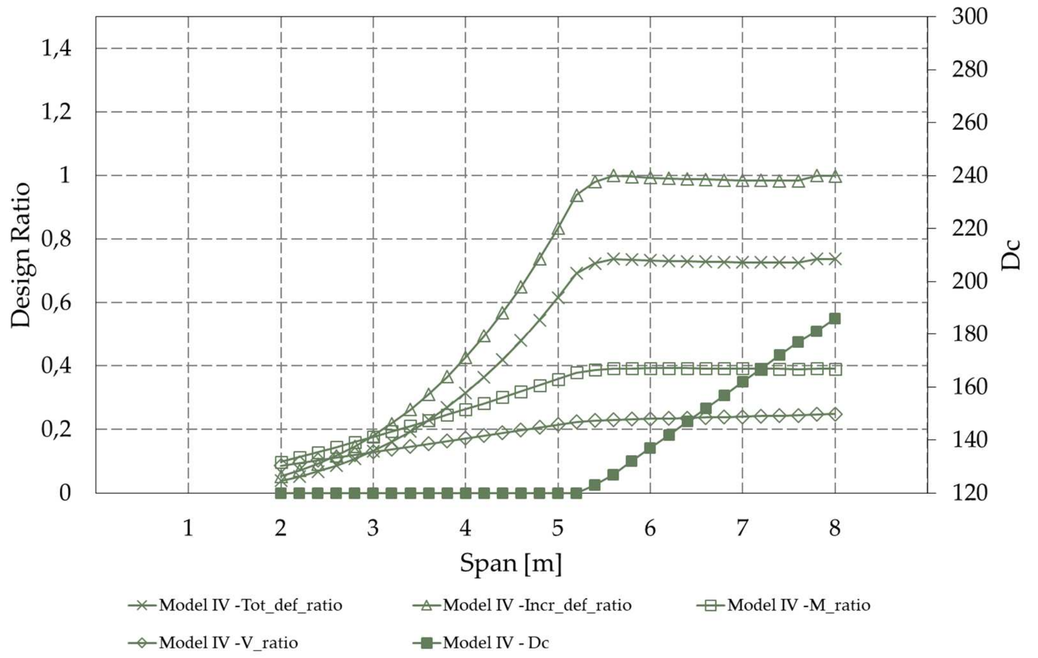

Figure 41: Thickness depth slab and design ratios for an unpropped slab with profile 2 in the case of Model IV

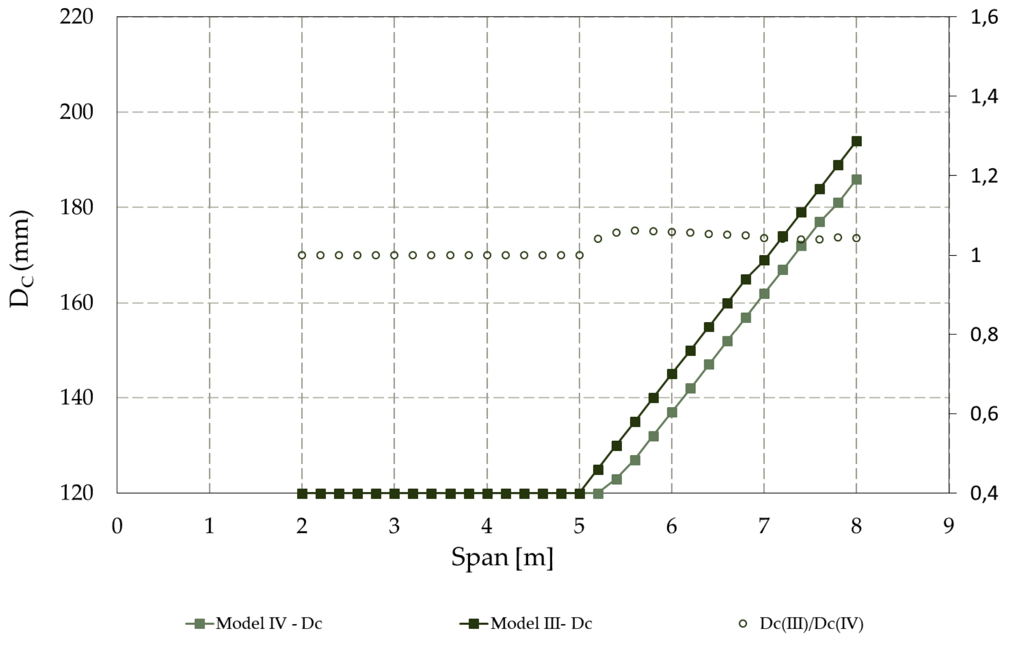

Figure 42: Thickness depth slab and design ratios for an unpropped slab with profile 2 in the case of Model IV

The results of all these studies have shown that the serviceability limit state governs the design in all analysing cases with the Model I and Model II. While for the Model III and Model IV the Ultimate limit state curves become important for small span.

Figures 43 and 44 summarize the comparison among the four model for propped and unpropped slab with profile 1 and 2. The values of design slab thickness obtained with the Model I, III and Model IV are dimensionalised against the results computed from the Model I.

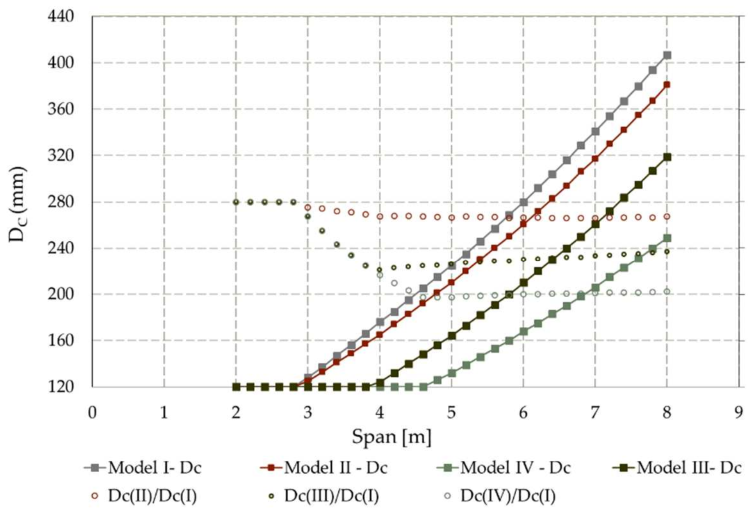

(a) Propped

(b) Unpropped

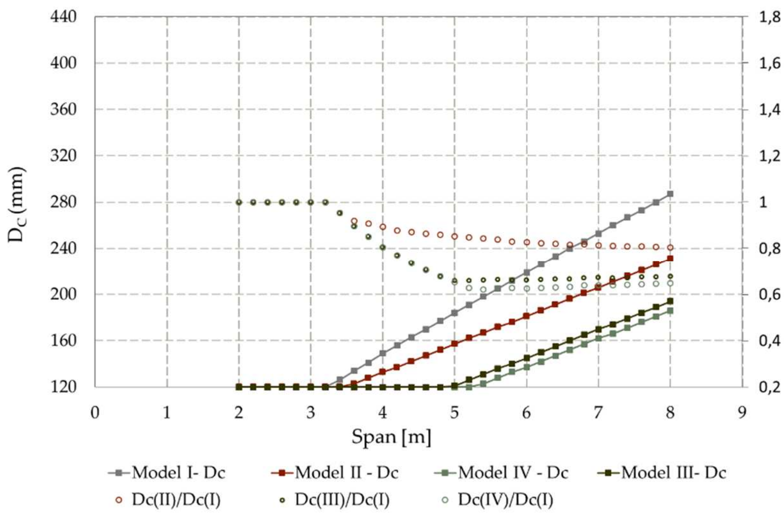

Figure 43: Comparison among design thickness depth using Model I, II, III and IV for profile 1.

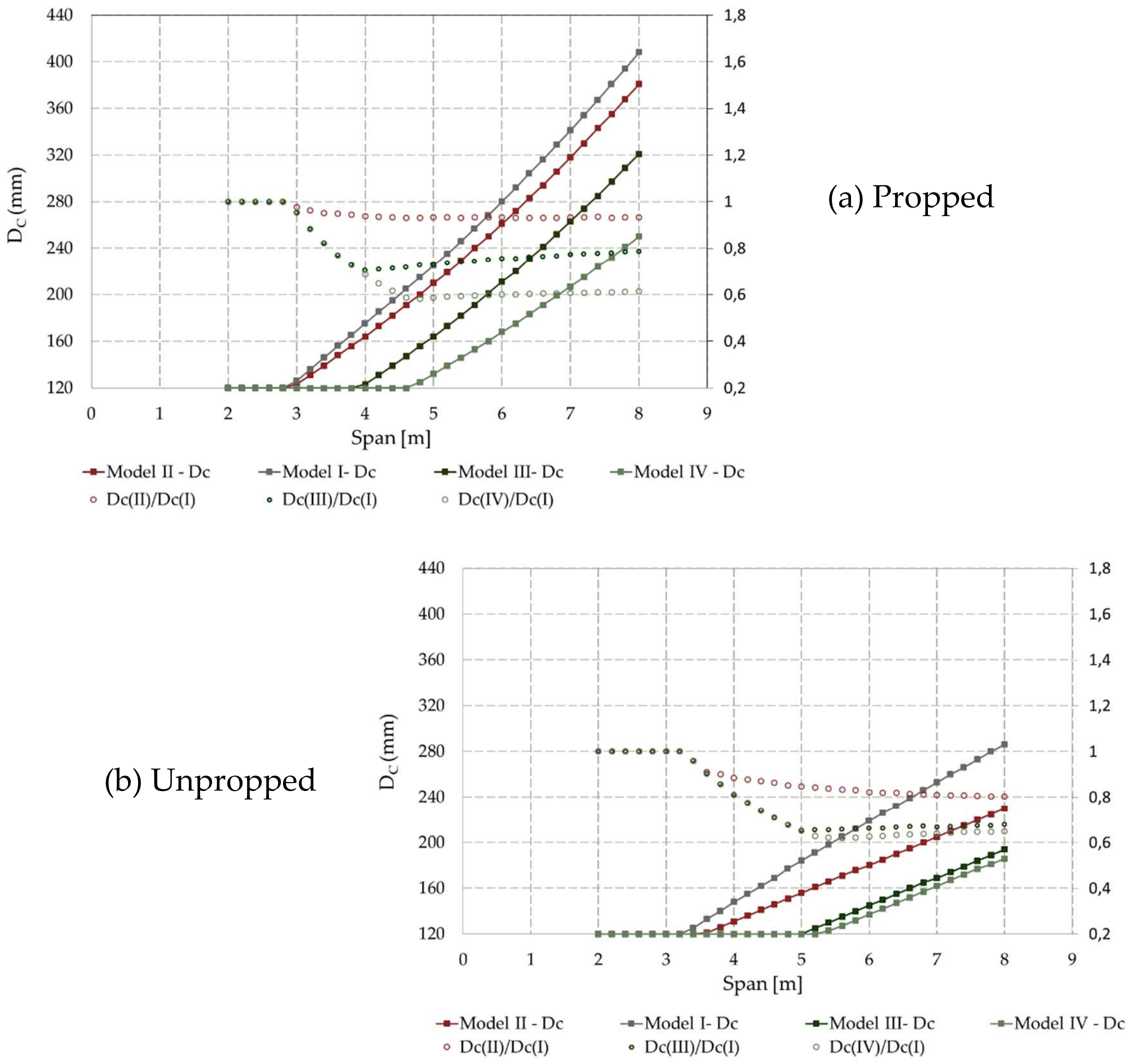

Figure 44: Comparison among design thickness depth using Model I, II ,III and IV for profile 2.

The results are also calculated ignoring the incremental limit check in the design process. In the cases of the Models I and II, the serviceability limit state still controls the design thickness for all lengths of the slab (figure 45a and 46a), while in the case of Model III and IV it continues to prevail on the ultimate behaviour only for the spans where no minimum thickness is required (figure 45b,45c,46b and 46c). Therefore, if the effect of shrinkage is neglected, the ultimate limit state condition (that in all other cases is far to govern the design of the composite slab) becames important for small spans.

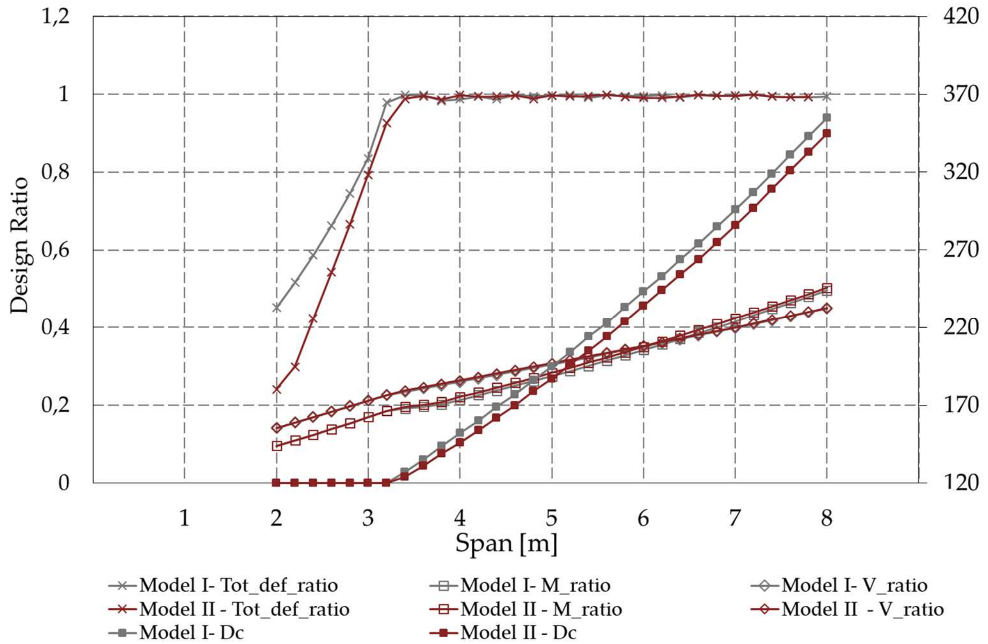

(a) Model I and II

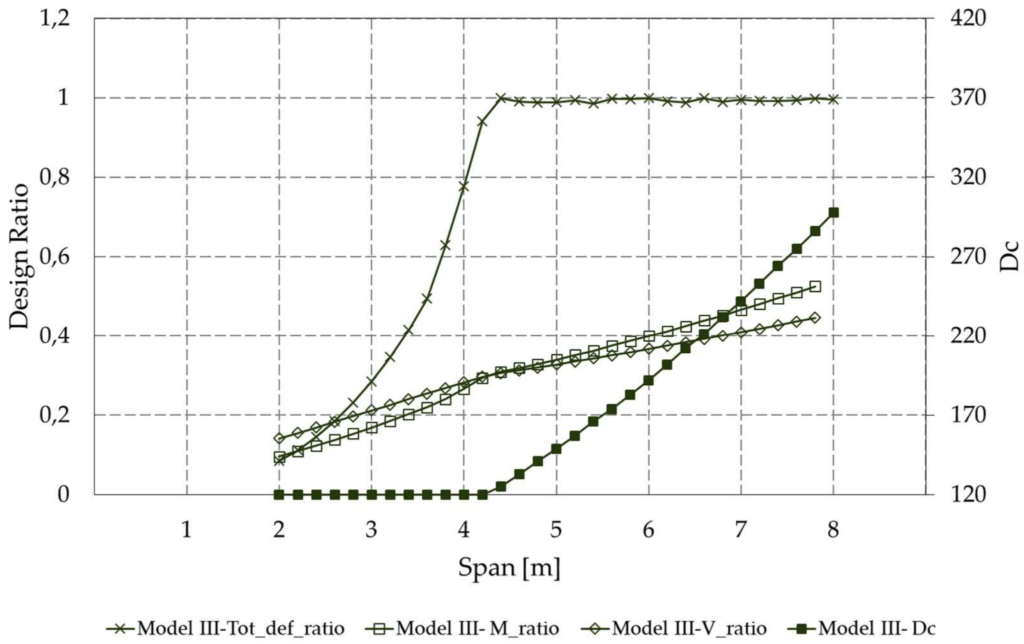

(b) Model III

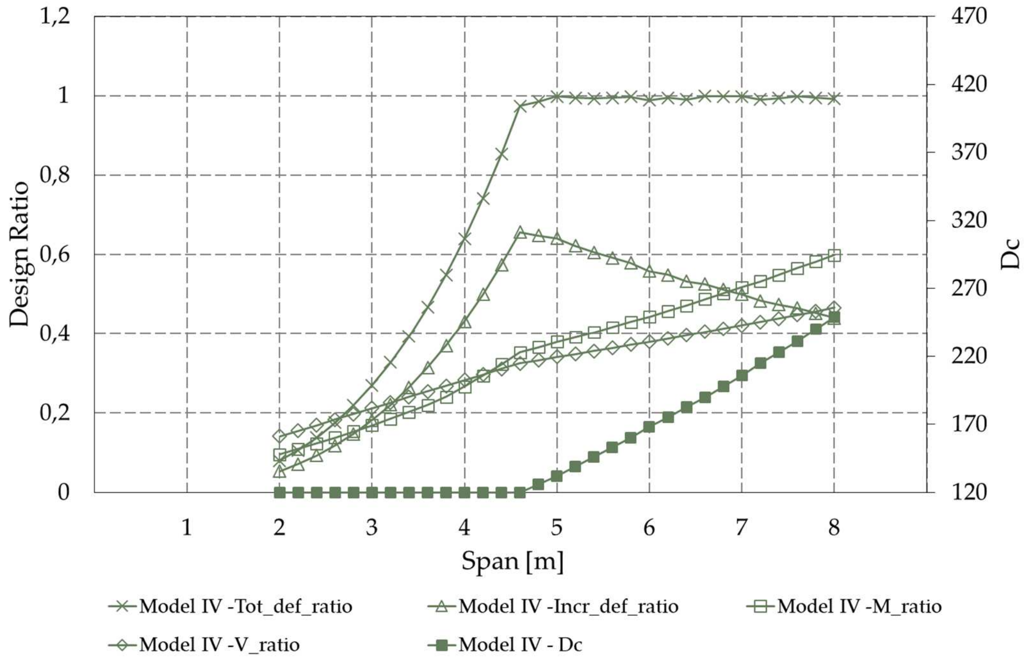

(c) Model IV

Figure 45: Thickness depth slab and design ratios for a propped slab with profile 1 without considering the incremental deflection limit.

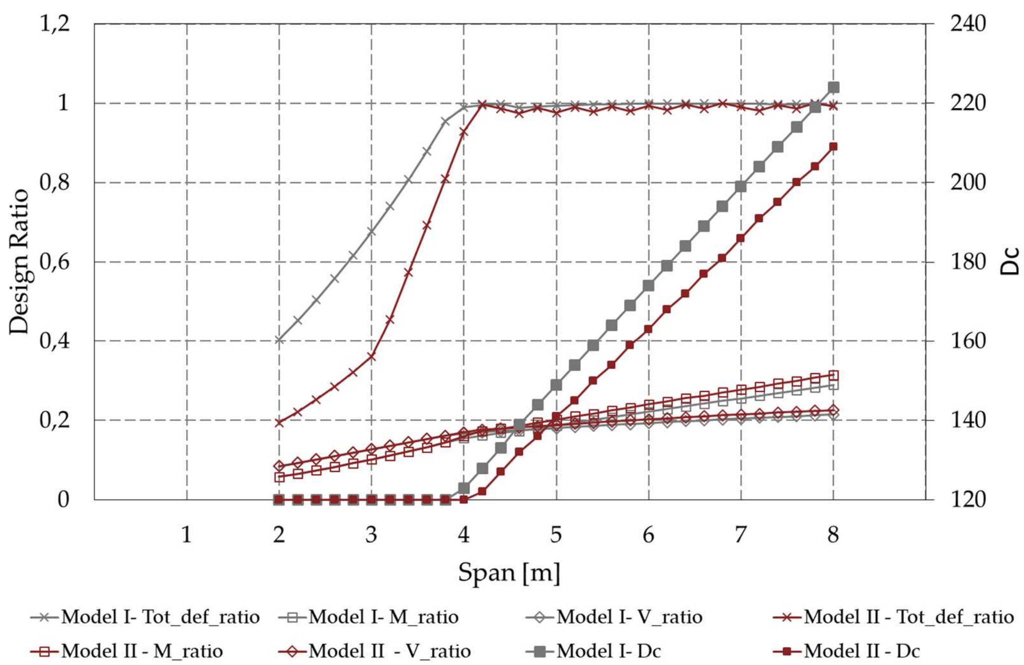

(a) Model I and II

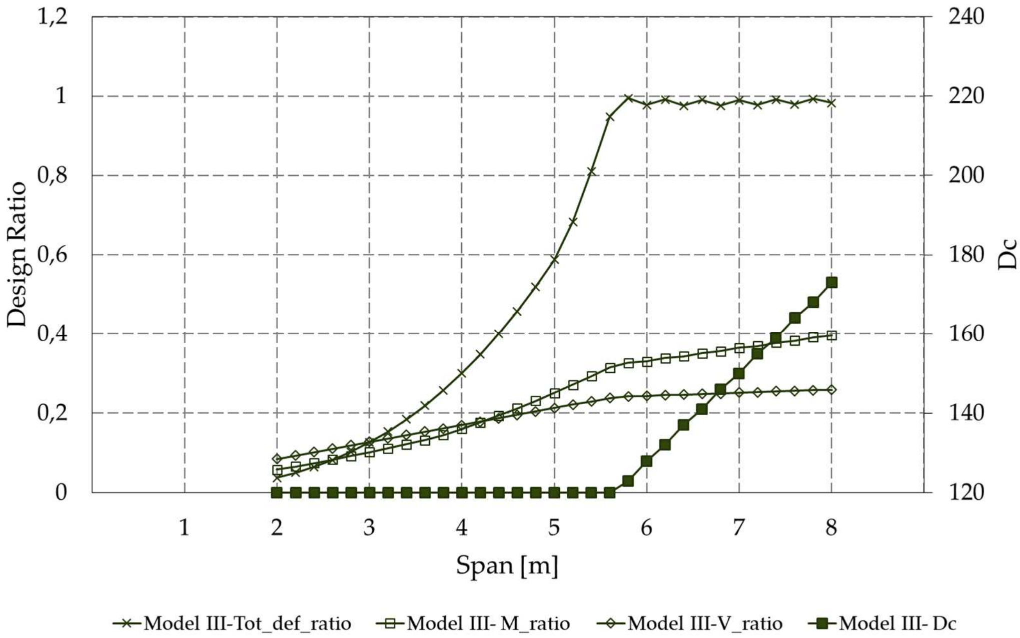

(b) Model III

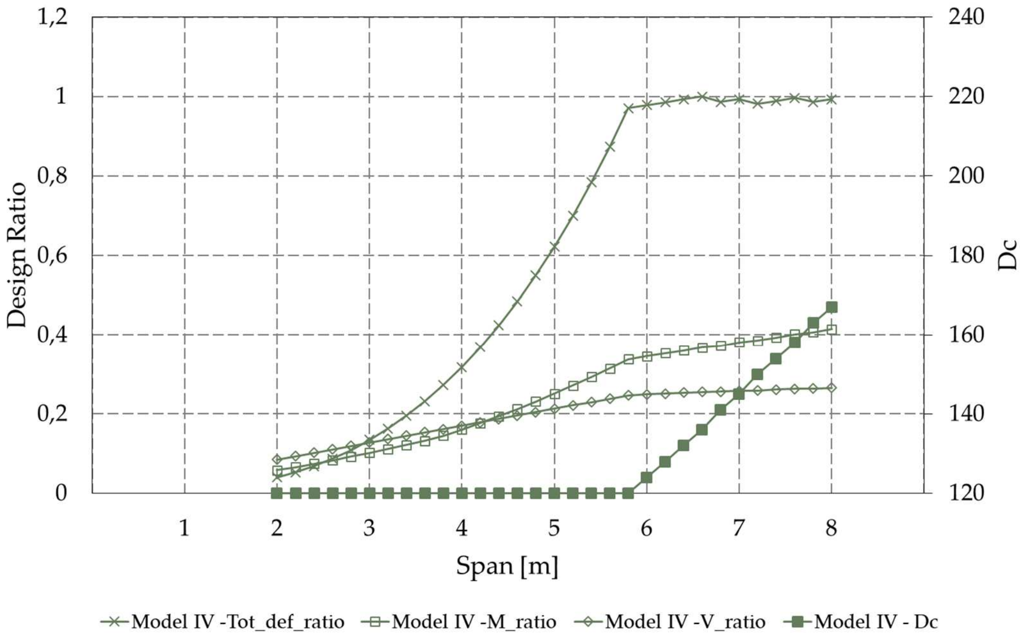

(c) Model IV

Figure 46: Thickness depth slab and design ratios for an unpropped slab with profile 1 without considering the incremental deflection limit

7.3. Consideration about the deflection

The parametric study has been also performed to show the influence to use different numerical models on the calculation of deflections. The figure 47 and 48 show the comparison of the total deflection for profile 1, in the case of propped and unpropped slab, respectively. In order to obtain comparable results, for all models the deflections are calculated with the design depths of the Model I as reference. Furthermore, to observe the real difference between the models, it was necessary blocking the cracking and uncracked condition has been considered for all span lengths.

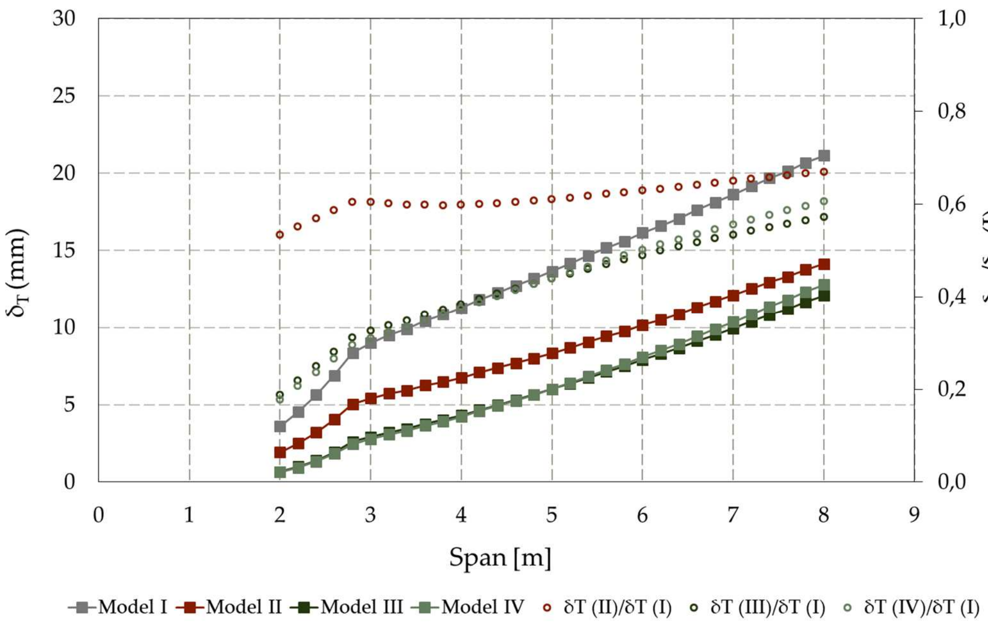

Figure 47: Comparisons among total deflection in the case of a propped slab with profile 1.

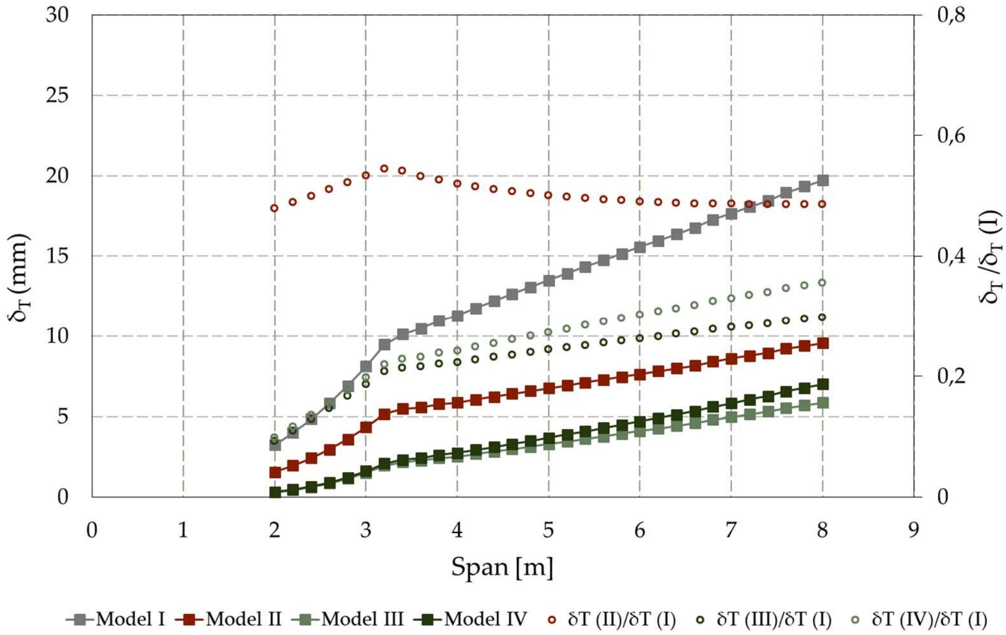

Figure 48 : Comparisons among total deflection in the case of an unpropped slab with profile 1.

The deflections calculated with Model I are typically higher than those obtained with the other models. Furthermore, it is possible observing that the all ratios of deflection showed in the figure 47 and 48 are far from 1, it shows that the difference between the Model I and all other models is substantial in each case. Despite both, Model I and Model II, take into account of the shrinkage component in the calculation of deflection, the difference among the total deflections of these models is not negligible.

The figure 49 presents the three components of the total deflection (instantaneous, creep and shrinkage deflection) already showed in the figure 47, in order to show the influence of each component on the total structural response in terms of deflection. In the case of instantaneous and creep deflection the curves coincide, while the results of shrinkage deflections two models are totally different for the two models and the curves are far . It shows the relevance of the shrinkage component and that the choice of the approach used to calculate shrinkage effects influences significantly the structural response in term of total deflection. The aim of these consideration is to highline the result of not take into account the development of shrinkage gradients, which occurs through the depth of composite slab, on the deflection calculation. The use of uniform shrinkage profile prove to be more conservative than the shrinkage gradient underestimating the defection.

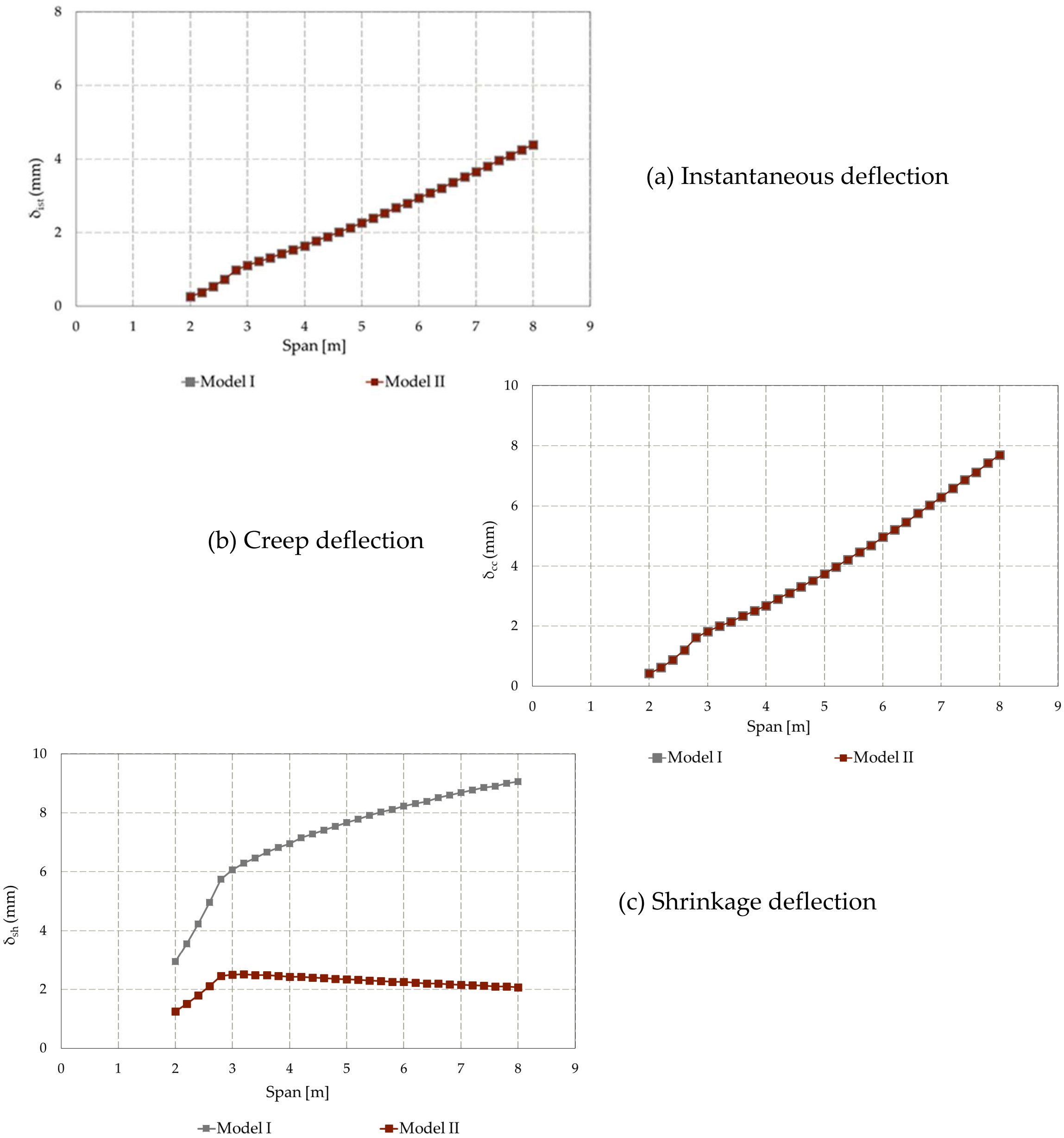

Figure 49: Components of deflection in the case of a propped slab with profile 1

Despite all the difference between the four models, real slab not use to suffer of excessive deflections in the real structures. It is probably due to the fact that real slabs use to be continuous over two spans (at least) and, for this reason, they tend to deflect less than a simply supported slab, as international standards allow to consider a continuous slab. Another possible explanation could be the presence of the floor finishes that could mitigate the shrinkage effects and, therefore, the deflection of the slab. It can be restored the uniform profile of shrinkage.

7.3.1. Other design models for the prediction of deflection

The possibility to use different design models for the calculation of the materials properties of concrete has been introduced in the paragraph (3.2.3). The figure 50 shows the influence of using of these different design models in the prediction of the total deflections. In order to allow a better comparison among the models, the deflection has been calculated assuming unrealistically an uncracked section for all span lengths and the same slab depths (obtained considering linear shrinkage) for all the models. The propped condition for the slab with profile 1 is presented, as reference.

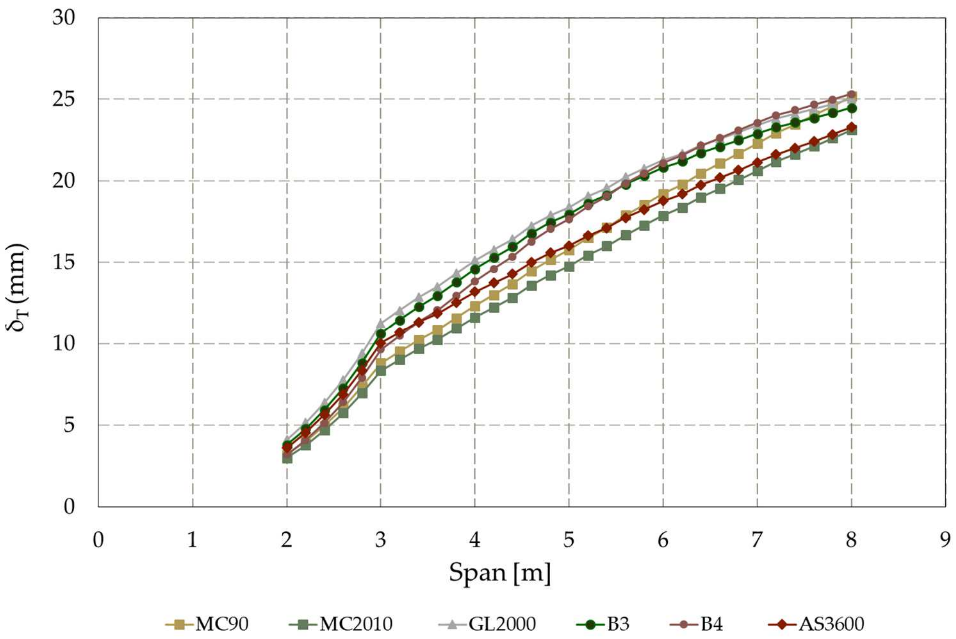

Figure 50: Comparison of total deflection computed using different design models for the calculation of the material properties (t_final= 30 anni).

According the formula (5.1) the total deflection is the sum of three components: instantaneous deflection, creep deflections and shrinkage deflections. The components of the deflection can be compensate each other. For example, despite the final creep coefficient (30 years) calculated with the Model B4 is significantly higher than the other models, the value of total deflection is close to the other ones. The creep deflection is compensated by shrinkage deflection due to the low value of design shrinkage coefficient (figure 51).

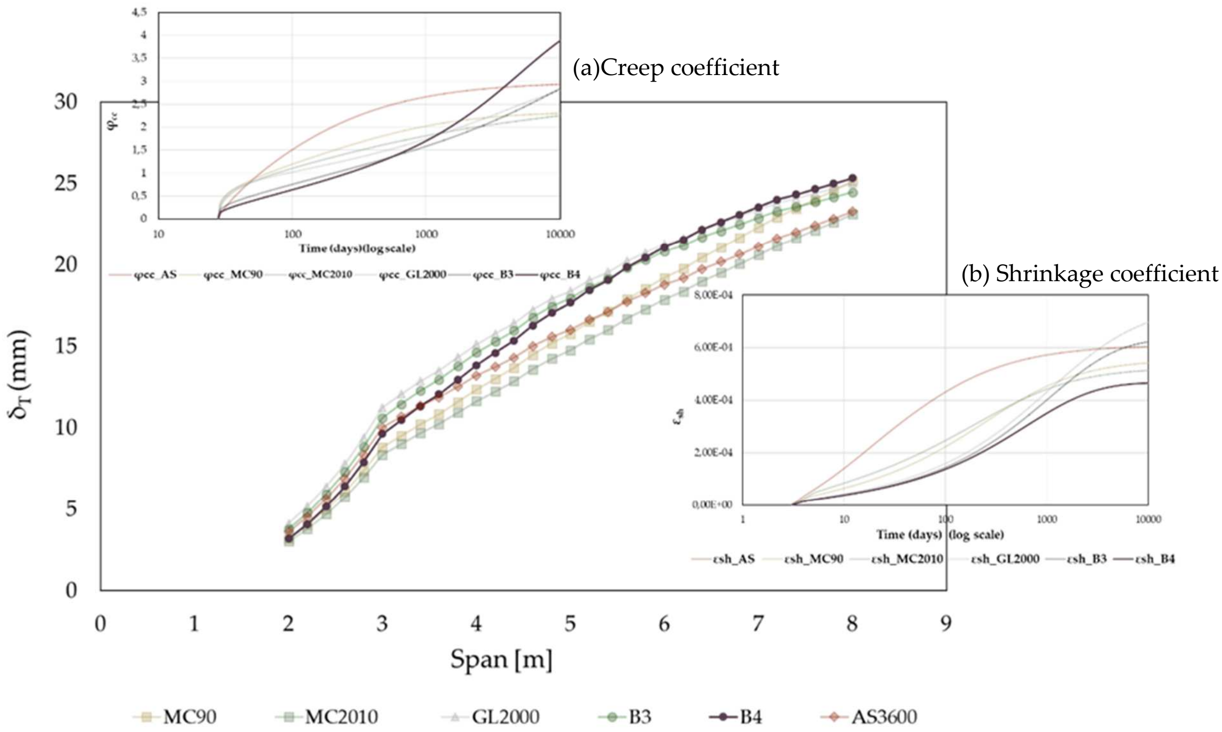

Figure 51 : Total deflection in the case of Model B4

For completeness, in order to understand which component of deflection governs the structural response, instantaneous, creep and shrinkage deflections of each models are presented in the figure 52-54.

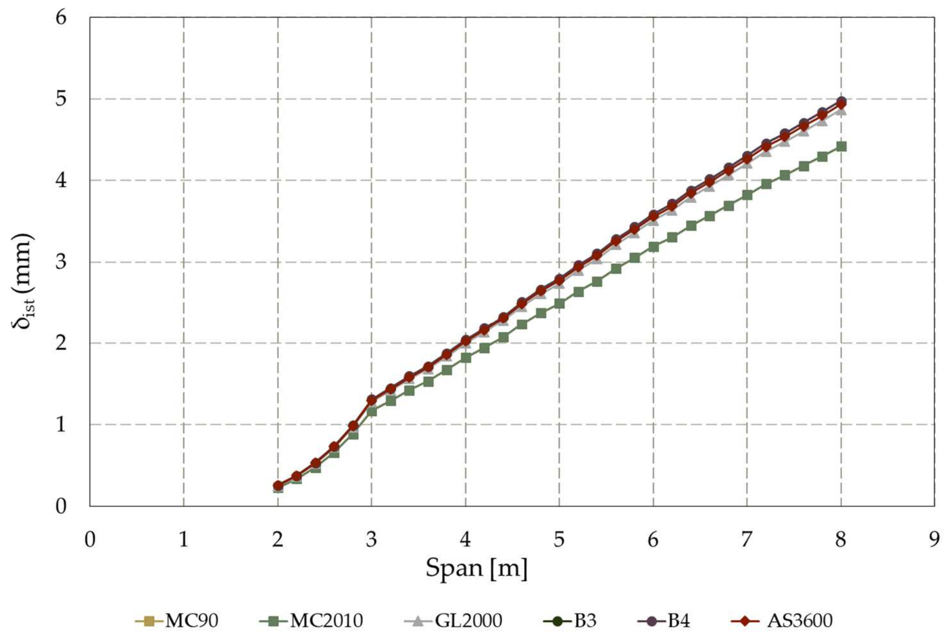

Figure 52: Comparison of instantaneous deflection computed using different design models for the calculation of the material properties (t_final= 30 anni).

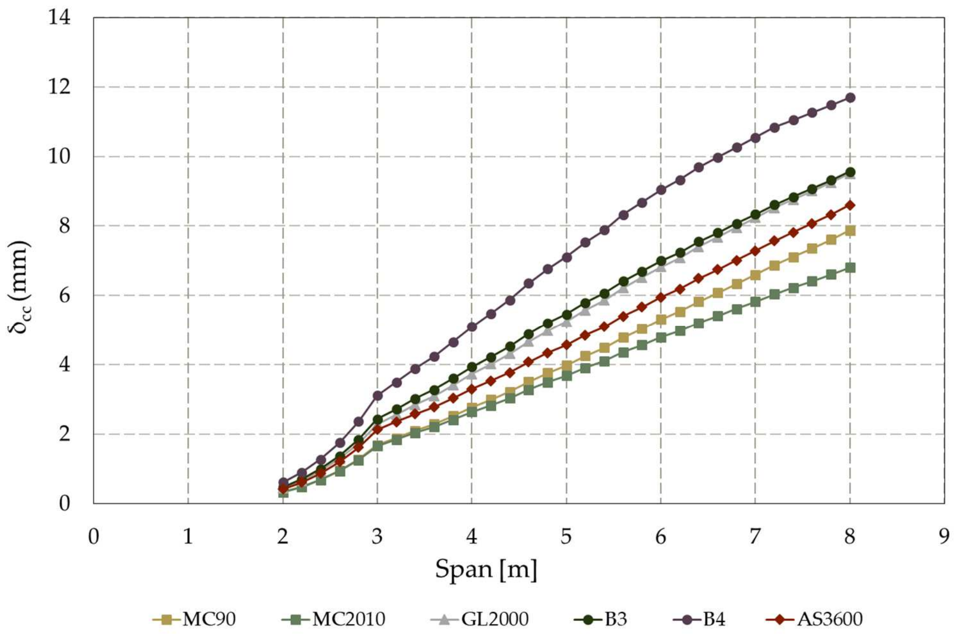

Figure 53: Comparison of creep deflection computed using different design models for the calculation of the material properties (t_final= 30 anni).

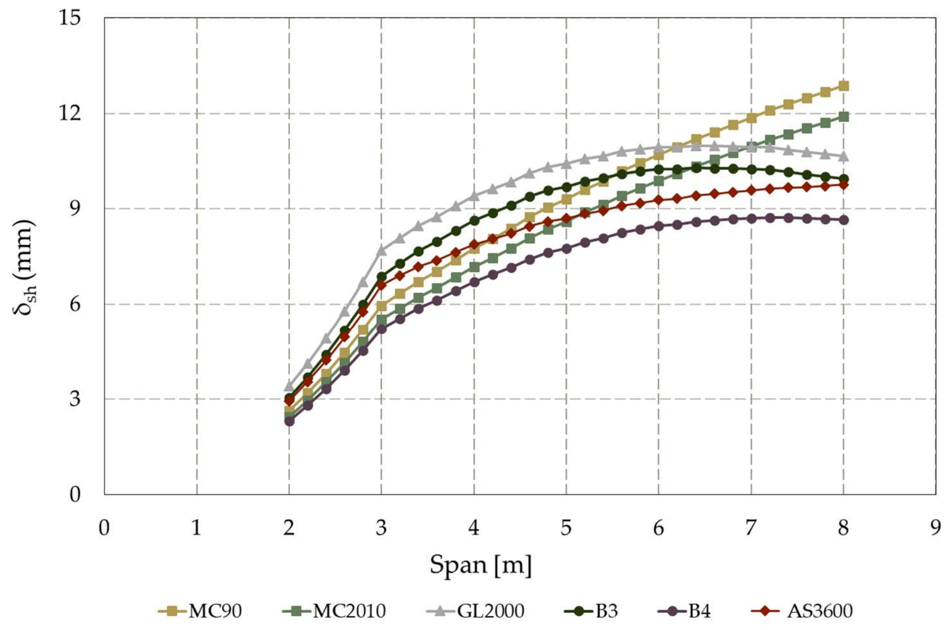

Figure 54: Comparison of shrinkage deflection computed using different design models for the calculation of the material properties (t_final= 30 anni).

In conclusion, this chapter highlights the importance of serviceability limit state on the design of composite steel-concrete structure, and shows the priority of the shrinkage effects over the design calculation. It also focusses on the study of material properties, which is intrinsically linked to the structural behavior.

Conclusion

8.1.Introduction

The conclusion based on the results of this study is summarized in this chapter followed by the recommendations for future work.

8.2. Concluding remarks

This thesis represents an evaluation of the service behaviour of composite steel-concrete slabs. Particular attention is given to a review of the design serviceability models available in current international guidelines (European and Australian) and literature.

The comparison of design procedures specified in the European and Australian guidelines and the parametric study conducted in this thesis, identify the importance of the occurrence of shrinkage gradient in the deflection calculation of composite steel-concrete slabs. The presence of steel sheeting modify the profile of shrinkage through the depth of the slab due the inability of the concrete to dry from the underside of the slab. The parametric study was performed to show the influence of using different models to account the shrinkage effects and also to evaluate the key parameters controlling the composite slab design for building floors. The assumption of linear shrinkage profile (Model I), uniform shrinkage profile (Model II) and no shrinkage effects (Model III and IV) were considered. These models followed the procedures suggest by the international guidelines (AS2737 (1), AS3600-2009 (3), and EN 1994-1-1 (2)).In the parametric study the slab length has been varied and the thickness of the slab has been obtained. The design has taken into consideration the ultimate limit states and the serviceability limit states of composite slabs. Different values of design depth have been obtained for the four models and the difference has been result considerable. Neglect the shrinkage effects leads the most conservative results follow by the uniform shrinkage model and at the end the linear shrinkage model. The result of this study highlights that the serviceability limit state requirements are most stringent than the ultimate ones . The serviceability limit states govern the design of composite steel-concrete slab.

Relevant differences between the four models can be observable also in term of shrinkage deflection, which affects the total deflection. The deflections computed with the Model I result significantly higher than the values obtained with the other models, which underestimate the deflections. This highlighted the importance of including shrinkage effects in the deflection measurements. In the case of composite slab, the real shrinkage profile can be assumed linear, and it is recommended to consider this in the design of such slabs. In general, the differences on the four models tend to amplify for large span. This is due to the fact the shrinkage deflection linearly depends on the span length. If the span is large, the shrinkage deflection tend to get importance on the overall deflection.

In conclusion, the design of composite slabs is usually governed by serviceability limit state requirement associated with deflection.

8.3.Future work

This thesis focuses on the behaviour of simply supported slabs disregards the fact that real slabs use to be continuous over two or more spans because the international standards allow to consider a continuous slab as a series of simply supported slabs. Despite this simplification is generally adopted, this work should be extended evaluating the shrinkage effects on the continuous slabs, in order to obtain more realistic result.

The floor finishes could also influence the drying shrinkage reducing the deflection of the slab. The presence of floor could avoid the free drying of the concrete from upside of the slabs acting like the steel sheeting in the underside. In this case the drying conditions could be the same for both side and the uniform shrinkage profile could be considered. This leads to lesser values of deflection of composite slabs.

For these reasons, experimental studies could be performed to evaluate the influence of floor finishes on the shrinkage profile. Thinner design slab and reduced effect of shrinkage could be obtained.

These possible future works could show a more realistic behaviour of composite steel-concrete slab and explain why real slabs do not use to suffer of excessive deflection in real structures.

References

1. Australian Standards. *AS 2327-2017*.

2. Eurocode. *1994-1-1*.

3. Australian Standard. *3600-2009*.

4. Al-Deen, Ranzi, Uy. *Non-uniform shrinkage in simply-supported composite steel-concrete slabs.* 2015.

5. Al-Deen S, Ranzi G. *Effects of Non-uniform Shrinkage on the Long-term Behaviour of Composite Steel-Concrete Slabs.* 2015.

6. Ghali A, Favre R. *Concrete structures: stresses and deformations.* 1986.

7. RI, Gilbert. *Time effects in concrete structures.* 1988.

8. *Time-dependent analysis of composite steel–concrete sections.* 1990.

9. B, Uy. *Long-term service-load behaviour of simply supported profiled composite slab.* 1997.

10. Koukkari, H. *Steel sheet in a post-tensioned composite slab.* 1999.

11. Gilbert R.I, G. Ranzi. *Time-dependent Behaviour of Concrete Structures.* 2011.

12. Shayan S, Al-Deen, Ranzi G,Vrcelj Z. *Long-term behaviour of composite concrete slabs: an experimental study.* 2010.

13. Al-Deen S, Ranzi G and Vrcelj Z. *Full-scale long-term and ultimate experiments of simply-supported composite beams with steel deck* . 2011.

14. Gilbert RI, Bradford MA, Gholamhoseini A and Chang ZT. *Effects of shrinkage on the long-term stresses and deformations of composite concrete slabs.* 2012**.**

15. Ranzi G, Al-Deen S, Ambrogi L and Uy B. *Long-term behaviour of simply-supported post-tensioned composite slabs .* 2013.

16. Ranzi G, A.Ostinelli. *An experimental study on the shrinkage and ultimate behaviour of post tensioned composite slab.* 2012.

17. Vrcelj, Ranzi G and. *Closed form solutions for the long-term analysis of composite steel-concrete members subjected to non-uniform shrinkage distributions.* 2009.

18. Lambe K, Siddh S. *Analysis and design of composite slab by varing different parameters.* 2018.

19. Ranzi G, Leoni G, Zandonini R. *State of the art on the time-dependent behaviour of composite steel-concrete structures.* 2013**.**

20. Nakai H, Kurita A, Ichinose LH. *An experimental study on creep and concrete filled steel pipes.* Fukuoka (Japan) : Proceedings of the 3rd International Conference on Steel–Concrete Composite Structures, 1991.

21. Terrey PJ, Bradford MA, Gilbert RI. *Creep and shrinkage in concrete-filled steel tubes.* s.l. : Proceedings of 6th International Symposium on Tubular Structures, 1994**.**

22. Kwon S-H, Kim T-H, Kim Y-Y, Kim J-K. *Long-term behaviour of square concrete-filled steel tubular columns under axial service loads .* s.l. : Mag Concr Res, 2007**.**

23. Ichinose LH, Watanabe E, Nakai H. *An experimental study on creep of concrete filled steel pipes.* s.l. : J Constr Steel Res, 2001.

24. An, Kwon and Kim. *Effect of wide-flange-steel geometry on the long-term shortening of steel-reinforced concrete columns.* s.l. : Magazine of Concrete Research, 2015.

25. Zhouyi Chen, Tangzhen Dai. *Effects of sustained axial loads on steel-reinforced concrete columns.* s.l. : HKIE Transactions, 2015.

26. Chang-Soo Kim, Hong-Gun Park, Kyung-Soo Chung and In-Rak Choi. *Eccentric Axial Load Capacity of High-Strength Steel-Concrete Composite Columns of Various Sectional Shapes.* 2013 : American Society of Civil Engineers.

27. Kwon SH, Kim YY, Kim JK. *Long-term behaviour under axial service loads of circular columns made from concrete filled steel tubes.* s.l. : Mag Concr Res, 2005.

28. Chang-Soo Kim, Hong-Gun, In-Rak Choi, and Kyung-Soo Chung. *Effect of Sustained Load on Ultimate Strength of High-Strength Composite Columns Using 800-MPa Steel and 100-MPa Concrete.* s.l. : American Society of Civil Engineers, 2016.

29. Yang YF, Han LH and Wu X. *Concrete Shrinkage and Creep in Recycled Aggregate.* 2008.

30. Geng Y, Wang Y, Chen J. *Time- dependent behaviour of steel tubular columns filled with recycled coarse aggregate concrete.* s.l. : Adv Struct Eng, 2016.

31. Wang, By Y. C. *Deflection of steel-concrete composite beams with partial shear interaction.* 1998.

32. Zuk, W. *Thermal and shrinkage stresses in composite beams.* 1961.

33. Tarantino AM, Dezi L. Creep effects in composite beams with flexible shear. *Creep effects in composite beams with flexible shear connectors.* 1992.

34. MA, Bradford. *Generic modelling of composite steel–concrete slabs subjected to shrinkage, creep and initial thermal strains including partial interaction* . 2010.

35. RP, Johnson. *Shrinkage-induced curvature in composite beams with a cracked concrete flange.* 1987.

36. Alsamsam, I. *Shrinkage measurements in composite beam slabs.* 1992.

37. Wright HD, Vitek JL, Rakib SN. *Long-term creep and shrinkage in composite beams with partial connection.* 1992.

38. Fragiacomo M, Amadio C, Macorini L. *Influence of viscous phenomena on steel–concrete composite beams with normal and high performance slab.* 2002.

39. —. *Finite-element model for collapse and long-term analysis of steel–concrete composite beams.* 2004.

40. Virtuoso F, Vieira R. *Time dependent behaviour of continuous composite beams with flexible connection. .* 2004.

41. G., Ranzi. *Short- and long-term analyses of composite beams with partial shear interaction stiffened by a longitudinal plate.* 2006.

42. Gara F, Ranzi G, Leoni G. *Time analysis of composite beams with partial interaction using available modelling techniques: a comparative study.* 2006.

43. Chaudhary S, Pendharkar U, Nagpal AK. *Control of creep* ***and shrinkage effects in steel concrete composite bridges with precast decks.*** **2009.**

44. Chaudhary S, Pendharkar U, Nagpal AK. *Hybrid procedure for cracking and time-dependent effects in composite frames at service loads.* 2007.

45. Sakr MA, Sakla SSS. *Long-term deflection of cracked composite beams with non linear partial shear interaction.* 2008.

46. Mirza O, Uy B. *Finite element model for long-term behaviour of composite steel–concrete push tests.* 2010.

47. Erkmen RE, Bradford MA. *Nonlinear quasi-viscoelastic behavior of composite beams curved in plan.* 2011.

48. Nguyen Q-H, Hjiaj M, Aribert J-M. *A space-exact beam element for time-dependent analysis of composite members with discrete shear connection.* 2010.

49. Nguyen Q-H, Hjiaj M, Uy B. *Time-dependent analysis of composite beams with continuous shear connection based on a space-exact stiffness matrix.* 2010.

50. Ranzi G, Bradford MA. *Analytical solutions for the time dependent behaviour of composite beams with partial interaction.* 2006.

51. Fan J, Nie X, Li Q, Li Q. *Long-term behavior of composite beams under positive and negative bending. I: experimental study.* 2010.

52. *Long-term behavior of composite beams under positive and negative bending. II: analytical study.* 2010.

53. Al-Deen S, Ranzi G, Vrcelj Z. *Full-scale long-term experiments of simply supported composite beams with solid slabs.* 2011.

54. Ranzi G, Vrcelj Z. *Closed form solutions for the long-term analysis of composite steel–concrete members subjected to non-uniform shrinkage distributions* . 2009.

55. Furtak.K. *Evaluation of the influence of shrinkage strain on the fatigue strength of the connection in steel–concrete composite beams.* 2015.

56. Zanuy, C. *Analytical Equations for interfacial stresses of composite beams due to shrinkage.* 2015.

57. Xiang T, Yang C, Zhao G. *Stochastic Creep and Shrinkage Effect of Steel-Concrete Composite Beam.* 2014.

58. Katwal U, Tao Z, Hassan K. *Finite element modelling of steel-concrete composite beams with profiled steel sheeting.* 2018.

59. Tazawa, Miyazawa. 1992.

60. *Australian Standard.* 2327-2017.

61. *Australian Standard.* 3600-2009.

62. *Material computation-4D timber construction: Towards building-scale hygroscopic actuated, self constructing timber surface.* D. M. Wood, D. Correa, O. D. Krieg, A. Menges. 2016, International Journal of Architecture Computing , Vol. 14 (1), p. 49-62.

63. *Quantitative and qualitative research in the built environment: application of "mixed" research approach.* D. Amaratunga, D. Baldry, M. Sarshar, R. Newton. 2013, MCB UP Ltd.

64. *An autonomous shading system based on coupled wood bilayer elements.* C. Vailati, E. Bachtiar, P. Hass, I. Burgert, M. Ruggerberg. 2017, Elsevier - Energy and Building , Vol. 158, p. 1013-1022.

65. *CTBUH Journal.* 2017 Issue II, 2017, Tall Buildings in Numbers, p. 48-49.

66. *Meteorosensitive architecture: Biomimetic building skin based on materially embedded and hygroscopically enabled responsiveness.* S. Reichert, A. Menages, D. Correa. 2015, Computer - Aided Design, Vol. 60, p. 50-69.

67. *Lesson from tall wood buildings.* R. Holt, K. Wardle. 2014, Perkins+Wil - Research journal, p. 7-19.

68. *Bio-Inspired Wooden Actuators For Large Scale Application.* M. Ruggemberg, I. Burgert. 2015, Journal.pone .

69. *An innovative building envelope (kinetic façade) with Shape Memory Alloys used as actuators and sensors.* M. Formentini, S. Lenci. 2018, Elsevier - Automation in Construction , p. 220-231.

70. *Adaptive facade network - Europe.* L. Aelenei, M. Brzezicki, U. Knaack, A Luible, M. perino, F. Wellershoff. 2015.

71. *Kinetics and mechanism of Dionaea muscipula trap closing.* Ag. Volkov, T. Adesina, VS. Markin, E. Javanok. 2008, p. 694-702.

72. *Shape morphing solar shading: A Review.* F. Fiorito, M. Sauchelli, D. Arroio, M. Pesenti, G. Masera, G. Ranzi. 2015, Elsavier - Renovable and Sustainable Energy Reviews, Vol. 55, p. 883-884.

73. *Structural Analysis: Principles, Methods.* Gilbert, Gianluca Ranzi and Raymond Ian. Sydney : s.n., 2015.

74. *Wood: Strenght and Stiffness.* Green, D. W. p. 9732-9735.

75. *CLT Handbook: Cross-Laminated Timber.* S. Gagnon, C. Pirvu. s.l. : FPInnovations, 2011.

76. *Solid Timber Construction: Process Practice Performance.* E. R. Smith, G. Griffin, T. Rice,. 2015.

77. *Mid-rise Timber Building, Class 2, 3 and 5 Buildings.* P. England, B. Iskra. September 2016.

78. *Timber Towers.* Architect, Waugh Thistleton. s.l.: BluePrint, 2011.

79. *Internationa Conference - Alternative and Renewable Energy Quest.* Mohamed, Abeer Samy Yousef. 2017.

80. *E3 Berlin - Europe's first wooden high-rise.* Moore, C. s.l. : bigEE, 2016.

81. *Solid timber construction - Process, practice, performance.* R. E. Smith, G. Griffin, T. Rice. 2015.

82. Gholamhoseini, Gilbert, Bradford. *Long-term behaviour of continuous composite concrete slabs with steel decking*. 2018.

83. MA, Bradford. *Shrinkage behaviour of steel–concrete composite beams.*

84. Neville, AM., Dilger, W.H and Brooks, J.J. *Creep of Plain and Structural Concrete.* 1983**.**

Appendix

GL2000

$$\varepsilon(t) = \varepsilon_{ist} + \varepsilon_{sh} + \varepsilon_{cr}$$

$$\varepsilon_{sh} = \varepsilon_{shu}\beta(h)\beta(t)$$

$$\varepsilon_{cr}(t, t_0) = \frac{\sigma_c(t_0)}{E_c(t_0)}\Phi(t, t_0)$$

$$\beta(t)=\left(\frac{t-t_c}{t-t_c+0{,}15\cdot({}^{V}/_{S})^2}\right)^{0{,}5}$$

$$E_{cmt} = 3500 \cdot 4300\sqrt{f_{cmt}}$$

$$f_{cmt} = f_{cm28}\frac{t^{3/4}}{a + bt^{3/4}}$$

$$\beta(h)=(1\text{-}1{,}8h^4)$$

$$\Phi_{28} = \Phi(t_c)\left[2\left(\frac{(t-t_0)^{0{,}3}}{(t-t_0)^{0{,}3}+14}\right)+\left(\frac{7}{t_0}\right)^{0{,}5}\left(\frac{(t-t_0)}{(t-t_0)+7}\right)^{0{,}5} +2{,}5(1-1{,}086h^2)\left(\frac{t-t_0}{t-t_0+0{,}15({}^{V}/_{S})^2}\right)^{0{,}5}\right]$$

$$\varepsilon_{shu}=1000\cdot K\cdot\left(\frac{30}{fcm_{28}}\right)^{1/2}\cdot 10^{-6}$$

$$f_{cm28} = 1{,}1f_{ck28} + 5$$

$$\Phi(t_c)=1 \qquad if\ t_0 = t_c$$

$$\Phi(t_c)=\left[1-\left(\frac{t-t_0}{t-t_0+0{,}15({}^{V}/_{S})^2}\right)^{0{,}5}\right]^{0{,}5} \qquad if\ t_0 > t_c$$

Figure A1: Creep strain and shrinkage strain according GL2000

Model B3

$$\varepsilon(t) = J(t,\ t')\sigma + \varepsilon_{sh}$$

$$J(t,t') = q_1 + R_T C_0(t,t') + C_d(t,t',t_0)$$

$$q_1 = p_1 / E_{28}$$

$$E_{28} = 4734\sqrt{f_{cm}}$$

$$C_0(t,t') = q_2 Q(t,t') + q_3\, ln\left[1 + \left(\frac{t-t'}{1\, days}\right)^{0{,}1}\right] + q_4\, ln\left(\frac{t}{t'}\right)$$

$$q_4 = 20.3(a/c)^{0.7}$$

$$q_3 = 0.29(w/c)^4 q_2$$

$$Q(t,t') = Q_f(t')\left[1 + \left(\frac{Q_f(t')}{Z(t,t')}\right)^{r(t')}\right]^{-1/r(t')}$$

$$q_2 = 185.4c^{0.5} f_c^{-0.9}$$

$$Q_f(t') = \left[0.086(t')^{2/9} + 1.21(t')^{4/9}\right]^{-1}$$

$$m = 0.5;\ n = 0.1$$

$$Z(t,t') = (t')^{-m} ln[1 + (t - t')^n]$$

$$r(t') = 1.7(t')^{0.12} + 8$$

$$C_d(t,t',t_0) = 0 \qquad if\ t < t_0'$$

$$C_d(t,t',t_0) = q_5[exp\{-8H(t,t_0)\} - exp\{-8H_c(t_0',t_0)\}]^{1/2}$$

$$H(t,t_0) = 1 - (1 - h)S(t)$$

$$H_c(t_0',t_0) = 1 - (1 - h)\, tanh\sqrt{\frac{t_0', t_0}{\tau_{sh}}}$$

$$q_5 = 7.57 \cdot 10^5 f_{ck}^{-1} |\varepsilon_{sh\infty}|^{-0.6}$$

$$\varepsilon_{sh\infty} = \varepsilon_{s\infty}\frac{E(607)}{E(t_0 - \tau_{sh})}$$

$$E(t_0 + \tau_{sh}) = E(28)\left(\frac{t_0 + \tau_{sh}}{4 + 0{,}85(t_0 + \tau_{sh})}\right)^{1/2}$$

$$E(607) = E(28)\left(\frac{607}{4 + 0{,}85(607)}\right)^{1/2}$$

$$\varepsilon_{sh}(t,t_0) = \varepsilon_{sh\infty}\kappa_h S(t)$$

$$k_h = \begin{cases} 1 - h^3 & h \le 0{,}98 \\ -0{,}2 & h = 1 (swelling\ in\ water) \\ linear\ interpolation & 0{,}98 \le h \le 1 \end{cases}$$

$$S(t) = tanh\sqrt{\frac{t}{\tau_{sh}}}$$

$$\tau_{sh} = \kappa_t(\kappa_s D)^2$$

$$\kappa_t = 8{,}5 t_0^{-0{,}08} f_{ck}^{-1/4}$$

$$k_s = \begin{cases} 1.00 \text{ for} & \text{an infinite slab} \\ 1.15 \text{ for} & \text{an infinite cylinder} \\ 1.25 \text{ for} & \text{an infiniter square prism} \\ 1.30 \text{ for} & \text{a sphere} \\ 1.55 \text{ for} & \text{a cube} \end{cases}$$

$$\varepsilon_{s\infty} = -\alpha_1\alpha_2[1{,}9 \cdot 10^{-2}\omega^{2{,}1} f_{ck}^{-0{,}8} + 270]$$

$$\alpha_1 = \begin{cases} 1{,}0 & \text{Type I } cement \\ 0{,}85 & \text{Type II } cement \\ 1{,}1 & \text{Type III } cement \end{cases}$$

$$\alpha_2 = \begin{cases} 0{,}75 & \text{steam } curing \\ 1{,}2 & \text{sealed o normal } curing \\ 1{,}0 & \text{curing in water } 100\%\omega \end{cases}$$

Figure A2: Creep strain and shrinkage strain according Model B3

Model B4

$$\varepsilon(t) = \mathrm{J}(t,\ t')\sigma + \varepsilon_{sh}$$

$$J(t,t') = q_1 + R_T C_0(t,t') + C_d(t,t',t_0)$$

$$\varepsilon_{sh}(t,t_0) = \varepsilon_{sh\infty}\kappa_h S(t)$$

$$q_1 = p_1 / E_{28}$$

$$E_{28} = 4734\sqrt{f_{cm}}$$

$$C_d(t,t',t_0) = 0 \qquad if\ t < t_0'$$

$$k_h = \begin{cases} 1 - h^3 & h \le 0,98 \\ 12,94(1-h) - 0,2 & 0,98 \le h \le 1 \end{cases}$$

$$C_d(t,t',t_0) = q_5[exp\{-8H(t,t_0)\} - exp\{-8H_c(t_0',t_0)\}]^{1/2}$$

$$S(t) = tanh\sqrt{\frac{t}{\tau_{sh}}}$$

$$C_0(t,t') = q_2 Q(t,t') + q_3\, ln\left[1 + \left(\frac{t-t'}{1\ days}\right)^{0,1}\right] + q_4\, ln\left(\frac{t}{t'}\right)$$

$$\tau_{sh} = \tau_0 \kappa_{ta}\left(\kappa_s \frac{D}{1\ mm}\right)^2$$

$$H(t,t_0) = 1 - (1-h)S(t)$$

$$q_4 = \frac{p_4}{1\ Gpa}\left(\frac{a/c}{6}\right)^{p_{4w}}\left(\frac{w/c}{0.38}\right)^{p_{4w}}$$

$$\tau_0 = \tau_{cem}\left(\frac{a/c}{6}\right)^{p_{\tau a}}\left(\frac{w/c}{0.38}\right)^{p_{\tau w}}\left(\frac{6,5c}{\rho}\right)^{p_{\tau c}}$$

$$H_c(t_0',t_0) = 1 - (1-h)\, tanh\sqrt{\frac{t_0', t_0}{\tau_{sh}}}$$

$$q_3 = p_3 q_2\left(\frac{a/c}{6}\right)^{p_{3w}}\left(\frac{w/c}{0.38}\right)^{p_{3w}}$$

$$\varepsilon_{sh,tot}(t,t_0) = \varepsilon_{sh}(t,t_0) + \varepsilon_{au}(t,t_0)$$

$$q_5 = \frac{p_5}{1\ Gpa}\left(\frac{a/c}{6}\right)^{p_{5w}}\left(\frac{w/c}{0.38}\right)^{p_{5w}} |\kappa_h \varepsilon_{sh\infty}|^{p_{5\varepsilon}}$$

$$Q(t,t') = Q_f(t')\left[1 + \left(\frac{Q_f(t')}{Z(t,t')}\right)^{r(t')}\right]^{-1/r(t')}$$

$$\varepsilon_{au}(t,t_0) = \varepsilon_{au\infty}\left[1 + \left(\frac{\tau_{au}}{t+t_0}\right)^{\alpha}\right]^{r_t}$$

$$\varepsilon_{sh\infty} = -\varepsilon_0 \kappa_{\varepsilon a}\frac{E(\beta_{Th} + 600\beta_{Ts})}{E(t_0 - \tau_{sh}\beta_{Ts})}$$

$$q_2 = \frac{p_1}{1\ Gpa}\left(\frac{w/c}{0.38}\right)^{p_{2w}}$$

$$\varepsilon_{au\infty} = -\varepsilon_{au,cem}\left(\frac{a/c}{6}\right)^{r_{\varepsilon a}}\left(\frac{w/c}{0.38}\right)^{r_{\varepsilon w}}$$

$$Q_f(t') = \left[0.086\left(\frac{t'}{1\ days}\right)^{2/9} + 1.21\left(\frac{t'}{1\ days}\right)^{4/9}\right]^{-1}$$

$$E(t) = E(28)\left(\frac{t}{4days + (6/7)(t)}\right)^{1/2}$$

$$\tau_{au} = \tau_{au,cem}\left(\frac{w/c}{0.38}\right)^{r_{\tau w}}$$

$$m = 0.5;\ n = 0.1$$

$$Z(t,t') = \left(\frac{t'}{1\ days}\right)^{-m} ln\left[1 + \left(\frac{t-t'}{1\ days}\right)^{n}\right]$$

$$\alpha = r_\alpha\left(\frac{w/c}{0,38}\right)$$

$$r(t') = 1.7\left(\frac{t'}{1\ days}\right)^{0.12} + 8$$

Figure A3: Creep strain and shrinkage strain according Model B4